

**ALPHA -T-T and T-T-ALPHA-T DIAGRAMS**  
**IN INTELLIGENT PROCESSING OF THERMOSETTING COMPOSITES**

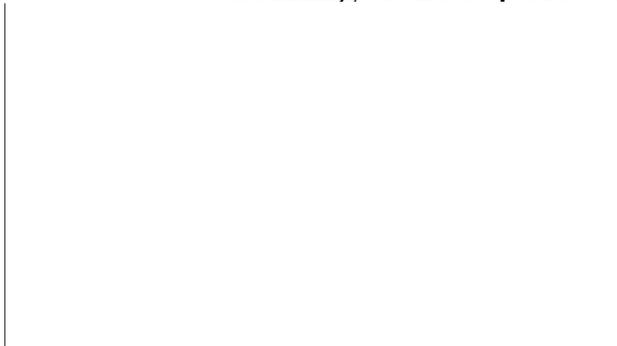
Barbara Osinski  
M.Sc. (Ceramics) University of Mining and Metallurgy, Krakow, Poland

A THESIS SUBMITTED IN PARTIAL FULFILLMENT OF THE  
REQUIREMENTS FOR  
THE DEGREE OF MASTER OF APPLIED SCIENCE

in

THE FACULTY OF GRADUATE STUDIES  
METALS AND MATERIALS ENGINEERING

We accept these thesis as conforming to the requested standard



THE UNIVERSITY OF BRITISH COLUMBIA

April 1993

© Barbara Osinski



## ABSTRACT

The majority of existing models for processing in thermoset matrix composites concentrate nearly exclusively on heat and mass transfer problems and account for material-related aspects in a very simplified manner. The objective of this work is to provide that missing element by proposing a clearly defined system which yields all the information of Gillham's T-T-T diagram but can be used for non-isothermal curing cycles. To build the system, three elements are needed: the gelation and vitrification curves, expressed as functions of degree of conversion; the kinetic model of conversion; and a diagram combining all complex information provided by the system. The proposed system for the Narmco 5208 resin incorporates a recently developed mechanistic model for the kinetics of conversion. The algorithm calculates and graphically presents the progress of thermoset processing using the developed diagrams which re-introduce time as an independent variable. The most important part of the system is its graphical output:  $\alpha$ -T-T diagrams, originally developed in this work. Their role is to enhance the understanding of the process by providing the rheological information.

Practical applications of the system, with an increasing degree of its sophistication, are presented using four examples. The first case demonstrates the basic value offered by the diagrams - prediction of the moment of gelation and vitrification in advance; the second application shows the advantage of the system in thick composite processing; the third is the generation of the T-T-T diagram for the Narmco resin based on the kinetic model of conversion; the fourth application, where the system is used in the reverse mode, in a new capability - the search for an optimum curing cycle in the RTP method.

In experimental part of the work, the kinetic model of conversion incorporated into the system was verified using the Differential Scanning Calorimetry (DSC) technique, and the rheology of the resin was investigated using the Rheometric Dynamic Analyser (RDA) and DSC apparatus.

## TABLE OF CONTENTS

	Page
ABSTRACT	ii
TABLE OF CONTENTS	iv
TABLES	vi
FIGURES	vi
NOMENCLATURE	x
ABBREVIATIONS	xii
ACKNOWLEDGEMENTS	xiii
1. INTRODUCTION	1
1.1 Scope of the Work	5
2. CHEMICAL SYSTEM OF EPOXY RESIN	7
2.1 Introduction	7
2.2 Reaction Mechanism and Kinetics of Narmco Resin	10
3. MODELLING OF KINETICS OF CONVERSION	12
3.1 Introduction	12
3.2 Degree of Cure	13
3.3 Review of Existing Models	14
3.4 Conversion of Epoxide Groups	20
3.5 Experimental Verification of Cole's Model	22
3.6 Results and Discussion	23
3.7 Contribution of the Author	23
4. CHEMORHEOLOGICAL CHANGES DURING CURE	35
4.1 Theory	35
4.1.1 Viscosity	38
4.1.2 Gelation	42
4.1.3 Vitrification	48
4.2 Experiments	51
4.2.1 Introduction	51

4.2.2	Review of Techniques for Rheological Characterization	52
4.2.3	Determination of Gelation and Vitrification Point Using RDA Technique	57
4.2.4	Discussion of the Results	63
4.2.5	Determination of Vitrification Point on the Basis of the DSC measurements	65
4.3	Contribution of the Author	65
5. CURE DIAGRAMS AS A METHOD OF DISPLAYING INFORMATION OF RHEOLOGICAL CHANGES IN MATERIAL UNDER PROCESSING		90
5.1	Gillham's T-T-T and C-H-T Diagrams	90
5.2	$\alpha$ -T-T Diagram - the Concept	94
5.3	Structure and Operation of the Developed "System"	95
5.4	Interaction of the Proposed System With a Thermal Model of Composite Processing	98
5.5	$\alpha$ -T-T and T-T- $\alpha$ -T Diagrams - the Graphical Output of the System	100
5.6.	Applications	104
5.6.1	RDA Tests	104
5.6.2	$\alpha$ -T-T Diagram in Processing of Thick Composites	130
5.6.3	Generation of T-T-T Diagram for Narmco Resin	133
5.7	Contribution of the Author	135
6. APPLICATION OF ALPHA-T-T DIAGRAM TO RTP METHOD		136
6.1	Contribution of the Author	137
7. CONCLUSIONS		139
8. REFERENCES		143

## TABLES

	Page:
1. Gelation Point - Experimental Data	84
2. Vitrification - Experimental and Theoretical Data	85
3. List of RDA Tests	104

## LIST OF FIGURES

	Page
1. Schematic of prepreg lay-up	1
2. The principal events occurring during a cure cycle	2
3. Epoxy group	7
4. Schematic form of a typical epoxy reaction	7
5. Network formation in epoxy resin	9
6. Main reactions in a cure of Narmco resin	11
7. Isothermal DSC curve obtained at temperature 130°C.	25
8. Isothermal DSC curve obtained at temperature 170°C.	26
9. Isothermal DSC curve obtained at temperature 190°C.	27
10. Dynamic DSC curve obtained at heating rate 3°/min.	28
11. Dynamic DSC curve obtained at heating rate 5°/min.	29
12. Calibration curve for dynamic tests	30
13. Verification of conversion kinetic model - isothermal 130°C.	31
14. Verification of conversion kinetic model - isothermal 170°C.	32
15. Verification of conversion kinetic model - dynamic 3°/min.	33

16.	Verification of conversion kinetic model - dynamic 5°/min.	34
17.	Schematic representation of the cure of a thermoset	37
18.	Measurement of viscosity	39
19.	Types of amine units	44
20.	Possible configurations for TGDDM-DDS system	45
21.	Specific volume as a function of temperature	49
22.	Time dependence of the stress and strain during a test	53
23.	Rheometrics Dynamic Analyzer	58
24a.	RDA record of processing - 140 °C/30 min.	66
24b.	Degree of conversion for experiment 140°C/30 min.	67
25a.	RDA record of processing - 170/140 °C/180 min.	68
25b.	Degree of conversion for experiment 180/140°C/180 min.	69
26a.	RDA record of processing - 170°C/60 min. (A).	70
26b.	Degree of conversion for experiment 170°C/60 min.(A).	71
27a.	RDA record of processing - 170 °C/60 min. (B)	72
27b.	Degree of conversion for experiment 170°C/60 min. (B)	73
28a.	RDA record of processing - 170°C/120 min. (A).	74
28b.	Degree of conversion for experiment 170°C/120 min. (A).	75
29a.	RDA record of processing - 170°C/120 min. (B).	76
29b.	Degree of conversion for experiment 170°C/120 min. (B).	77
30a.	RDA record of processing - 190°C/180 min. (A).	78
30b.	Degree of conversion for experiment 190°C/180 min. (A).	79
31a.	RDA record of processing - 190°C/180 min. (B).	80
31b.	Degree of conversion for experiment 190°C/180 min. (B).	81

32a.	RDA record torsion mode	82
32b.	RDA record torsion mode	83
33.	DSC record, rate of temperature increase 10°/min.	86
34.	DSC record, rate of temperature increase 10°/min.	87
35.	DSC record, rate of temperature increase 5°/min.	88
36.	DSC record, rate of temperature increase 5°/min.	89
37.	TTT cure diagram	92
38.	CHT cure diagram	93
39.	Structure of the system	97
40.	Interaction of the system with a thermal model	99
41.	Comprehensive $\alpha$ -T-T diagram	101
42.	T-T- $\alpha$ -T diagram	102
43.	T-T- $\alpha$ -T diagram without surfaces of gelation and vitrification	103
44a.	Temperature cycle in test 140°C/30 min.	106
44b.	History of degree of conversion	107
44c.	$\alpha$ -T-T diagram	108
45a.	Temperature cycle in test 170°C/140°C/180 min.	109
45b.	History of degree of conversion	110
45c.	$\alpha$ -T-T diagram	111
46a.	Temperature cycle in test 170°C/60 min.(A).	112
46b.	History of degree of conversion	113
46c.	$\alpha$ -T-T diagram	114
47a.	Temperature cycle in test 170°C/60 min.(B).	115
47b.	History of degree of conversion	116

47c.	$\alpha$ -T-T diagram	117
48a.	Temperature cycle in test 170°C/120 min.(A)	118
48b.	History of degree of conversion	119
48c.	$\alpha$ -T-T diagram	120
49a.	Temperature cycle in test 170°C/120 min.(B).	121
49b.	History of degree of conversion	122
49c.	$\alpha$ -T-T diagram	123
50a.	Temperature cycle in test 190°C/180 min.(A).	124
50b.	History of degree of conversion	125
50c.	$\alpha$ -T-T diagram	126
51a.	Temperature cycle in test 190°C/180 min.(B).	127
51b.	History of degree of conversion	128
51c.	$\alpha$ -T-T diagram	129
52.	$\alpha$ -T-T diagram in thick composite processing	131
53.	T-T- $\alpha$ -T diagram in thick composite processing	132
54.	T-T-T diagram for Narmco resin	134
55.	$\alpha$ -T-T diagram in RTP processing	138

## NOMENCLATURE

B	= initial ratio of primary amine N-H bonds to epoxide group
D	= diffusivity
E	= activation energy
E'	= storage moduli
E''	= loss moduli
F	= structure factor
f	= fractional free volume
f <sub>e</sub>	= functionality of epoxy group
f <sub>a</sub>	= functionality of hardener
G'	= storage modulus
G''	= loss modulus
g	= gyration factor
H <sub>t</sub>	= heat developed during the reaction between the starting point and a time (t)
H <sub>tot</sub>	= total heat developed during the cure
M <sub>a</sub>	= moles of epoxy
M <sub>e</sub>	= moles of hardener

- $M_w$  = weight-average molecular weight
- $P_e$  = fraction of epoxy active group
- $P_a$  = fraction of hardener active group
- $r$  = initial ratio of hardener to epoxy groups
- $R$  = gas constant (8314.4 J kmol<sup>-1</sup>)
- $T$  = temperature
- $T_{g_0}$  = glass transition temperature at  $\alpha=0$
- $t$  = time
- $T_{g_\infty}$  = maximum glass transition temperature
- $\alpha$  = fractional degree of conversion of epoxide groups
- $\beta$  = fraction of amine N-H bonds which have reacted
- $\dot{\gamma}$  = rate of shear
- $\delta$  = shear stress
- $\epsilon$  = tensile strain
- $\zeta$  = friction factor
- $\eta_*$  = complex viscosity
- $\eta'$  = dynamic viscosity
- $\eta''$  = imaginary viscosity

- $\kappa$  = branching coefficient
- $\omega$  = frequency of oscillations in dynamic testing
- $\sigma$  = tensile strain

## ABBREVIATIONS

DMA Dynamic Mechanical Analyzer

DSC Differential Scanning Calorimeter

RTP Rapid Thermoset Processing

TBA Torsional Braid Analyzer

TMA Thermal Mechanical Analyzer

## ACKNOWLEDGEMENTS

I would like to extend special thanks to Professor K. Gillham of Princeton University from whose work my idea is conceived. Professor's Gillham diagrams served not only as a starting point but also as a continuous standard for my Thesis throughout its development. His encouragement and inspiration are deeply appreciated.

I would also like to express my gratitude to Professor B. Hawbolt and Professor P. Steiner of University of British Columbia for their support, constructive criticism, and helpful recommendations.

Special thanks are also due to Professor G. Springer of Stanford University for his time spent discussing my work and for his hospitality.

Finally I would like to thank Mr. A. Russell of National Defence Research and Professor P. Steiner from University of British Columbia for giving me an opportunity to work on their equipment, as well as Dr. K. Cole National Research Council of Canada and Mr. D. Wilson Bombardier Inc. for supplying the materials essential to the completion of my work.

I am also deeply indebted to the Government of Canada for providing the financial support for my work in a form of a student loan.

## 1. INTRODUCTION

During the last few years great progress has been made in the development of high-performance composites. Most are fabricated using carbon or aromatic fibers with an epoxy matrix based on tetraglycidyl diamino diphenyl sulphone (TGDDM-DDS) formulations. The laminates are generally produced by the Autoclave/Vacuum Degassing Laminating Process where the polymerization reactions of the thermoset matrix are activated and the composite is consolidated. In this process, prepreg plies of desired shape are laid up in a prescribed orientation to form a laminate. The laminate is placed upon a smooth metal tool surface and covered with successive layers of an absorbent material (bleeder), a fluorinated film to prevent sticking, and finally a vacuum bag. The entire system is placed into an autoclave, vacuum is applied to the bag, and the temperature is increased at a constant rate in order to promote the resin flow and polymerization. Figure 1<sup>43</sup> represents a simple lay-up.<sup>42,43</sup> The principal physical events occurring during such a cure cycle are illustrated in Figure 2.<sup>40</sup>

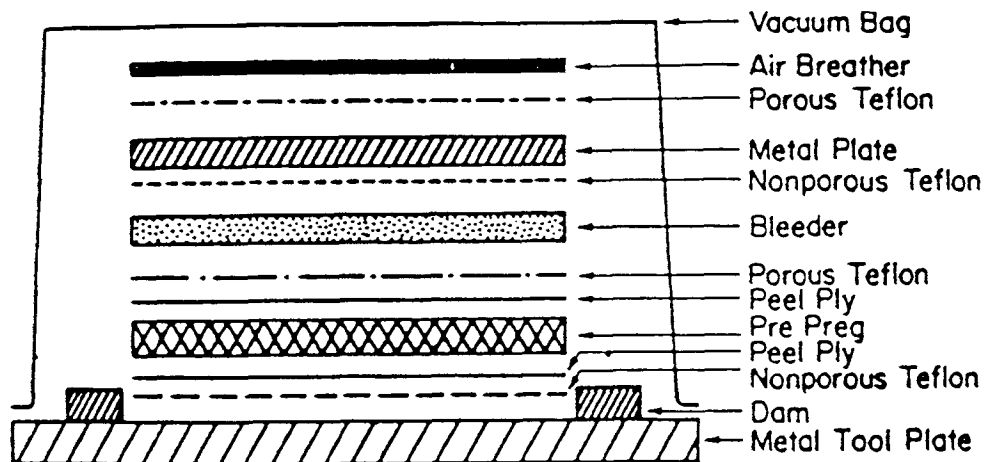


Figure 1. Schematic of the prepreg lay-up.

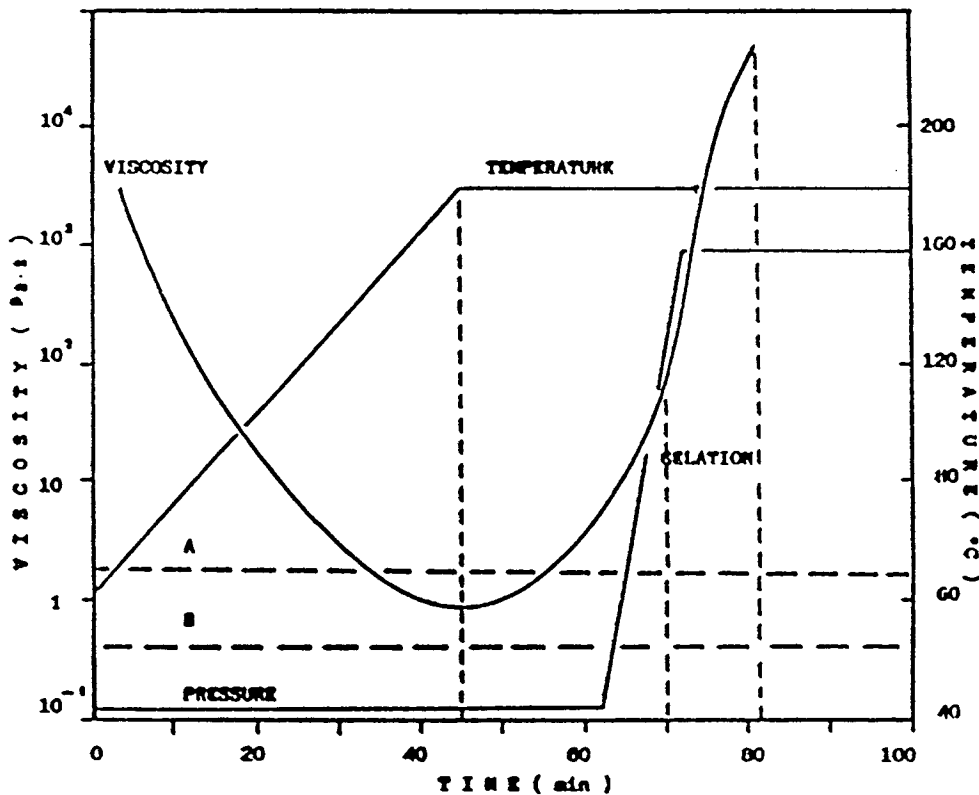


Figure 2. The principal events occurring during a cure cycle

The processing conditions in the autoclave are dictated by the chemoreological properties of the epoxy matrix and by heat transfer characteristics of the composite-tool-autoclave system. The relative rates of heat generation and of heat transfer determine the values of the advancement of the reaction and the viscosity through the thickness of the laminate. The processing of a polymeric composite based on thermoset matrices, requires the optimization of the cure cycle parameters as well as an adequate rheological characterization of the reacting system.<sup>29,43</sup>

The mentioned optimization of the cure cycle may be attempted on the basis of a mathematical model of the process. Unfortunately, the existing models for processing of thermoset matrix

composites are poorly suited for the task. To some extent, the existing knowledge on the material under processing is responsible for this fact; it does not provide all of the information necessary for a full optimization in the quantitative form required for algorithmization. However, the existing models of the old generation fail to provide the essential information even if this information may be generated on the basis of the existing knowledge. They account typically for three aspects of the process: heat transfer, fluid flow, and kinetics of resin conversion, concentrating nearly exclusively on the first two and using simplified, experimentally-determined expressions for the third. The heat transfer model, combined with the model of conversion are to ensure that the temperature in any location of the material during processing does not exceed the value, liberally assumed as the acceptable maximum, and that the degree of conversion of the material at the end of processing does reach a value liberally assumed as the acceptable minimum. The resin flow model is to ensure the proper level of material compaction reached before the resin becomes too viscous to flow. It also may be used, to some extent, to control the behaviour of gaseous discontinuities in the processed material. The element missing in those models is a model of rheological behaviour of the resin. Yet, rheological transformations taking place during processing have a serious impact either on the process itself, or on the final properties of the product. The phenomenon of gelation marks the end of resin flow and carries a special meaning for the precipitation of an additional phase in the case of toughened resin processing. Vitrification not only defines the moment when a material acquires mechanical properties of a solid, but causes the diffusion-controlled slow-down of the conversion reaction and may determine the final degree of conversion obtained in the product. It also may determine the density of cross-linking, specific volume, and final contraction of the material - the properties of the semi-finished product. In cases when these parameters vary from location to location, additional stresses, and eventual deformations may be generated. In fact, the stresses may be generated simply because vitrification does not occur at different locations simultaneously.

This study is an attempt to fill the existing gap in the modelling of thermoset-based composite processing by developing an additional model segment representing material behavior. The

segment accounts for the kinetics of resin conversion, as well as for rheological transformations of the material, and could be used as a part of a comprehensive model of composite processing, as a stand-alone model of resin behaviour or combined with a thermal model, to simulate the processing of a non-reinforced resin system. The advanced kinetics of conversion expressions utilized in the segment are of the mechanistic approach reported by Cole.

A very specific problem resulting from the kinetics of conversion application is the complexity of the produced information. At any moment of processing there are three variables involved: time, temperature and degree of conversion, as well as at least three phenomena: gelation, initial vitrification, and final vitrification. If a heat transfer model is additionally employed, for thick, or non-uniformly shaped material under processing, the complexity is amplified by a number of characteristic locations at which the mentioned variables must be monitored. This complexity calls for especially effective means of conveying the produced information to the user of the model in a comprehensive and transparent form. The perfect example of a well-suited form for the application are Gillham's Time-Temperature-Transformation (TTT) diagrams<sup>23,51,53,70</sup> The diagrams, however, are built for, and can be applied to isothermal curing only, while in industrial practice, especially in case of thick materials, the processing cycles are non-isothermal. The concept of the diagrams presented in this study which could be applied to any processing cycle stems from the fact that the point of gelation and the point of final vitrification, for a resin system, can be quite easily expressed as a function of the degree of conversion and temperature<sup>67</sup>. Gelation is expected to occur at a constant value of conversion, while the point of vitrification is described by the DiBenedetto equation<sup>54</sup>. Both curves may be plotted on the grid of the degree of conversion versus temperature of processing. In order to place the point of processing in the same figure, its coordinates - the momentary temperature of processing and the degree of conversion must be determined. The latter can be calculated if the kinetic model of conversion is available.

The objective of this study was to create an algorithm based on the presented concept and to develop diagrams comprehensively displaying the complex information produced. The algorithm consists of different elements, and is therefore called a 'system'. The elements of the system are: material-dependent gelation, initial vitrification, and final vitrification; material - and - cycle - dependent kinetics of conversion; and the original alpha-T-T and T-T-alpha-T diagrams, which provide a comprehensive characterization of processing by displaying all the information produced by the system graphically. The diagrams are the most valuable and innovative part of the system. The system itself is limited to the well-known aspects of material behavior and does not address all the problems involved in optimization of the processing cycle. However, it creates the basis on which further efforts leading in this direction can be made by providing a basis for a comprehensive understanding of the process.

The best way to understand and to assess the real value of the system, and the diagrams, is to study the examples of their practical application. The presented applications include a manufacturer-suggested processing cycle, followed by the cycles applied in Rheometrics Dynamic Analyser (RDA) experiments, and reproduction of the Gillham diagram. An original method of Rapid Thermoset Processing (RTP) takes a distinctive place among these applications, proving the extensive potential capabilities of the concept presented in this study.

### 1.1 Scope of the work

Of the three elements of the 'system'- kinetics of conversion, rheological characteristics of the material, and the diagrams - the kinetics of conversion is investigated first. After reviewing typical models of the kinetics of conversion a decision was made to use an approach developed by Cole specifically for the resin system under consideration. This excellent kinetics expression for the conversion reaction was incorporated into the computer code of the model of conversion. The model

is verified by comparing its results with the results of experiments conducted on the same resin system using Differential Scanning Calorimetry (DSC) technique, with either isothermal or linearly increasing temperature cycles.

The second objective of the work is to measure/verify rheological parameters of the resin system related to gelation and vitrification phenomena. The suitability of different techniques for determination of rheological parameters was assessed. The moment of gelation is determined using the RDA apparatus, the vitrification is investigated using RDA and DSC techniques.

Since the original  $\alpha$ -T-T and T- $\alpha$ -T-T diagrams, proposed by the author, cannot stand alone, but are generated by the system for each specific temperature cycle, both, the system and the diagrams are developed and presented simultaneously. It is important to realize that the diagram concept has grown out of Gilham's T-T-T diagrams. The T-T-T diagrams, however, are for a specific type of a thermal cycle (isothermal, or linear temperature increase), and contain the kinetics of conversion within, while the proposed diagrams may be applied to any temperature cycle, no matter how complex, and require the support of the system. The main problem of the proposed diagrams is that there are three variables to be shown simultaneously: time, temperature and degree of conversion. To deal with this problem, either a special arrangement of three different graphs is employed ( $\alpha$ -T-T diagram), or a 3-dimensional graph is used (T- $\alpha$ -T-T diagram)<sup>51,52</sup>.

A number of examples of the diagrams application are presented. These are either for the temperature cycle as suggested by the manufacturer of the resin, or for temperature cycles used in the investigation of the rheological properties of the resin. An interesting, although hypothetical exercise, was conducted by using the system to generate Gilham's diagram for isothermal processing. Another interesting application of the diagrams and the system is demonstrated for the newly developed RTP method<sup>9,52</sup>. The system provides the necessary information for this processing method to allow for its optimization.

## 2. CHEMICAL SYSTEM OF EPOXY RESIN

### 2.1 Introduction

Thermosetting epoxy resin is a synthetic organic polymers that cures to a solid infusible mass by forming a three dimensional network of covalent chemical bonds. These network polymers possess a variety of useful properties, including high chemical and solvent resistance, outstanding adhesion to many substrates, low shrinkage on cure, good impact resistance, flexibility, and good electrical properties. As a result, epoxy resins have gained wide acceptance in composite materials for demanding structural application.

The key to the excellent performance of epoxy resins is the chemistry involved in network formation. The epoxy resins (also known as epoxide resins and occasionally as ethoxyline resins) are characterized by the possession of more than one epoxy group per molecule (Figure 3). The three-membered epoxy ring is highly reactive to many substances, particularly with proton donors, so that reactions of the schematic form can occur (Figure 4).

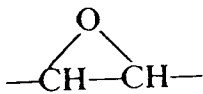


Figure 3.

Epoxy group

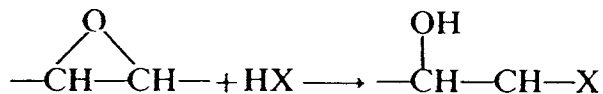
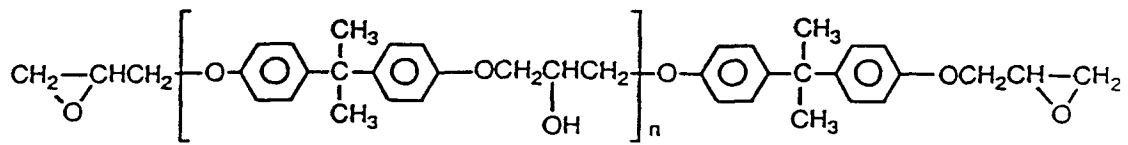


Figure 4.

Schematic form of a typical epoxy reaction.

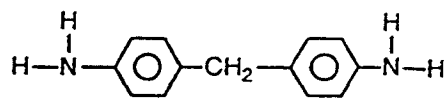
Such reactions allow chain extension and/or crosslinking to occur without elimination of small molecules such as water. As a consequence, these materials exhibit a lower curing shrinkage than many other types of thermosetting plastics. The non-epoxy part of the molecule may be aliphatic, cycloaliphatic, or highly aromatic hydrocarbon or it may be non-hydrocarbon. Similar remarks also apply to the chain extension/cross linking agents so that cross-linked products of great diversity may be obtained. In practice, however, the commercial scene is dominated by the diglycidyl ether of bisphenol A (BPA) and its higher homologs. The glycidyl ethers of various novolac resins are the second most important class of epoxy resins. The glycidyl novolacs are characterized by better elevated-temperature performance than BPA-based resin.

The cross-linking of epoxy resins may be carried out either through the epoxy groups or the hydroxy groups. Three chemical reactions are of major importance to the curing of epoxy composite matrices: the amine/epoxide reaction, the anhydride/epoxide reaction, and the Lewis acid-catalyzed epoxide homopolymerization. The most common curing agents are the amines, in which each of the amino-hydrogens reacts with an epoxide group (Figure 5). Depending on the number of amino hydrogens on the curing agent, their reactivity, the number of epoxide group per resin molecules, and the supporting structures of each, a wide variety of mechanical properties can be obtained and various laminating processes can be used. Chain extension and crosslinking of epoxy resins depend on the reaction of epoxy groups with themselves and with the hydrogen of donor compounds. The reaction may be promoted by heat, by catalysts, or by agents which chemically interact with the epoxide. The rate of cure of the epoxy system is significantly increased by agents such as boron trifluoride complexes, organic sulphides or tertiary amines.



DIFUNCTIONAL

+

TETRAFUNCTIONAL  $f = 4$ 

- ANHYDRIDES,
  - LEWIS ACIDS,
  - 3° AMINES
- ALSO CURE

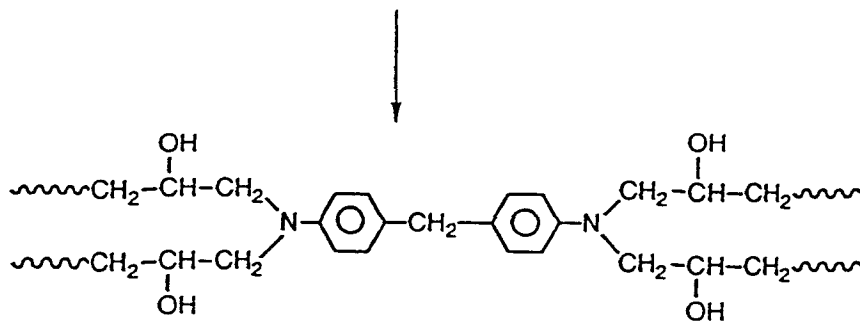


Figure 5.

Network Formation In Epoxy Resin

## 2.2 Reaction Mechanism and Kinetics of Narmco Resin

The Narmco Rigidite 5208 epoxy resin, which was chosen for this study, basically consists of Tetraglycidyl Diamino Diphenyl Methane (TGDDM) and Diamino Diphenyl Sulphone (DDS) curing agent. The third component of the Narmco resin is based on a bisphenol A Novolac. The TGDDM-DDS system is widely used in the manufacture of graphite fiber reinforced structural composites for aerospace application. The chemistry involved in the Narmco curing process is complex. The epoxy amine reaction produces hydroxyl groups which have two effects: (1) they catalyze the reaction which produces them, and (2) they themselves react with epoxy rings to form ether linkages.<sup>6,34,47</sup> Therefore, the reaction mechanism is both a stepwise (epoxide-amine addition) and chain (etherification) polymerization. The sequence of main reactions presented in Figure 6 was suggested in the literature.<sup>5,34,47</sup>

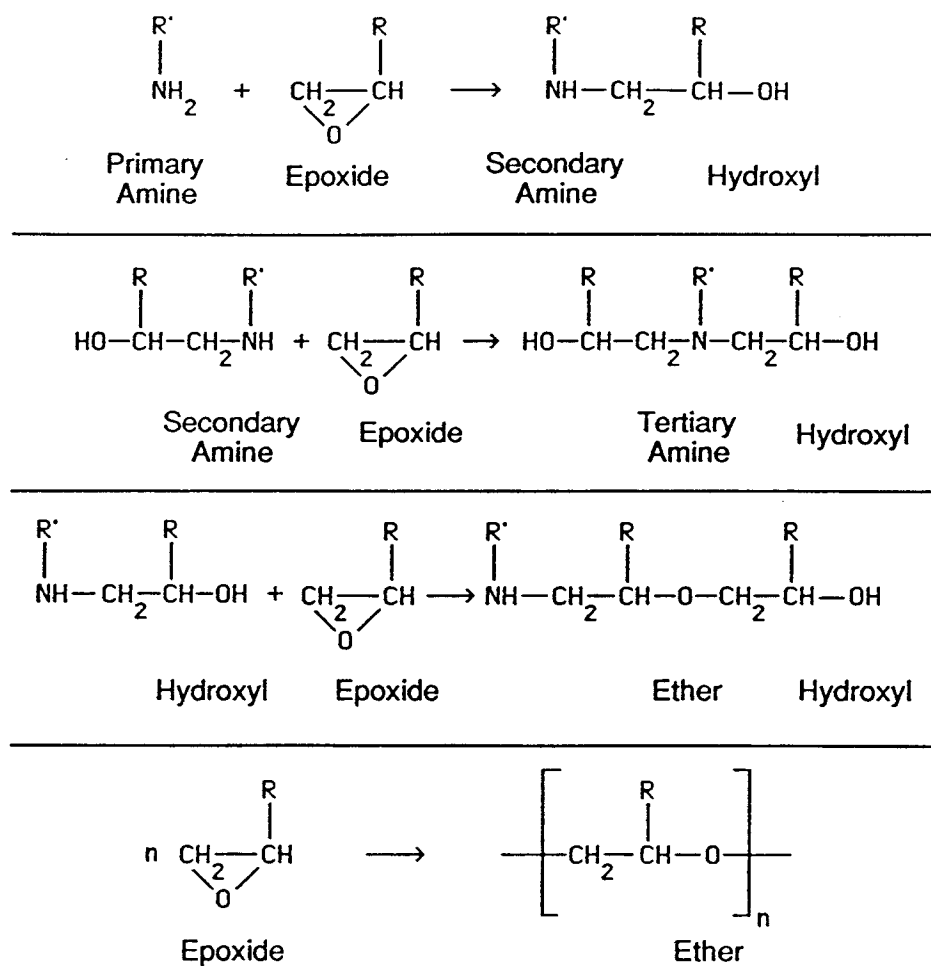


Figure 6.

Main Reactions In The Cure of Narmco Resins

### 3. MODELLING OF KINETICS OF CONVERSION

#### 3.1 Introduction:

The first step for the development of an intelligent system leading to the design optimization and control of the processing of high performance composites is to obtain adequate information about the reaction kinetics of the epoxy matrix. The polymerization of a thermoset polymer generally involves the transition of a fluid resin into a rubber, and then into a solid glass, as a result of the chemical reaction between active groups present in the system, which develop a progressively denser polymeric network. The reaction kinetics of thermoset matrices is strongly dependent on the physical properties characterizing the different stages of the curing process. The dependency is strong near vitrification where a cessation of the reaction is generally observed although the reaction is not complete. The rate of chemical reactions in condensed systems is controlled by the reactivity of functional groups and by their mobility. The reaction rate is controlled by the chemical reactivity of groups according to the mass action law, based on the average concentration of reactive groups and the Arrhenius dependence of the rate constant on temperature. This case is observed if the rate of displacement of the group (diffusion) is much faster than the formation of the chemical bond itself. If, however, the mobility of the medium is reduced, the control by chemical reactivity (kinetic control) is accompanied by control of the reaction rate by diffusion (diffusion control).

The diffusion control may be of two types: (a) specific, when the apparent reactivity depends on the diffusion coefficient of the species (molecules) to which it is attached, and (b) overall, when the mobility of all groups is hindered by the reduced mobility of the medium. The specific diffusion control is typical for fast reactions, such as chain polymerization, whereas, the overall diffusion control is typical for polymer system where in the course of the reaction the system passes into a glassy state. This latter phenomenon is quite common in the curing of epoxy resins, when the glass

transition temperature  $T_g$ , increases so much that it approaches the reaction temperature  $T_{cure}$ . The reaction is known to still continue at  $T_{cure} \leq T_g$ , but the reaction rate decreases considerably until it stops completely. When the reaction is quenched by vitrification, a subsequent exposure to temperature greater than the cure temperature could result in further reaction.<sup>23,27,34,42</sup>

### 3.2 Degree of Cure

The progress of the curing reaction is expressed quantitatively in terms of the fractional degree of conversion of epoxide groups ( $\alpha$ ). Mathematically, it is described with a dimensionless number ranging from zero for an uncured resin to one for a fully cured resin. The degree of conversion varies accordingly to resin kinetics and applied conditions. Initially the resin has a zero degree of conversion meaning none of the resin component (amine and epoxy) has reacted. At the end of a cure cycle, if all component have reacted, the resin has a degree of conversion of one. Since the polymerization reaction of the epoxy system is exothermic the generic degree of conversion is defined as:

$$\alpha = \frac{H_t}{H_{tot}} \quad (1)$$

where  $H_t$  is the heat developed during the reaction between the starting point and a time (t), and  $H_{tot}$  is the total heat developed during the cure.

In a kinetic model, an expression  $\frac{d\alpha}{dt} = f(\alpha, T)$  must be derived where T is a temperature of processing.<sup>2,16,47</sup>

### 3.3 Review of Existing Models

The most common and one of the simplest models corresponds to an empirical n-th order of reaction, first proposed for epoxy resins by Kenny and Apicella.<sup>40</sup>

$$\frac{d\alpha}{dt} = K(1 - \alpha)^n \quad (2)$$

where K is the temperature-dependent kinetic constant (Arrhenius Equation),

$$K = A \exp \frac{-\Delta E_i}{RT} \quad (3)$$

n is the reaction order, and  $\alpha$  is the degree of conversion.

This simple approach does not reflect an autocatalytic character of conversion and it does not account for the diffusion controlled phenomena.

Assuming that the reactivity towards epoxy groups is the same for the primary amine groups initially present and for the secondary amine groups formed during the reaction, Horie<sup>37</sup> has proposed the following equation:

$$\frac{d\alpha}{dt} = (K_1 + K_2\alpha)(1 - \alpha)(B - \alpha) \quad (4)$$

where  $K_1$  is a rate constant for the reaction catalyzed by groups initially present in the resin,  $K_2$  is a rate constant for the reaction catalyzed by newly-formed hydroxyl group, and B is the initial ratio of amine N-H bonds to epoxide rings. This equation takes into account the autocatalytic character of the epoxy-amine reaction but it does not account for the possibility of an etherification reaction.

For the epoxy-amine system with a significant excess of epoxy with respect to amine and for a system containing aromatic amines, where etherification reaction is important, the Horie equation is not adequate. The diffusion control is not included in the reaction.

Kamal<sup>38,39</sup> has proposed a semi-empirical equation:

$$\frac{d\alpha}{dt} = (K_1 + K_2\alpha^m)(1 - \alpha)^n \quad (5)$$

The model includes an element responsible for an autocatalytic behavior of epoxy systems and the equation provides a good fit to experimental data by introducing the variable  $m$  and  $n$  exponents, but it does not provide a description of the chemistry of the curing process. Additionally, the  $m, n$ , exponents are temperature-dependent (according to Arrhenius) and this dependency must be determined.

Springer and Loos<sup>43</sup> have proposed two different patterns of behavior for the  $\alpha$  divided by a critical value of  $\alpha = 0.3$ .

$$\frac{d\alpha}{dt} = (K_1 + K_2\alpha)(1 - \alpha)(\beta - \alpha) \quad (6)$$

$$\frac{d\alpha}{dt} = K_3(1 - \alpha)$$

It is assumed that in the beginning ( $\alpha < 0.3$ ) the epoxide-amine reaction is prevailing and must be considered. When the epoxide-amine reaction is completed, the epoxide hydroxyl reaction takes over, and the reaction is assumed to be of first order. This equation gives a reasonably good fit to the experimental data but again it does not provide a description of the network formation.

Sanford and McCullough<sup>61</sup> have proposed a more advanced model for the epoxy-amine cure reaction. They assumed a stoichiometric mixture of epoxy-amine, and described the autocatalytic reaction by:

$$\frac{d\alpha}{dt} = \{K_1 + K_2(1 - \alpha)\}\alpha^2 \quad (7)$$

where  $K_1$  and  $K_2$  have an Arrhenius temperature dependence.

The equation describes correctly the early stages of the cure. As the cure progresses and the resin crosslinks, the glass transition temperature  $T_g$  of the system rises. When it approaches the curing temperature, the resin passes from a rubbery to a glassy state, the mobility of the reactivity group is hindered, and the reaction is controlled by diffusion rather than by chemical factors. If Equation 7 was to remain correct also for advanced stages, the diffusional effect must be incorporated into it. Following the approach of Huguenin and Klein<sup>61</sup>, the reaction rate may be modified via the Rabinowitch equation yielding:

$$K_i = \frac{A_i \exp\left(-\frac{E_a}{RT}\right)}{1 + \left(\frac{\delta}{D}\right) \exp\left(-\frac{E_a}{RT}\right)} \quad (8)$$

where  $D$  is diffusivity,  $\delta$  essentially includes the vibration frequency and geometric factor,  $E_a$  is the activation energy in the Arrhenius equation, and  $A_i$  is the frequency factor in the Arrhenius equation.

The diffusivity  $D$  is a function of temperature, as well as  $\alpha$ , and may be described by free-volume theory. Using Macedo and Litovitz approach<sup>61</sup>, which accounts for both, the activation and segmental mobility, the diffusivity may be expressed as:

$$D = D_0 \exp\left(-\frac{E_d}{RT}\right) \exp\left(-\frac{b_d}{f}\right) \quad (9)$$

where  $D_0$  is a constant,  $E_d$  is an activation energy of diffusivity,  $b_d$  is a constant accounting for critical free volume for motion, and  $f$  is a fractional free-volume.

Combining Equations 7, 8 and 9:

$$\begin{aligned} \frac{d\alpha}{dt} = & \left[ \frac{A_1 \exp\left(-\frac{E_{a1}}{RT}\right)}{1 + \left(\frac{\delta}{D_0}\right) \exp\left(-\frac{E_d}{RT}\right) \exp\left(-\frac{b_d}{f}\right) \exp\left(-\frac{E_{a1}}{RT}\right)} + \right. \\ & \left. + \frac{A_2 \exp\left(-\frac{E_{a2}}{RT}\right) (1 - \alpha)}{1 + \left(\frac{\delta}{D_0}\right) \exp\left(-\frac{E_d}{RT}\right) \exp\left(-\frac{b_d}{f}\right) \exp\left(-\frac{E_{a2}}{RT}\right)} \right] \alpha^2 \quad (10) \end{aligned}$$

It should be noted that the fractional free volume ( $f$ ) in Equation 9 and 10 is a function of an actual temperature and the glass transition temperature of a material and is therefore also a function of  $\alpha$ .

$$f = f_g + a_f(T - T_g) \quad (11)$$

where  $f_g$  is a fractional free volume at  $T_g$ ,  $a_f$  is a thermal expansion coefficient of the free volume, and  $T_g$  is a glass transition temperature described by the DiBenedetto equation.

If Equation 11 is substituted into Equation 9:

$$D = D_o \exp\left(-\frac{E_d}{RT}\right) \exp\left(-\frac{b_d}{\{f_g + \alpha_f[T - Tg(\alpha)]\}}\right) \quad (12)$$

A new mechanistic approach to modelling the cure kinetics of epoxy-amine thermosetting resins was recently (1991) proposed by Cole.<sup>15,16</sup> The model is based on the model proposed by Horie, but it takes into account both the epoxide-amine reactions and the subsequent etherification reaction [Figure 6]. The kinetics is completely described by three rate constants of the Arrhenius type. The effect of the diffusion control is included and described by a simple equation. The model provides an excellent prediction of the degree of conversion over the whole range of cure (160°C-200°C) without introducing empirical parameters or making approximations such as separating the reaction into distinct regimes. The constants were derived specifically for the Narmco 5208 epoxy-amine system.

The basic assumptions inherent in the model are: (1) the epoxide-amine reactions are hydroxyl-catalyzed, (2) the secondary amine groups have the same reactivity with respect to epoxide as the primary amine groups, (3) the etherification reaction is first order with respect to epoxide concentration, and may also involve hydroxyl groups, tertiary amine groups, or both. The progress of the polymerization is described in terms of two parameters  $\alpha$  and  $\beta$ . The first ( $\alpha$ ) is the overall degree of conversion as expressed in terms of the fraction of epoxide groups reacted. The second ( $\beta$ ) is the fraction of amine N-H bonds which have reacted.<sup>15,16</sup>

$$\frac{d\beta}{dt} = [(K_1 + BK_2\beta)(1 - \beta)] \cdot (1 - \alpha) \cdot f(\alpha, T) \quad (13)$$

$$\frac{d\alpha}{dt} = [B(K_1 + BK_2\beta)(1 - \beta) + K_3\beta^3] \cdot (1 - \alpha) \cdot f(\alpha, T) \quad (14)$$

The diffusion control factor  $f(\alpha, T)$  is given by:

$$f(\alpha, T) = [1 + \exp(30.1\alpha + 4.06 - 0.1617T)]^{-1} \quad (15)$$

The diffusion control factor  $f(\alpha, T)$  was based on a semi-empirical relationship based on free volume considerations. When the degree of cure reaches the critical value  $\alpha_c$ , diffusion control takes over and the diffusion-controlled rate constant  $k_d$  is given by:

$$K_d = K_c \exp[-C(\alpha - \alpha_c)] \quad (16)$$

where  $k_c$  is the rate constant for chemical kinetics, and C is a constant.

The equation corresponds to a rather sudden onset of diffusion control at  $\alpha = \alpha_c$ . In reality, the onset is gradual and there is a region where both chemical and diffusional control are significant. According to Rabinowitch, the overall effective rate constant  $K_e$  can be expressed:

$$\frac{1}{K_e} = \frac{1}{K_d} + \frac{1}{K_c} \quad (17)$$

Combining Equation 16 and Equation 17, the diffusion control factor  $f(\alpha)$  can be defined:

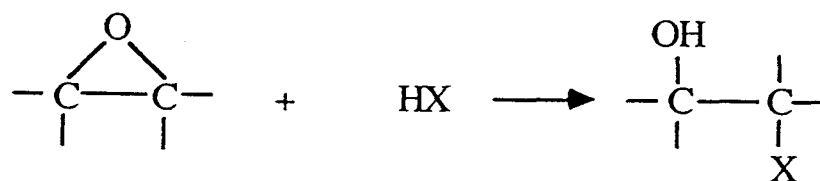
$$f(\alpha) = \frac{K_e}{K_c} = \frac{1}{1 + \exp[C(\alpha - \alpha_c)]} \quad (18)$$

The effective reaction rate is equal to the chemical reaction rate multiplied by the diffusion factor. For values of  $\alpha$  significantly lower than  $\alpha_c$ ,  $f(\alpha)$  is approximately equal to 1 and diffusion control is negligible. When  $\alpha$  approaches  $\alpha_c$ ,  $f(\alpha)$  begins to decrease, reaching 0.5 when  $\alpha = \alpha_c$ . Beyond this point it continues to decrease, eventually approaching zero, so that the reaction becomes very slow and finally stops.<sup>15,16</sup>

### 3.4 Conversion of Epoxide Groups

In order to compare empirically determined parameters in the kinetic modelling, it is necessary to accurately measure the conversion of functional groups. Three methods may be used for following the extent of reaction in an epoxide-amine system: titration, infra-red spectroscopy, and thermal analysis.

The classical method for monitoring the extent of reaction in epoxy-amine system is chemical titration. The most commonly used titration technique is based on the addition of a hydrogen halide to the epoxide group<sup>6</sup>



The difference between the amount of acid added and the amount unconsumed determined by back titration with standard base, is a measure of the epoxy content.

Infra-red spectroscopy has also been used to analyze the conversion of epoxy resin with amine. The method is based on the fact that change in the IR absorbance band at a frequency associated with a certain functional group are related to changes in the concentration of that particular group in the sample. The infra-red spectroscopy technique for monitoring the extent of reaction has several advantages. The disappearance and formation of all the types of functional groups which occur during the cure reaction can be monitored. It is also possible to determine conversion for samples

in the pre- and post-gel regions. However, there are limitations involving the application of infra-red spectroscopy to quantitative analysis . One of the primary difficulties associated with this method concerns the complexity of the IR spectra and the sensitivity of the equipment, which enhance the probability of the overlap of absorbance peaks. Severe inaccuracies in the determination of the degree of cure can result by overlap of new bands which appears during the reaction.<sup>6,17</sup>

Differential Scanning Calorimetry (DSC) is the third, and probably the best, method which can be used to determine the extent of reaction in thermosetting systems. It measures the rate of enthalpy change as a sample is cured. It is assumed that the heat evolved during the reaction is proportional to the conversion of functional group [Equation 1]. Equation 1 assumes that the extent of the reaction at the end of the cure cycle is 100%. Ideally,  $H_{tot}$  is equal to the heat corresponding to the total conversion of all reactive groups. Equation 1 also assumes that a single type of reaction occurs during the cure or that the heat evolved during different reactions is the same.<sup>17</sup>

### 3.5 Experimental Verification of Cole's Model

The Narmco 5208 resin used in this study was provided compliments of Canadair Inc. The resin was in the form of a partially polymerized film. The actual initial degree of polymerization ( $\alpha_0$ ) in the received sample was 0.03, according to Narmco Inc.

The applicability of Cole's model to the above resin system was verified in the experimental portion of the work. The experimental process utilized to perform such a verification was conducted on a Differential Scanning Calorimeter (Du Pont 2910 module) under the conditions of nitrogen environment in accordance with the following procedural guidelines. The verification included both isothermal and non-isothermal tests. Isothermal DSC tests were performed to eliminate the eventual dependency on temperature of two types of reactions with different rates, occurring simultaneously during the cure of TGDDM-DDS system.

Approximately 10 mg samples of the material in question were placed in unsealed aluminum pans. The basic calibration process was conducted accordingly to the instrument operating manual. Isothermal runs were performed at three different temperature; 130°C, 170°C, and 190°C. The experimental results of these tests are visually depicted in Figures 7-10.

In the dynamic mode the samples were heated from room temperatures to 300°C and two heating rates 3°/min and 5°/min were used to obtain the results shown in Figure 10 and 11. In the dynamic mode, the accuracy of the results was additionally verified by introducing an extra procedure. Following the basic experiments each sample was heated for a short time interval at 300°C to assure a complete cure reaction. The sample was then cooled within the equipment and re-heated again at

the same heating conditions. The DSC record obtained during the re-heating contains nothing but that characteristic of the equipment and could be used as a calibration curve for a main experiment (Figure 12).

### 3.6 Results and Discussion

On the basis of Cole's kinetic model a computer program was developed which numerically integrates the rate of conversion as a function of time for a given temperature history.

The examples of the DSC records, plotted against the ones predicted from the model are presented in the Figures 13-16.

An excellent agreement between results predicted from Cole's model (smooth lines) and the experimental data (lines marked with circles) can be found. In the case of dynamic heating with the rate  $5^{\circ}\text{C}/\text{min}$  [Figure 16] there is virtually no difference between the predicted curve and the experimental data up to a temperature of  $210^{\circ}\text{C}$ .

Small differences are observed for a low temperature isothermal test ( $130^{\circ}\text{C}$ ) and for dynamic tests for temperature exceeding  $200^{\circ}\text{C}$ . It should be remembered, however, that the validity of the model was defined by Cole as  $140^{\circ}\text{C}$ - $190^{\circ}\text{C}$ . At  $130^{\circ}\text{C}$  the rate of the reaction is very slow and the sensitivity of the equipment is not sufficient to draw any conclusion.

### 3.7 Contribution of the Author

The authors own contribution within Chapter 3 consists of:

- (1) Development of a computer program for Cole's model of kinetics of conversion.
- (2) Verification of Cole's model, using the DSC technique.

Neither of the mentioned tasks contain an element of originality; Cole's model has been presented<sup>15,16</sup> as a complete package, including all related constants, and the DSC is a technique routinely applied for investigation of the kinetics of thermoset conversion.<sup>17</sup> The computer program of the kinetics model developed by the author employs the commonly used method of numerical integration. Using an assumed temperature history the code calculates and integrates the rate of conversion for consecutive time increments, producing a history of conversion as an output.

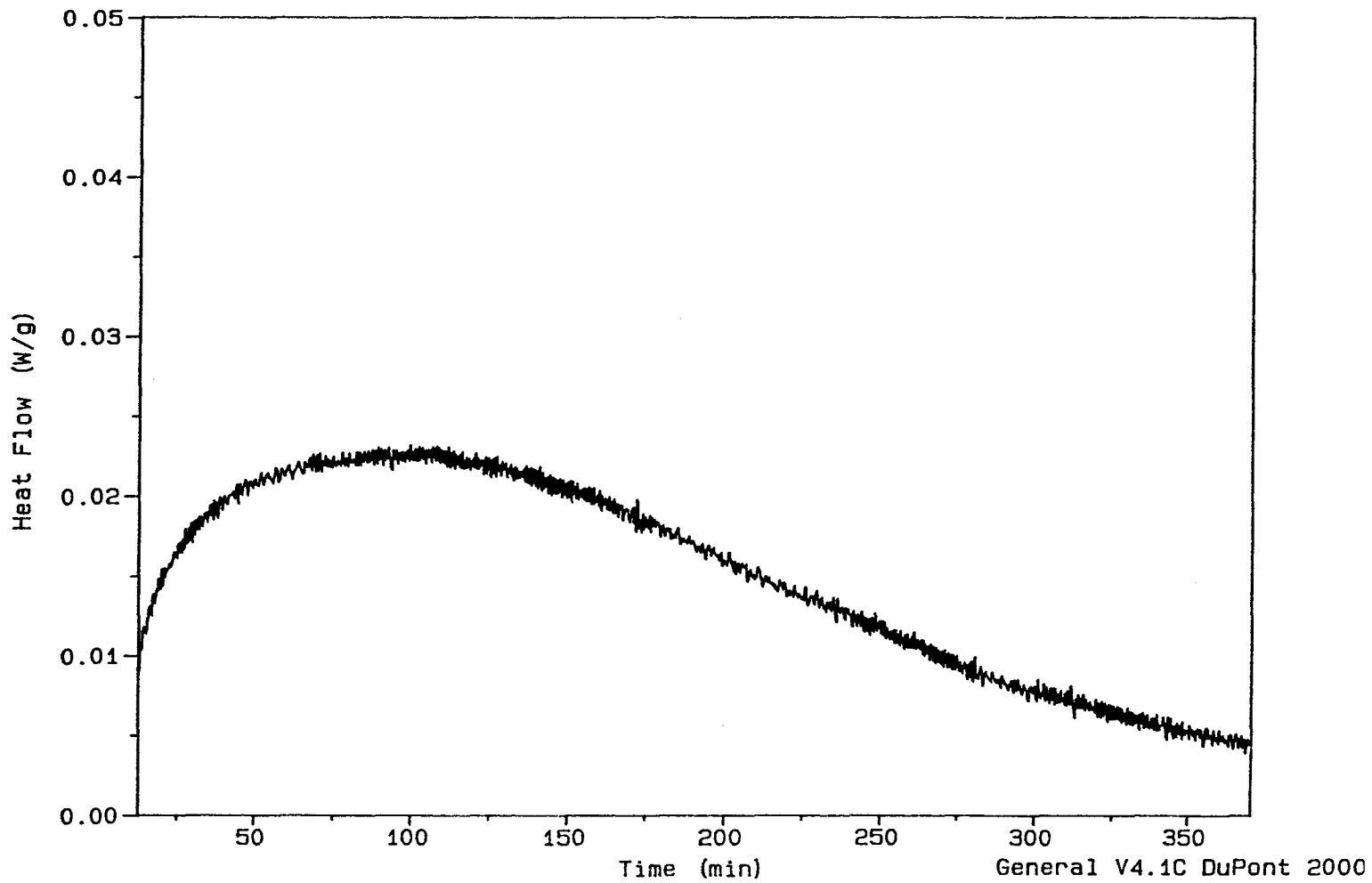
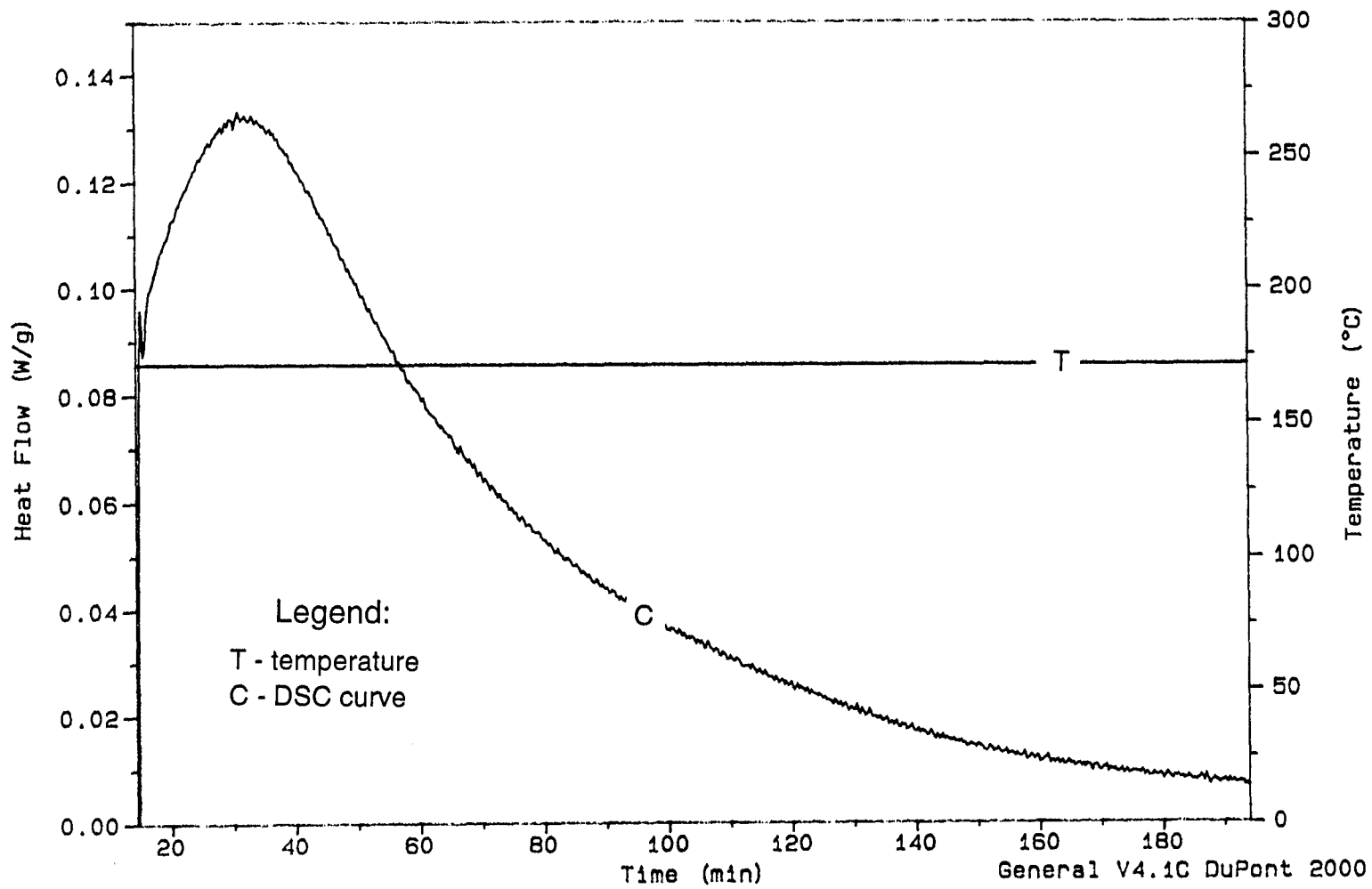


Figure 7.  
Isothermal DSC curve obtained at temperature 130 °C.

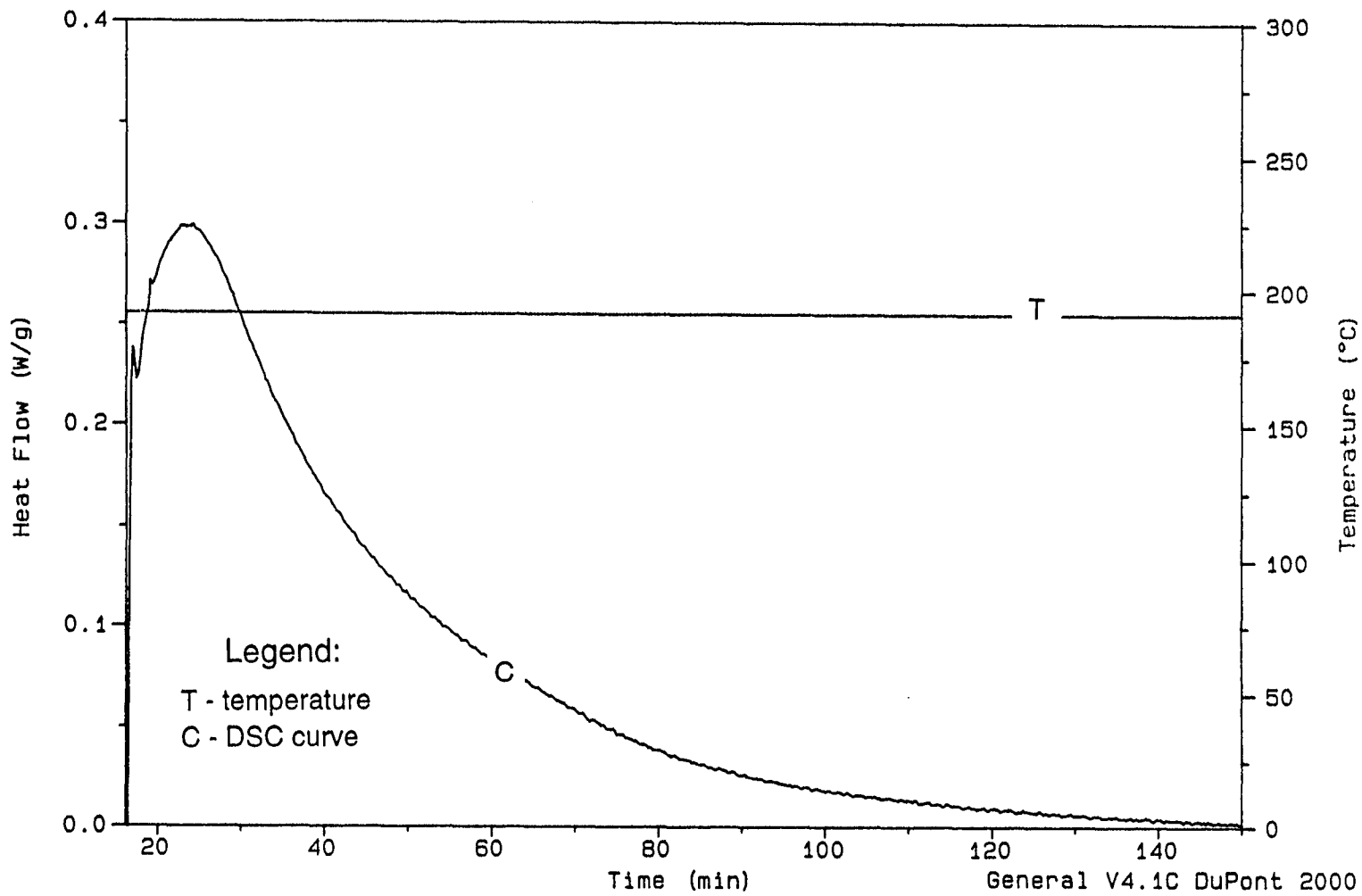
Isothermal DSC curve obtained at temperature 170°C.

Figure 8.



Isothermal DSC curve obtained at temperature 190°C.

Figure 9.



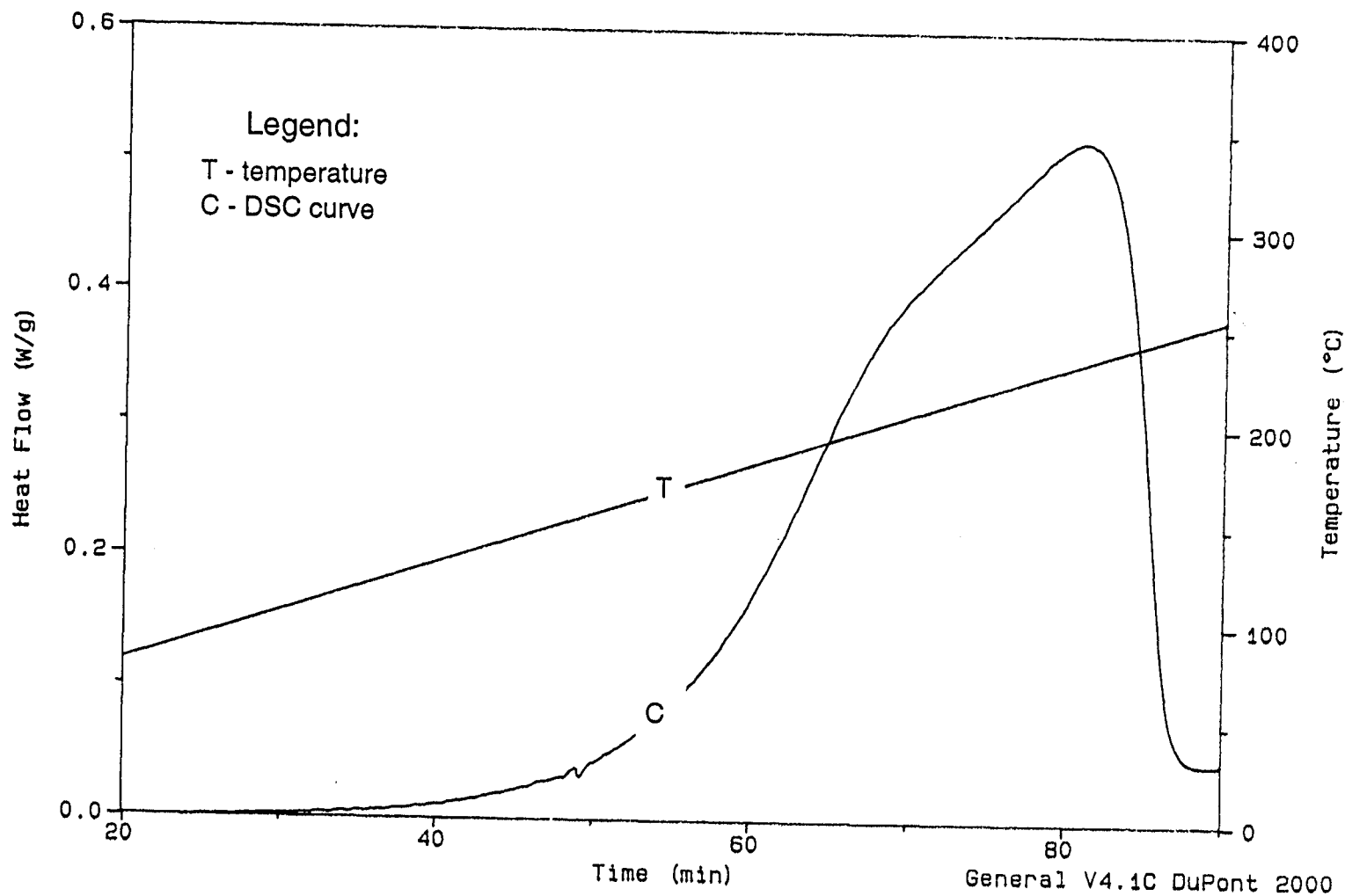


Figure 10.  
Dynamic DSC curve obtained at heating rate 3°/min.

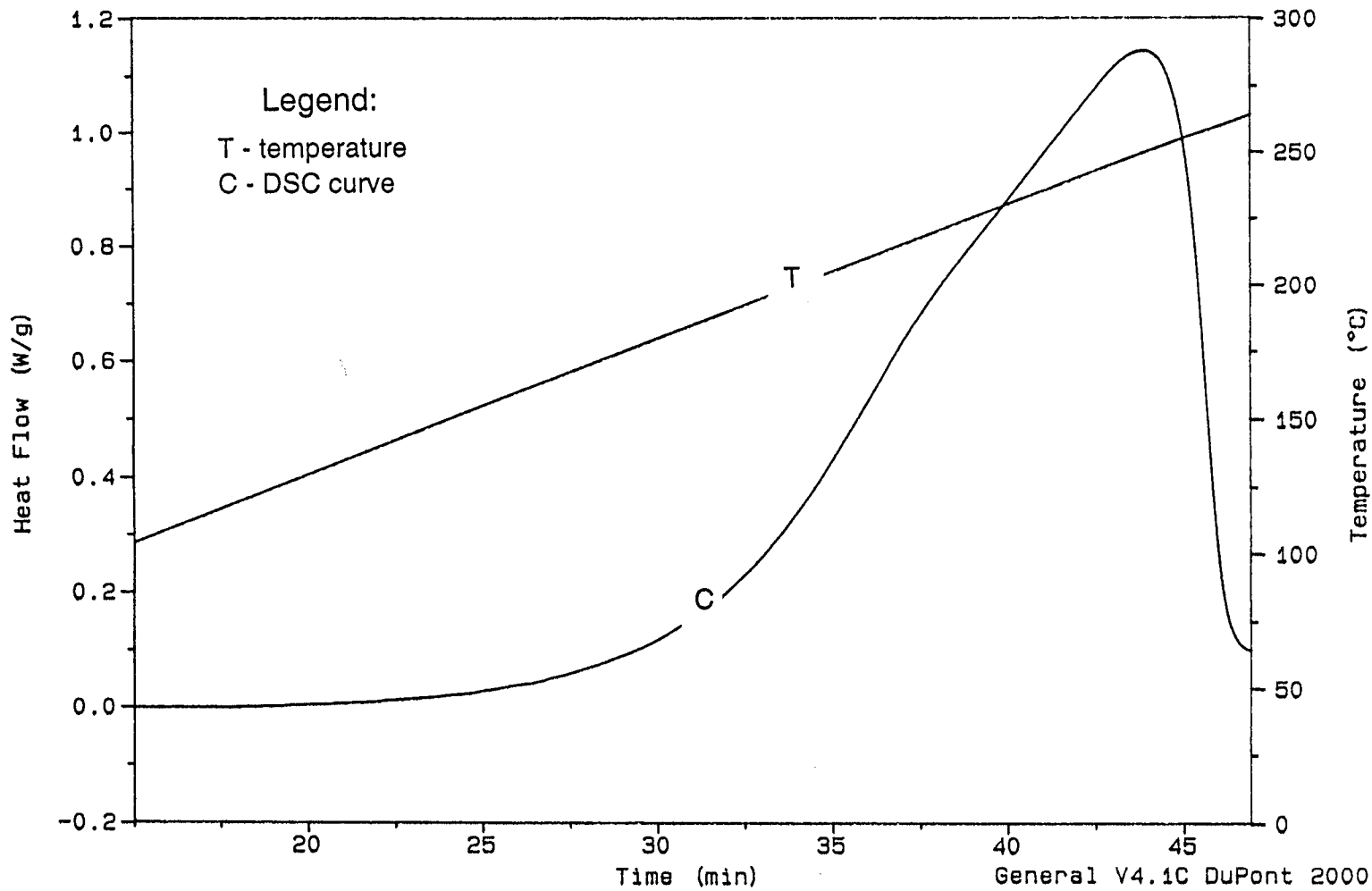


Figure 11.  
Dynamic DSC curve obtained at heating rate 5°/min.

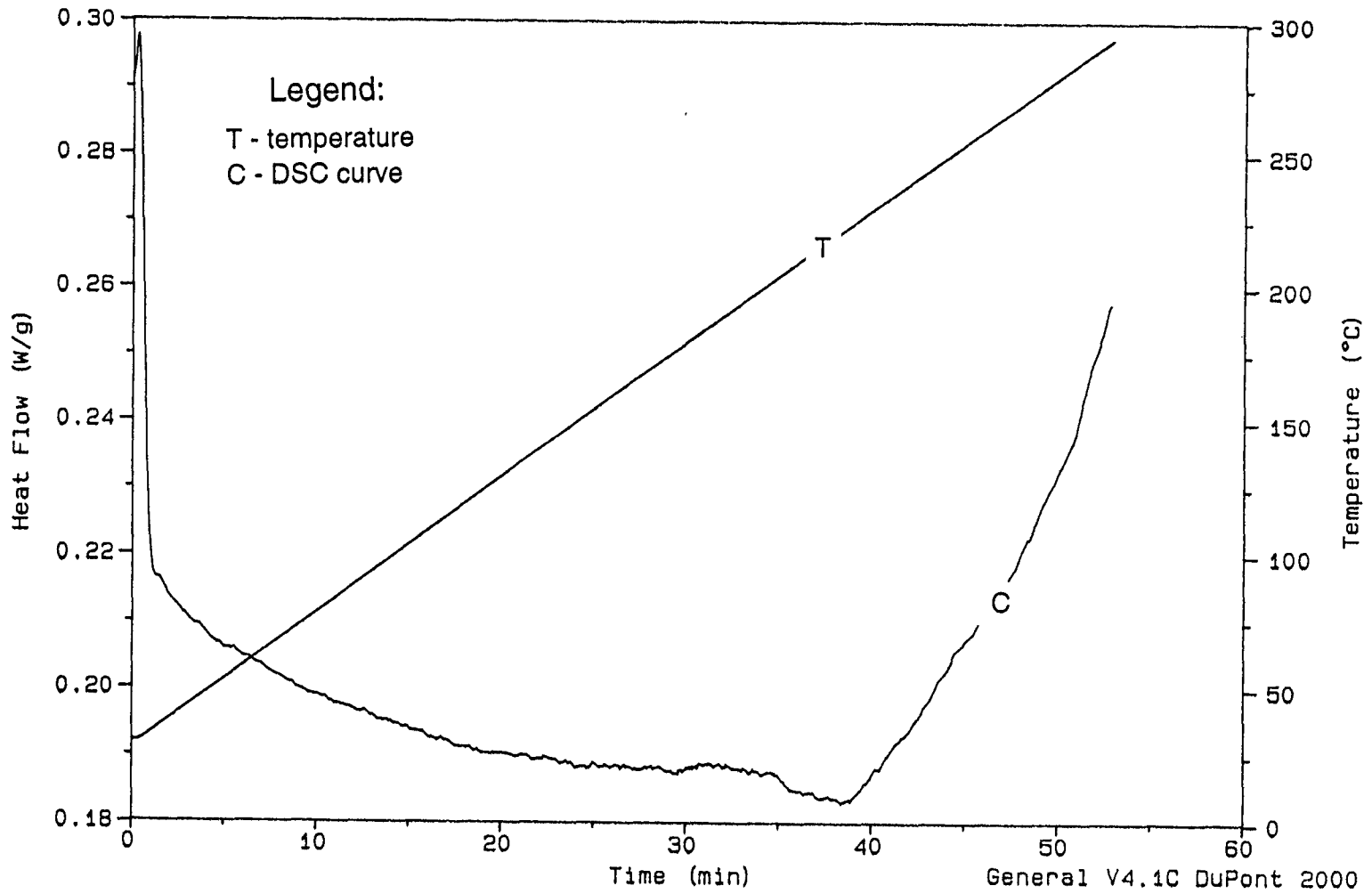


Figure 12.  
Calibration Curve for Dynamic Tests

## RATE OF CONVERSION

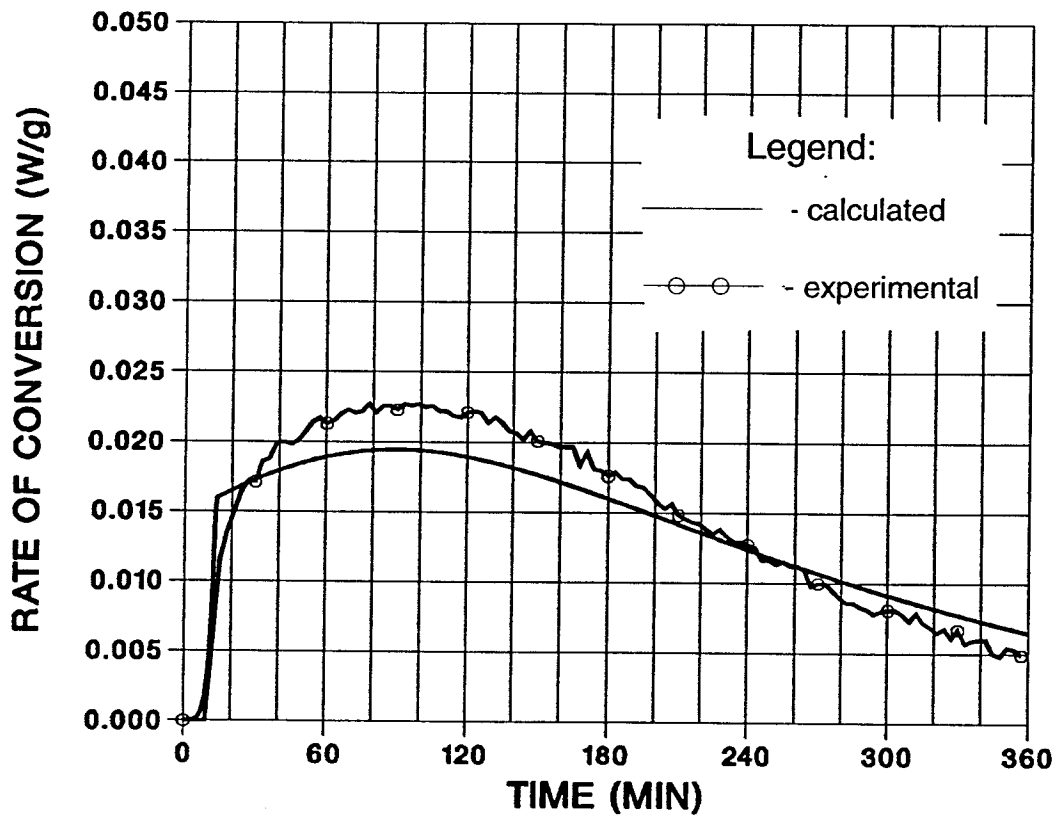


Figure 13.

Verification of conversion kinetic model.

Isothermal 130°C.

## RATE OF CONVERSION

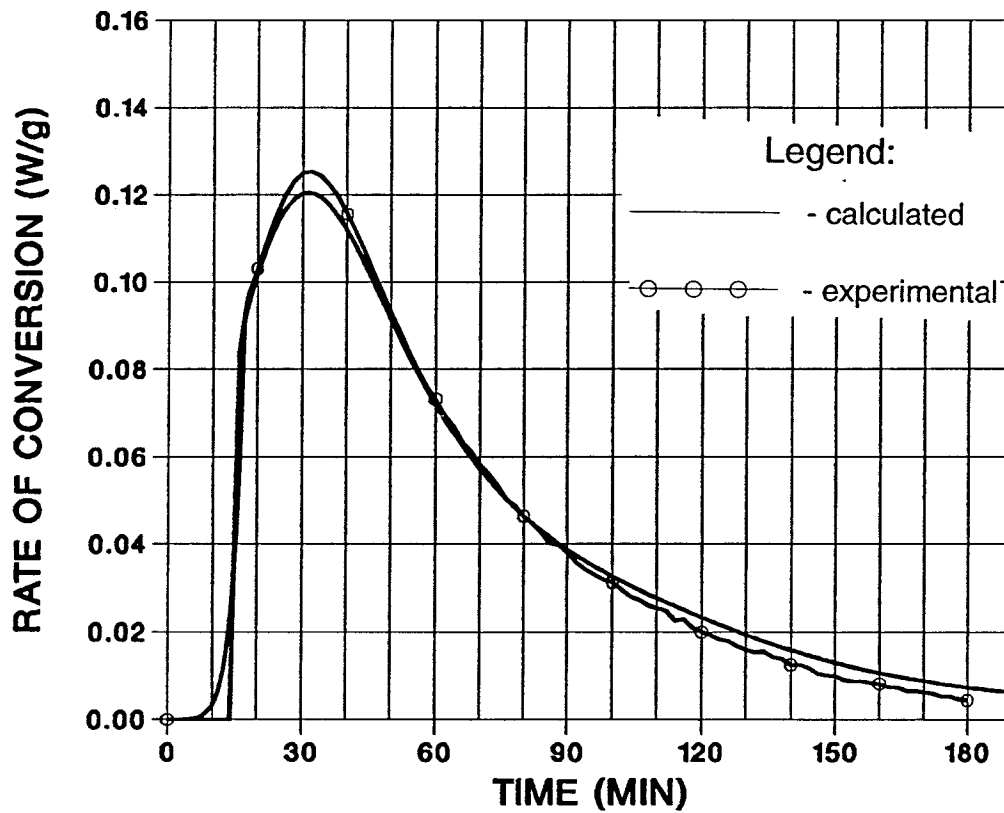


Figure 14.  
Verification of conversion kinetic model.  
Isothermal 170°C.

## RATE OF CONVERSION

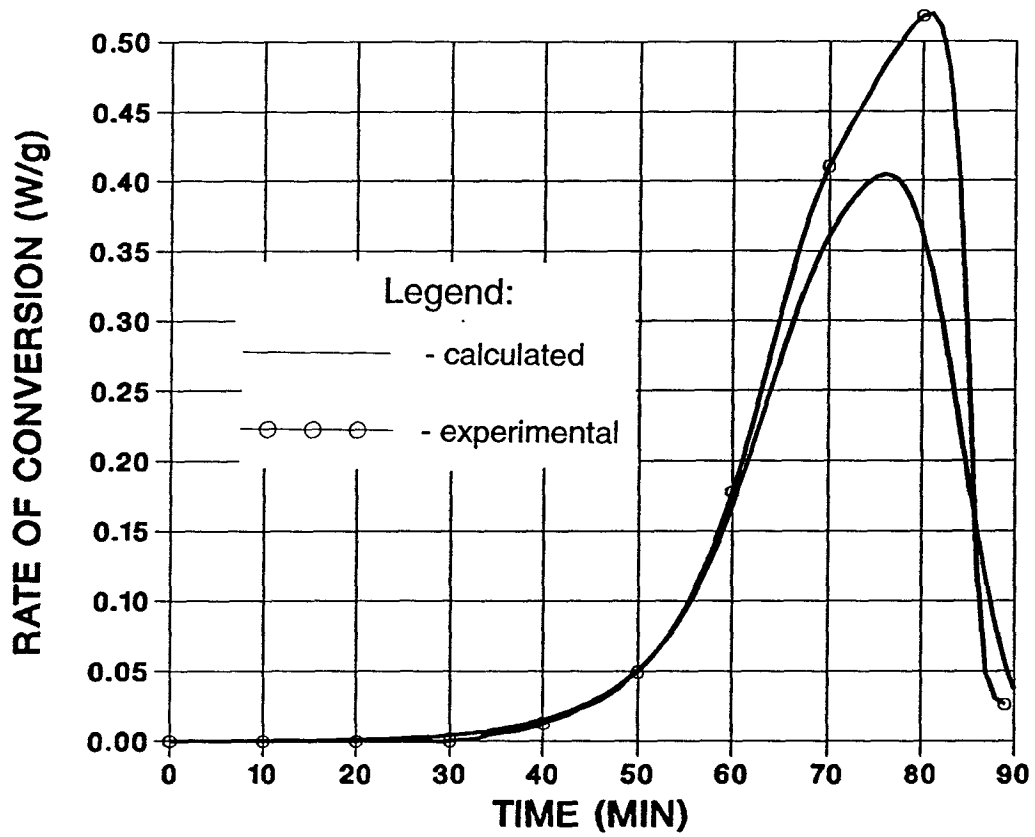


Figure 15.

Verification of conversion kinetic model.

Dynamic 3°/min.

## RATE OF CONVERSION

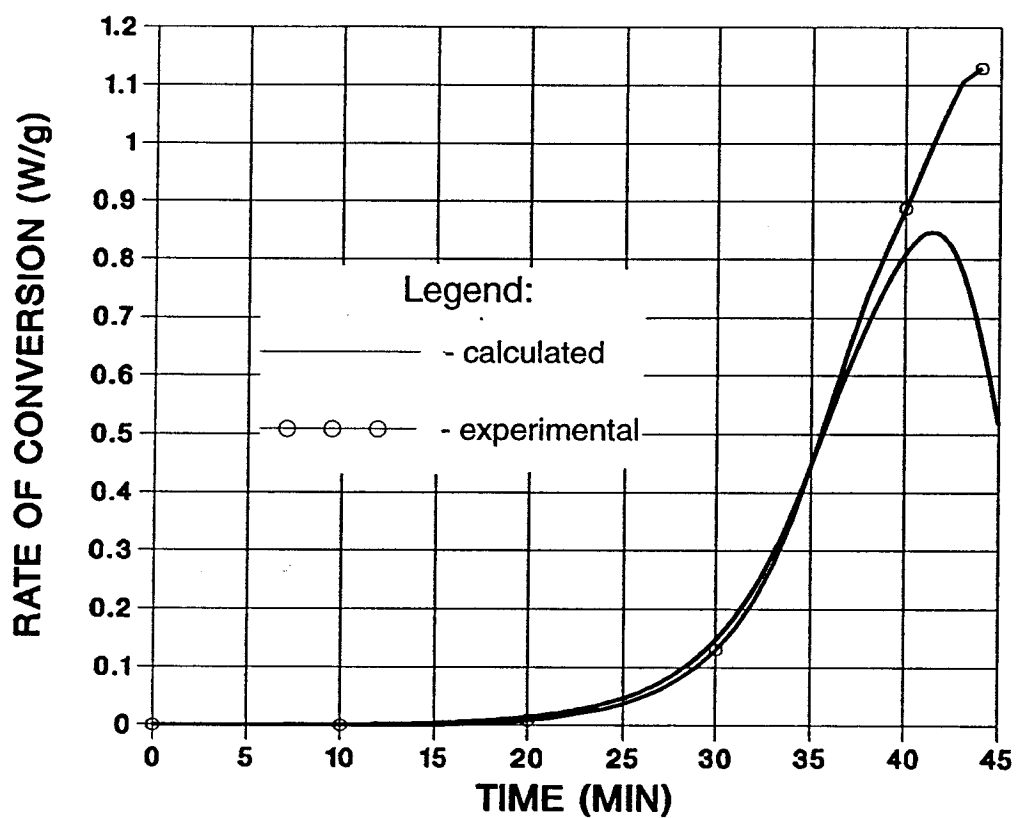


Figure 16.

Verification of conversion kinetic model.

Dynamic 5°/min.

## 4. CHEMORHEOLOGICAL CHANGES DURING CURE

### 4.1 Theory

Despite the widespread use of polymer composite materials there are still many technical problems to be solved. One of the major issues is processing of high performance thermoset composites with improved material quality and reliability. Today's choice of processing parameters is primarily based on extensive testing. This approach is not only costly but additionally, if the prepreg material or geometry of the parts is changed, the testing results are usually not applicable. Instead, a scientific approach can be used which is based on an understanding of the fundamental chemical and physical events characterizing the behavior of the composite during processing. This approach allows for a better choice of processing conditions and decreases the experimental work needed to determine the proper cure cycle. From a material point of view, not only chemistry but also the processing conditions should be selected to give the most uniform and reliable cure obtained in the shortest possible time. The characteristics of the curing process and the final properties are strongly dependent upon the chemorheological properties.<sup>2,4,14,41,60</sup>

The knowledge of the chemorheological characteristics is extremely important in the fabrication of advanced polymeric composites which requires precise resin cure control. This part of the work is focussed on the principal rheological phenomena governing the behavior of thermosets during their processing.<sup>31,45,55</sup>

Generally, the processing of thermoset matrix composites (curing process) involves a transition of the polymer from the liquid to the solid state as illustrated in Figure 17<sup>6</sup>. In the case of an epoxy

matrix a liquid consists of epoxy oligomers, a curing agent and often catalysts. The cure begins as a consequence of stepwise polymerization with simultaneous linear growth and branching of the chain. Whether branching or linear growth occurs faster depends on the relative rate of the epoxide with the primary or secondary amine hydrogens. As the reaction proceeds, the molecular weight increases rapidly, and eventually several chains become linked together into a network of semi-infinite molecular weight. The sudden and irreversible transformation from viscous liquid to an insoluble gel is known as the gel point. At the gelation point, small molecules are also present and often the majority of the reactive groups are still unreacted. Gelation does not inhibit the curing process; after gelation the reaction proceeds towards the formation of one infinite network with a substantial increase in cross-linking density, stiffness, glass transition temperature, and ultimate physical properties. The volume contraction which occurs during the cure is a result of the exchange of Van der Waals bonds for shorter covalent bonds. Because of increased molecular crowding the glass temperature is elevated.<sup>24,32,34,41</sup>

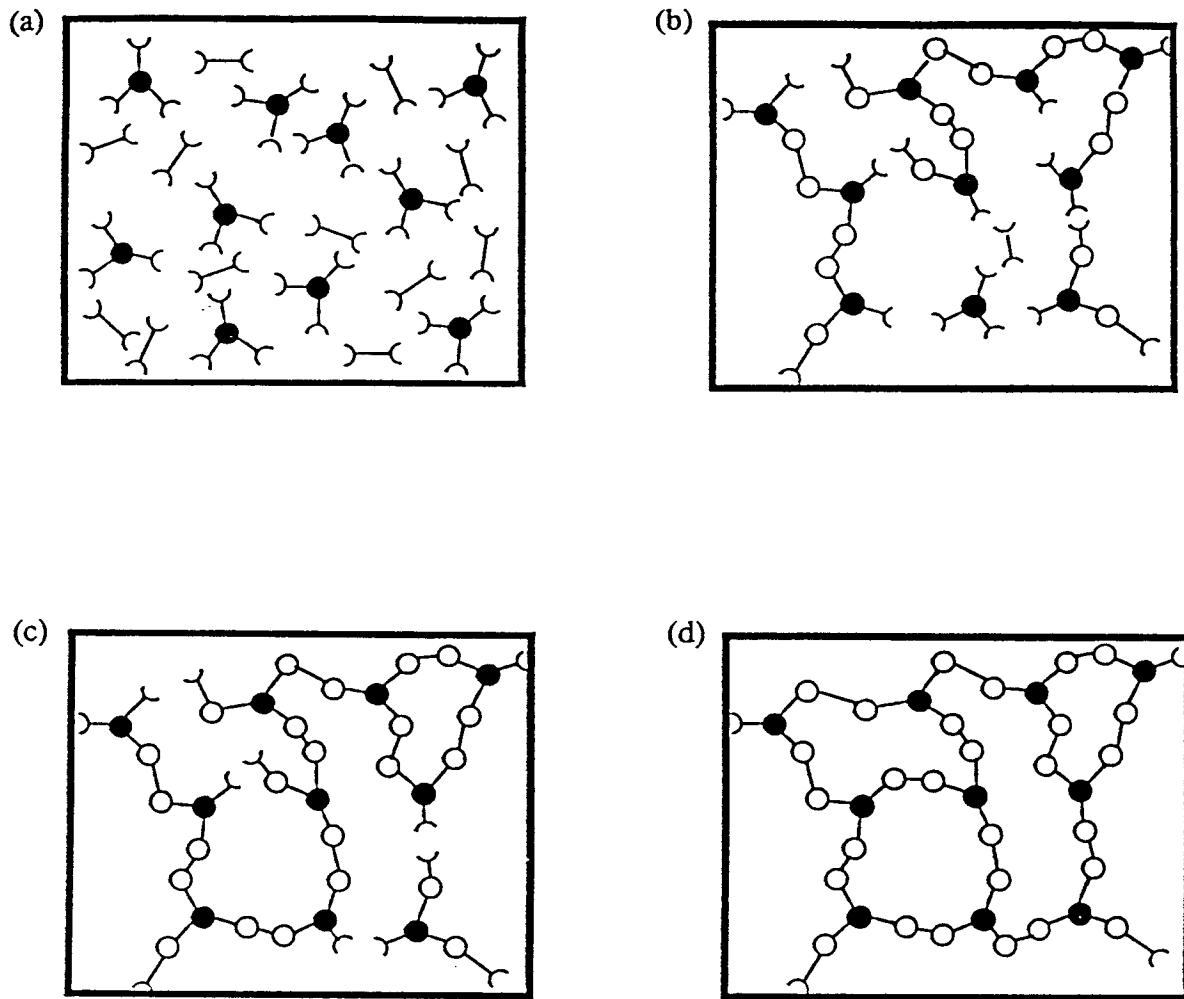


Figure 17.

Schematic representation of the cure of a thermoset, starting with monomers (a), proceeding via simultaneous linear growth and branching below the gel point (b), continuing with formation of a gelled but incompletely crosslinked network (c), and finally a fully cured thermoset (d).

#### 4.1.1 Viscosity

For many simple fluids, the study of rheology involves the measurement of viscosity only. For such fluids, the viscosity depends basically upon the temperature and hydrostatic pressure. However, the rheology of polymers is more complex because polymeric fluids do not show ideal behavior and their rheological properties depend upon the rate of shear, the molecular weight and structure of the polymer, the concentration of additives, and the temperature.<sup>50,66</sup>

For ideal, Newtonian fluids :

$$\text{Viscosity}(\eta) = \frac{\text{Shear stress}}{\text{Rate of shear strain}} = \frac{\tau}{\frac{d\gamma}{dt}} = \frac{\tau}{\dot{\gamma}} \quad (19)$$

If the fluid is not Newtonian, a plot of shear stress  $\tau$ , against the rate of shear  $\dot{\gamma}$ , is not a straight line but a curve, such as the solid line shown in Figure 18. The liquid may be Newtonian at very low shear rates to give a limiting viscosity  $\eta_0$  from the initial slope of the  $\tau$  versus  $\dot{\gamma}$  curve. When the  $\tau - \dot{\gamma}$  curve is not linear, the viscosity may be defined in two ways for any given rate of shear as illustrated in Figure 18<sup>50</sup>. The apparent viscosity  $\eta_a$ , is the slope of the secant line from the original to the shear stress at the given value of shear rate, that is,

$$\eta_a = \frac{\tau}{\dot{\gamma}} \quad (20)$$

The slope of the line at the chosen value of  $\dot{\gamma}$  is another viscosity called the consistency  $\eta_c$ .

$$\eta_c = \frac{d\tau}{d\dot{\gamma}} \quad (21)$$

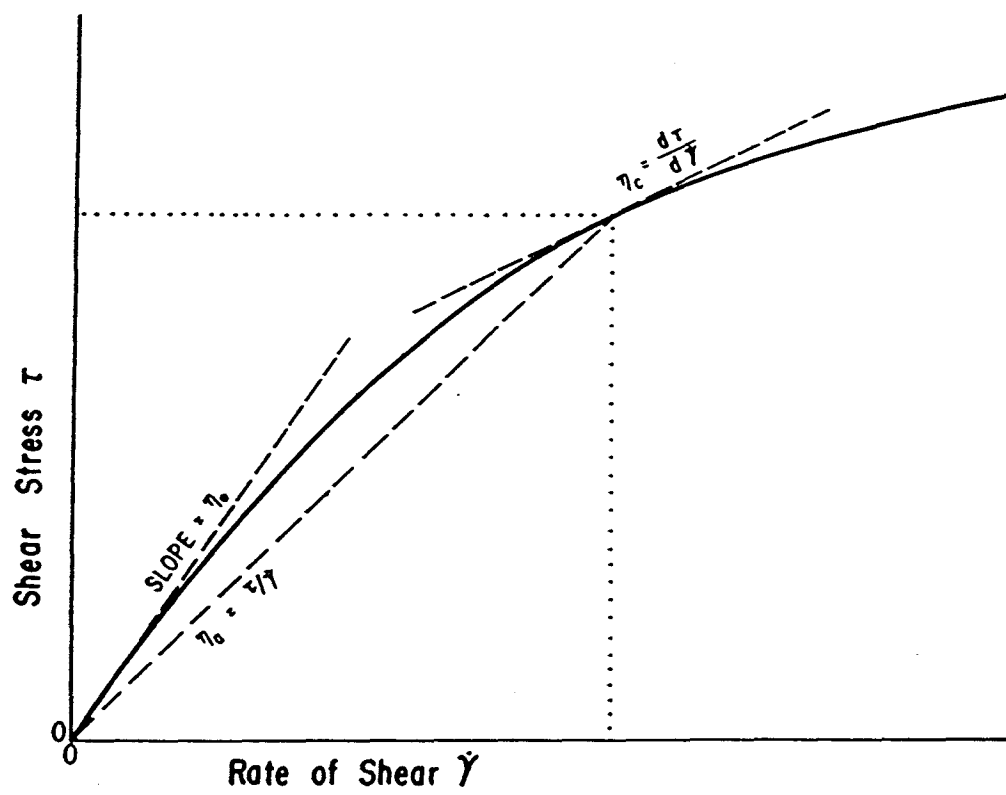


Figure 18.  
Measurement of viscosity

In the cases where the relative velocity of shearing plates is not constant but varies in a sinusoidal manner, a complex viscosity  $\eta^*$ , is measured. The complex viscosity contains an elastic component in addition to a term similar to the ordinary steady state viscosity. The complex viscosity is defined by:

$$\eta^* = \eta' - i\eta'' \quad (22)$$

The dynamic viscosity  $\eta'$ , is related to the steady state viscosity and is the part of the complex viscosity that measures the rate of energy dissipation. The real component of viscosity  $\eta'$ , measures the dissipation of energy and is related to the loss modulus  $G''$ , by:

$$G'' = \omega\eta' \quad (23)$$

The imaginary viscosity  $\eta''$ , measures the elasticity or stored energy and is related to the storage modulus  $G'$ , by<sup>50</sup>:

$$G' = \omega\eta'' \quad (24)$$

where  $\omega$  is the frequency of the oscillations in radians per second.

The zero shear viscosity of thermoset depends on the structural build-up during polymerization, and is equal, according to Berry and Fox, to:

$$\eta = \zeta F \quad (25)$$

where  $\zeta$  is a friction factor and  $F$  is a structure factor.

The friction factor depends on local intrachain and interchain forces between neighboring segments in the polymer and its magnitude is given, according to Sanford, by the equation:

$$\zeta = \zeta_0 \exp\left(\frac{E_\eta}{RT}\right) \exp\left(\frac{b}{f}\right) \quad (26)$$

where  $E_\eta$  is the activation energy,  $b$  is a constant which includes a critical free volume required for motion, and  $f$  is a frictional free volume, which equals:

$$f = f_g + a(T - T_g) \quad (27)$$

where  $f_g$  is the free volume at  $T_g$ , and  $a$  is an expansion coefficient. The structural factor  $F$ , in Equation 25 may be expressed:

$$F \propto g (M_w)^a \quad (28)$$

where  $g$  is a gyration factor,  $M_w$  is a weight average molecular weight, and  $a$  is a constant having a value in range of 2.5 - 3.5.

It should be noted that:

$$g, M_w = f(\alpha) \quad (29)$$

$T_g$  in Equation 27 may be found from the DiBenedetto Equation <sup>48,49</sup> and  $M_w$  can be calculated from the Macosco <sup>44</sup> Equation 33.

### 4.1.2 Gelation

From a rheological point of view, two major phenomena occur during thermoset processing; gelation and vitrification.<sup>19,27,40,48,53</sup> The gelation is of great technical importance since the flow of a resin is not possible after gelation. As a consequence, void diffusion and further compaction of the composite can no longer occur.<sup>2,43</sup> Gelation occurs at a specific point in the course of the chemical reaction and depends on functionality, reactivity, and stoichiometry of the reactants. The critical conversion at the gel point can be derived from the theory first proposed by Flory<sup>25</sup>. Flory introduced the branching coefficient ( $\kappa$ ) defined as the probability that a given reactive group of a branched unit of functionality greater than two is connected, via a chain of bifunctional units, to another branched molecule.

For a resin/hardener system,<sup>3,40</sup> if  $P_e$  and  $P_a$  are the fraction of epoxy and hardener active groups which have reacted, respectively, the branching coefficient is given by:

$$\kappa = P_e \cdot P_a = r P_a^2 = \frac{P_e^2}{r} \quad (30)$$

where  $r$  is the ratio of the hardener ( $m_a$ ), to epoxy ( $m_e$ ) groups initially present in the reactive mixture

$$r = \frac{m_a}{m_e} = \frac{f_a M_a}{f_e M_e} \quad (31)$$

where  $f_e, f_a$  are the functionalities and  $M_e, M_a$  are the moles of the epoxy resin and hardener molecules. The condition describing the incipient formation of an infinite network is derived by the theoretical dependence of the molecular weight on the branching coefficient.

When the branching coefficient reaches its critical value  $\kappa_c$ , the network leads to an infinite molecular weight:

$$\kappa_c = \frac{1}{(f_e - 1)(f_a - 1)} \quad (32)$$

For TGDDM-DDS system, weight - average molecular weight may be expressed as <sup>7,44</sup>:

$$M_w = \quad (33)$$

$$\left( \frac{f_e}{f_a \cdot r} \right) \left[ \frac{M_a^2 + f_a \cdot P_a \left[ 1 + \frac{P_{e-ea}}{P_{e-a} + P_{e-ea}} \left[ 1 + \frac{P_{e-ee}}{P_{e-e}} \right] \right] [M_e M_a + M_e^2]}{\left( \frac{f_e}{r \cdot f_a} \right) M_a + M_e} \right] +$$

$$+ \left[ \frac{\left[ 1 + \frac{P_{e-ea}}{P_{e-a} + P_{e-ea}} \left[ 1 + \frac{P_{e-ee}}{P_{e-e}} \right] \right] [(f_e - 1)M_a] + \frac{r \cdot M_e}{P_a}}{\left( \frac{r}{f_e \cdot P_a} \right) \left[ \left( \frac{f_e}{r \cdot f_a} \right) M_a + M_e \right]} \right].$$

$$\left[ \frac{\left[ P_e M_a + \left[ P_e(v - 1) + \left[ P_e(v - 1) \frac{P_{e-ea}}{P_{e-a} + P_{e-ea}} + 2P_{e-e} + 2P_{e-ee} \right] \left[ 1 + \frac{P_{e-ee}}{P_{e-e}} \right] \right] M_e \right]}{\left[ 1 - (f_e - 1) \left[ P_e(v - 1) + \left[ P_e(v - 1) \frac{P_{e-ea}}{P_{e-a} + P_{e-ea}} + 2P_{e-e} + 2P_{e-ee} \right] \left[ 1 + \frac{P_{e-ee}}{P_{e-e}} \right] \right] \right]} \right]$$

where:

$f_e$  - functionality of the TGDDM monomer = 4

$f_a$  - functionality of the DDS monomer = 4

$M_a$  - monomeric molecular weight of DDS = 248

$M_e$  - monomeric molecular weight of TGDDM = 422

$r$  - stoichiometric ratio of epoxide groups to amino-hydrogen group

$\nu$  - weight average extent of reaction =  $\frac{\sum i^2 P_{a,i}}{\sum i P_{a,i}}$

$P_{a,i}$  - fraction of amine units which have  $i$  reacted sites  $P_a$  - conversion of amino-hydrogens

$P_e$  - conversion of epoxide groups

$P_{e-a}, P_{e-e}, P_{e-aa}, P_{e-ee}$  - fractions of epoxide groups of  $E_A, E_E, E_{EA}, E_{EE}$  configurations, respectively (Fig. 19 and 20).

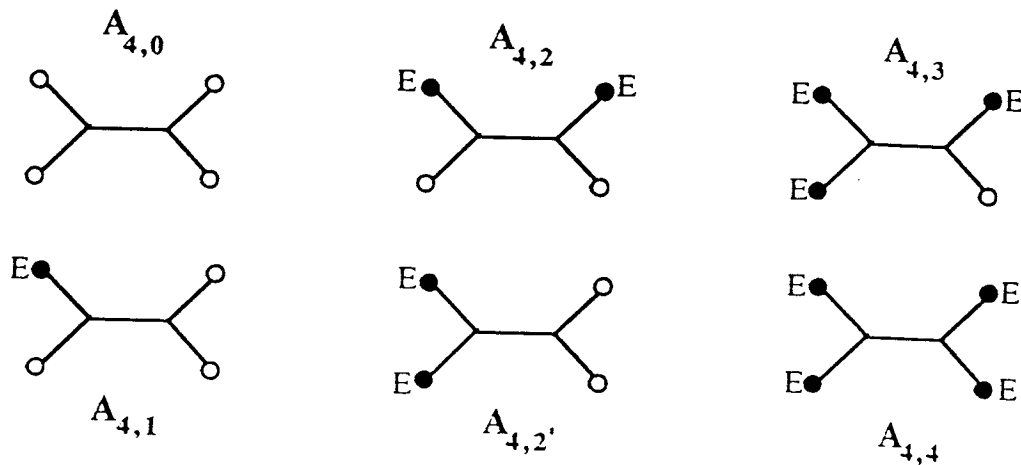
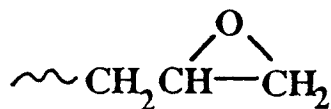
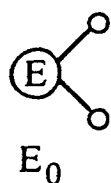
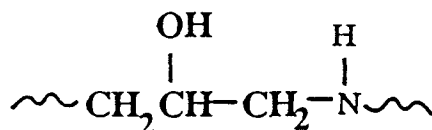
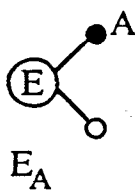


Figure 19.

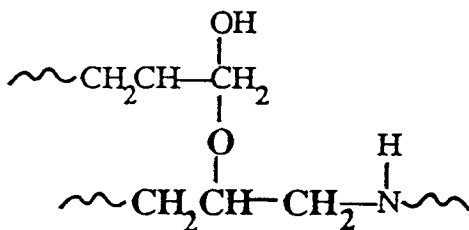
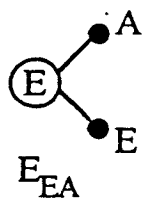
Types of amine units with 0,1,2,3, and 4 reacted sites

SchematicChemical StructureDescription of Reaction

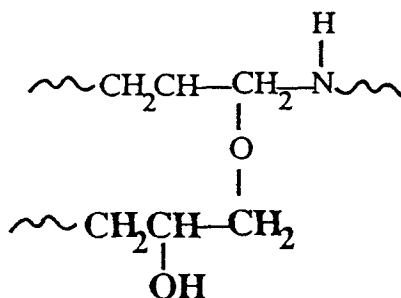
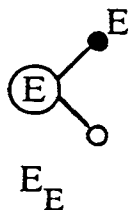
The epoxide group is completely unreacted



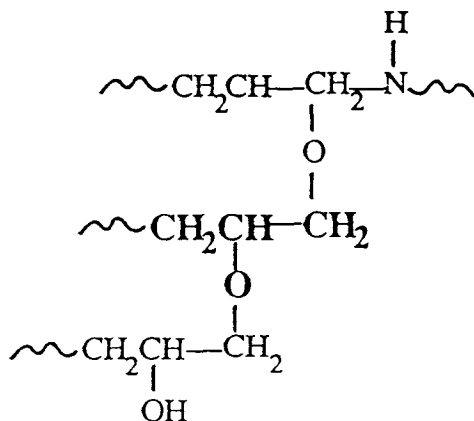
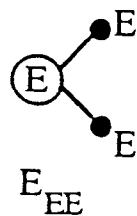
The epoxide group has reacted with an amino-hydrogen



The epoxide group has reacted with an amino-hydrogen and then the formed hydroxyl reacted with an epoxide group



The epoxide group has reacted with a hydroxyl group



The epoxide group has reacted with a hydroxyl group and then the newly formed hydroxyl reacted with another epoxide group

Figure 20.

Possible configurations for TGDDM-DDS system

At the gel point, the weight-average molecular weight becomes infinite.<sup>7,44</sup> This condition is met when the denominator of the last segment of Equation 33 is equal to zero:

$$1 - (f_e - 1) \left[ P_e(v-1) + \left[ P_e(v-1) \frac{P_{e-ea}}{P_{e-a} + P_{e-ea}} + 2P_{e-e} + 2P_{e-ee} \right] \left[ 1 + \frac{P_{e-ee}}{P_{e-e}} \right] \right] = 0 \quad (34)$$

The above equation allows for the calculation of the critical value of conversion at the gel point. However, the procedure of calculations is not straightforward since the conversion exists in the equation in an implicit form, being represented by elementary conversion ratios  $P_{e-a}, P_{e-e}, P_{e-ea}, P_{e-ee}$ .

In order to obtain the conversion at the gelation point, a kinetic model accounting for all mentioned elementary conversion ratios contributing to the overall conversion, must be run for the consecutive time increments until the condition in the Equation 34 is approached.

Under typical processing conditions the polymer at the critical gel point is neither a solid, since stress in a deformed critical gel can relax to zero, nor it is a liquid, since stress during flow grows to infinity. The polymer before the gel point (sol) is soluble, while the polymer beyond the gel point is no longer soluble. At the gel point the steady shear viscosity diverges to infinity. The steady shear measurements, however, can not be used in the close vicinity of the gelation point since they would result in breaking an existing molecular structure, and dynamic mechanical measurements are used instead. In such an experiment, the evolution of  $G', G''$  is measured in small amplitude oscillatory shear as a function of extent of crosslinking, ( $\alpha$ ).

At the gel point the dynamic moduli follow a power law<sup>69,70</sup>:

$$G' \approx G'' \approx \omega^n \quad (35)$$

The loss tangent,  $\tan \delta = \frac{G''}{G'}$ , is independent of frequency. Therefore, two methods to determine the gel point exist:

1. The gel point is reached when the loss tangent becomes independent of frequency, the method used successfully by Holly<sup>36</sup>.
2. For some polymers the gel point coincides with the  $G' - G''$  crossover, in experiments in which  $G', G''$  are measured at constant frequency,  $\omega$ , during the evolution of the crosslinking reaction. This method can be applied for stoichiometrically balanced polymers,<sup>6</sup> and networks with an excess crosslinker, at temperatures above the glass transition.<sup>32,33,62</sup>

These novel methods not only allow for the direct determination of the gel point but they also allow, by extrapolation, the prediction of the gel point when the polymer is close to gelation, but has not yet reached it.<sup>6,35,56,69,70</sup>

### 4.1.3 Vitrification

Distinct from gelation, vitrification may occur at any stage of the reaction. This transformation from a viscous liquid or elastic gel to a glass appears when the glass transition temperature of the material reaches the cure temperature, or vice versa. Further curing in the glassy state is slow and diffusion controlled. Vitrification is a reversible process. Curing of vitrified material can be accelerated by heating the partially cured thermoset above its glass temperature  $T_g$ .<sup>1,26,41,42,67</sup> The glass temperature  $T_g$ , is the temperature below which a material exhibits properties typical of glass. It is usually defined in terms of a specific volume or enthalpy as a function of the cooling rate. At temperatures above the glass transition the molecular mobility is great enough for a material to rearrange rapidly to a structure characteristic of its temperature. Upon cooling, the increase in molecular crowding decreases the mobility to the point where rearrangements necessary to achieve an equilibrium liquid configuration and chemistry can not keep up with the rate of cooling. The point of departure from this equilibrium state or break (abrupt decrease in slope) in the specific volume-temperature cooling curve depends on the rate of cooling. The departure or break comes sooner at a higher temperature with faster cooling. At slower cooling rates the sluggish molecular rearrangements can keep up with cooling until a lower temperature is reached. This break point is identified as a glass transition temperature and is a material-characterizing parameter. (Figure 21.)

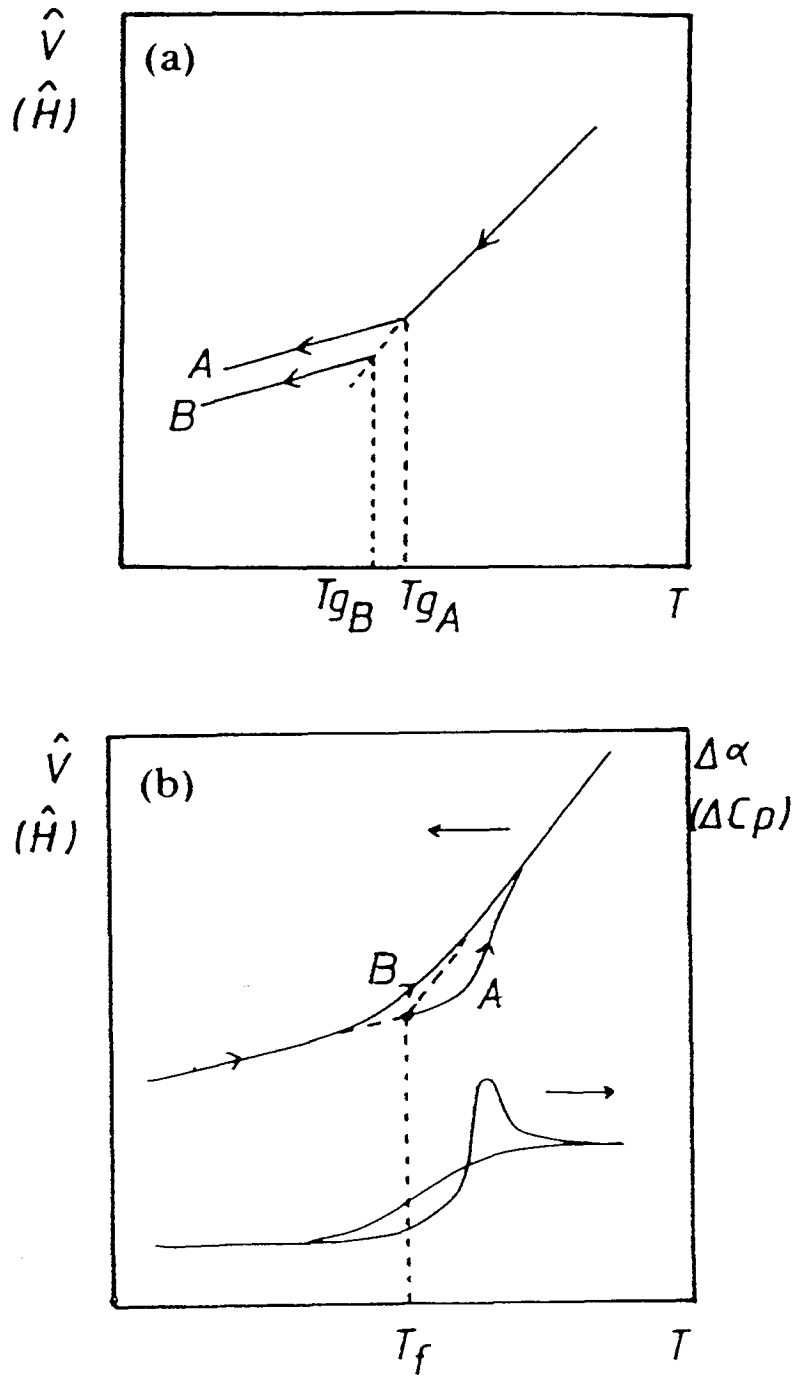


Figure 21.

Specific volume (enthalpy) as a function of temperature: (a) for two different cooling rates ( $A > B$ ) and (b) starting from a particular condition of the material in the glassy state at two different rates ( $A > B$ ).

The glass transition temperature  $T_g$ , is a sensitive and practical parameter for following the cure of a reactive thermosetting system.<sup>27,53,70,67</sup> A wide range of values of  $T_g$  is encountered during cure, and it can be measured throughout the entire range of cure. The fact that  $T_g$  increases nonlinearly with conversion in crosslinking system, makes it even more sensitive in the later stages of reaction, when the reaction rate is slow, for example at high conversion and after vitrification (solidification).

DiBenedetto<sup>48,49</sup> in his analysis of the crosslinking effect on the physical properties of the polymer, derived the equation relating the shift in the glass transition temperature to the extent of reaction.

$$\frac{T_g - T_{g_0}}{T_g} = \frac{\frac{\epsilon_x}{\epsilon_m} - \left(\frac{F_x}{F_m}\right)\alpha}{1 - \left(1 - \frac{F_x}{F_m}\right)\alpha} \quad (36)$$

where  $T_{g_0}$  is the glass transition temperature of the system at  $\alpha=0$ ,  $\frac{F_x}{F_m}$  is the ratio of segmental

mobilities for a certain extent of the reaction  $\alpha$ , and  $\frac{\epsilon_x}{\epsilon_m}$  is the corresponding ratio of lattice energies.

Enns and Gillham showed that an excellent fit of the overall experimental  $T_g$  versus  $\alpha$  relationship could be obtained when both  $\frac{\epsilon_x}{\epsilon_m}, \frac{F_x}{F_m}$  were taken as adjustable parameters. Moreover, the ratio of both parameters is given by

$$\frac{\frac{\epsilon_x}{\epsilon_m}}{\frac{F_x}{F_m}} = \frac{T_{g_\infty}}{T_{g_0}} \quad (37)$$

where  $T_{g_\infty}$  is the maximum glass transition temperature obtained when  $\alpha = 1$ .

## 4.2 Experiments

### 4.2.1 Introduction

From the main three rheological parameters of thermosets; viscosity, point of gelation, point of vitrification, only the latter two are of direct interest to the study. An attempt has been made to determine them experimentally. The objective of the experimental effort was twofold:

(1) To verify the suitability of modern methods for rheological parameter determination. Some of the methods are novel and eventual difficulties in their application or interpretation, as well as additional information they may provide, were of interest. It would be beneficial to suggest easy and dependable procedures for determining the necessary rheological information along with diagrams and concepts of modelling of thermoset processing proposed in the next chapter.

(2) To verify the overall accuracy of the modelling system consisting of two elements; kinetics of conversion and rheological characteristic of the resin. The system is presented in the following chapter.

Numerical values of the parameters obtained from the experiments are of secondary importance - they could be either derived from the theoretical considerations or found in literature.

#### 4.2.2 Review of Techniques for Rheological Characterization

During a cure cycle, the thermosetting material changes from liquid to a glassy solid state, and the extent of the viscoelastic modulus variation made the monitoring of the structural built-up very difficult. While polymers in the liquid state can be characterized by steady-state viscosity measurements, dynamic rheological techniques are needed to follow the cure behavior in the post-gel region. For thermosetting systems, dynamic measurements are generally easy to perform and data can be collected in both the liquid and the post-gel region.<sup>19,56,58,59,62,63,64,69</sup>

In the dynamic measurement, samples of a material are subjected to oscillating forces and the resulting deformations are measured. Dynamic moduli and loss tangents are evaluated as a function of forcing frequency, time/degree of cure, and temperature. These methods include low-frequency nonresonance and resonance methods.

For an isotropic sample that is subjected to a sinusoidally varying tensile strain  $\epsilon$ , at a frequency below that required to induce resonance vibration, for linear viscoelastic behavior, under steady-state conditions, the stress  $\sigma$ , sustained by the sample is also sinusoidal, but the stress cycle leads the strain cycle by a phase angle  $\delta$ , as illustrated in Figure 22.<sup>58</sup>

$$\epsilon = \epsilon_0 \cos \omega t \quad (38)$$

$$\sigma = \sigma_0 \cos(\omega t + \delta) \quad (39)$$

$$\sigma = \sigma_0 \cos \delta \cos \omega t - \sigma_0 \sin \delta \sin \omega t \quad (40)$$

where  $\omega$  is the angular frequency and  $\sigma_0, \epsilon_0$  are the amplitudes of  $\sigma$  and  $\epsilon$ .

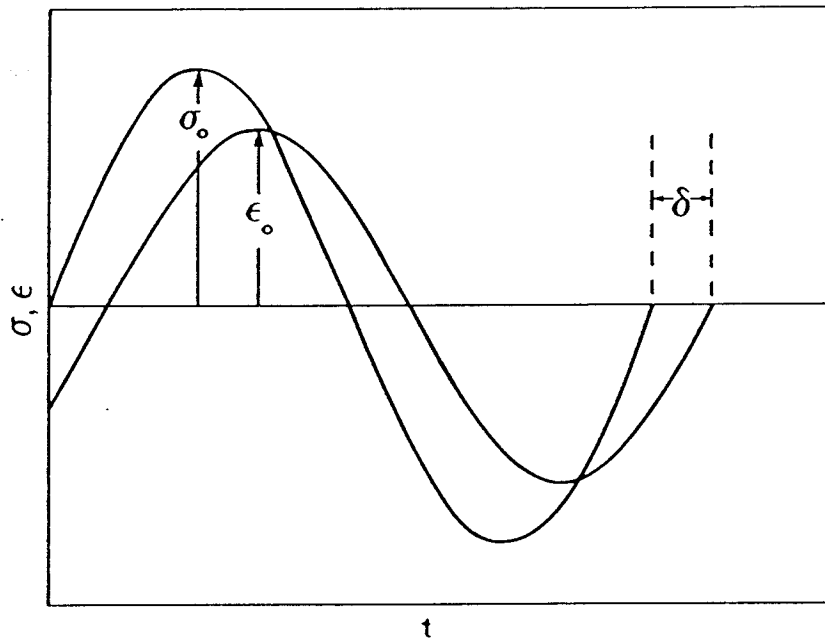


Figure 22.

Time dependence  $t$ , of the stress  $\sigma$ , and strain  $\epsilon$ , during a low-frequency (nonresonance) test.

Equation (40) demonstrates that the stress consists of two components. One component is of magnitude  $\sigma_0 \cos \delta$  and is in phase with the strain. The other component of magnitude  $\sigma_0 \sin \delta$  is  $90^\circ$  ahead of the strain and thus in phase with the strain rate. Therefore, the material behaves partly as an elastic solid and partly as a viscous liquid, and the stress - strain relationship is written:

$$\sigma = \epsilon_0 E' \cos \omega t - \epsilon_0 E'' \sin \omega t \quad (41)$$

where the component moduli are given by:

$$E' = \frac{\sigma_0}{\epsilon_0} \cos \delta \quad (42)$$

$$E'' = \frac{\sigma_0}{\epsilon_0} \sin \delta \quad (43)$$

These equations suggest that the tensile modulus can be specified in complex form. For this purpose the strain and stress cycles are represented by the real part of :

$$\epsilon^* = \epsilon_0 \exp(i\omega t) \quad (44)$$

$$\sigma^* = \sigma_0 \exp[i(\omega t + \delta)] \quad (45)$$

where

$$i = (-1)^{\frac{1}{2}} \quad (46)$$

Then:

$$E^* = \frac{\sigma^*}{\varepsilon^*} = \frac{\sigma_0}{\varepsilon_0} \exp(i\delta) \quad (47)$$

$$E^* = \frac{\sigma_0}{\varepsilon_0} (\cos \delta + i \sin \delta) = E' + iE'' \quad (48)$$

The real part of the modulus  $E'$ , which is in phase with the strain, is termed the storage modulus since it is proportional to the peak energy stored per cycle in the material. The imaginary part of the modulus  $E''$ , which is out of phase with the strain, is proportional to the net energy dissipation per cycle and is known as the loss modulus.

The ratio

$$\frac{E'}{E''} = \tan \delta_E \quad (49)$$

is termed the loss factor or damping factor.

It should be emphasized that  $E'$ ,  $E''$ , and  $\tan \delta_E$  depend on the test frequency and also on temperature, and each is used to characterize dynamic mechanical properties either at a given frequency or temperature or preferably, over a range of these variables.

Although the components of  $E^*$  are determined quite simply from dynamic tensile or flexural tests, it is often convenient to obtain dynamic properties for another mode of deformation - the shear. For isotropic materials, dynamic experiments yield the components of the complex shear modulus:

$$G^* = G' + iG'' = G'(1 + i \tan \delta_G) \quad (50)$$

where  $G'$ ,  $G''$ , and  $\tan \delta_G$ , are the shear storage modulus, loss modulus, and loss factor, respectively.

## Nonresonance Methods

At low frequencies (0.01 - 100 Hz) dynamic moduli and loss factors are determined directly from the amplitudes of, and phase angle between, the force and displacement cycles for samples subjected to a time-harmonic force of deformation. For polymer evaluation, the instruments working in nonresonance methods include thermal mechanical analyzers, and rheometers. The ideal instrument, in this category, is the Rheometrics Dynamic Analyzer (RDA) evaluating such viscoelastic properties as viscosity ( $\eta^*$ ), elastic modulus ( $G'$ ), viscous modulus ( $G''$ ), and damping ( $\tan \delta$ ). The RDA is capable of making these measurements on a material in its liquid or solid form in dynamic shear using parallel plates, cone and plate, and torsion fixtures. The combination of precision stress and strain detection, makes RDA the most accurate and convenient instrument available. RDA evaluates materials under an extremely broad temperature range (-150 to 600 °C). The wide dynamic range of the RDA's transducer (at least three decades) makes it ideally suited for thermoset characterization. Minimum viscosity, gel point, and vitrification moment of resins and prepregs can be determined during curing. With a temperature range of 1° to 60°C per minute almost any curing process can be simulated.<sup>8,14,20,58,59,64</sup>

## Resonance Method - Torsion Pendulum, Dynamic Mechanical Analyzer

Torsional deformations are more suitable than simple shear for determining the dynamic shear properties of rigid materials as they avoid the high force level associated with measurable deformation. Although less versatile than nonresonance techniques, this methods allow more accurate measurements. Values of the elastic modulus and loss modulus can be obtained for a specimen of known simple geometry (rectangular film or a cylindrical filament). The elastic shear modulus  $G'$ , is calculated from the frequency and the logarithmic decrement is calculated from the

decay of a damped oscillating wave. The times to macroscopic gelation and vitrification can be assigned from the times to reach consecutive maxima in the logarithmic decrement vs. time plot.<sup>9,24,27,47,58</sup>

#### 4.2.3 Determination of Gelation and Vitrification Points Using RDA Technique

For the determination of the gelation point the RDA technique seems to be the most promising. Alternative methods are: solubility testing and the Torsional Braid Analyzer (TBA). Solubility tests, however, are not very exact due to the subjectivity involved in the interpretation of their results. The TBA technique was reported<sup>23,24,27,47,70,71</sup> to be successfully used for defining gelation but the author of the Thesis did not have access to the equipment. To specify the vitrification moment a number of methods may be used: DSC<sup>19,71,73</sup>, TMA<sup>20</sup>, RDA<sup>59</sup>, and TBA<sup>23,24,27,46,47,71,72,73</sup>. Due to the complex behavior of thermosets only resonance techniques are commonly utilized for this purpose. However, in this work, lack of access to TBA and DMA equipments forced the author to investigate the possibility of using RDA and DSC methods instead.

The tests on the RDA apparatus (Figure 23), to which access was provided, courtesy of the Defence Research Establishment Pacific, were conducted by continuous monitoring of rheological parameters of the material undergoing a processing cycle. The applied processing cycles were usually isothermal using the processing temperature in the range of 140 - 190 °C and consisted of three parts: a rather rapid ramp from room temperature to the temperature of isothermal processing, extended period of isothermal processing, and a linear decrease of the temperature at the end of the cycle. Only in one instance, in order to speed up the conversion process, the temperature of 170 °C was applied initially, and later returned to the temperature of processing of 140°C.

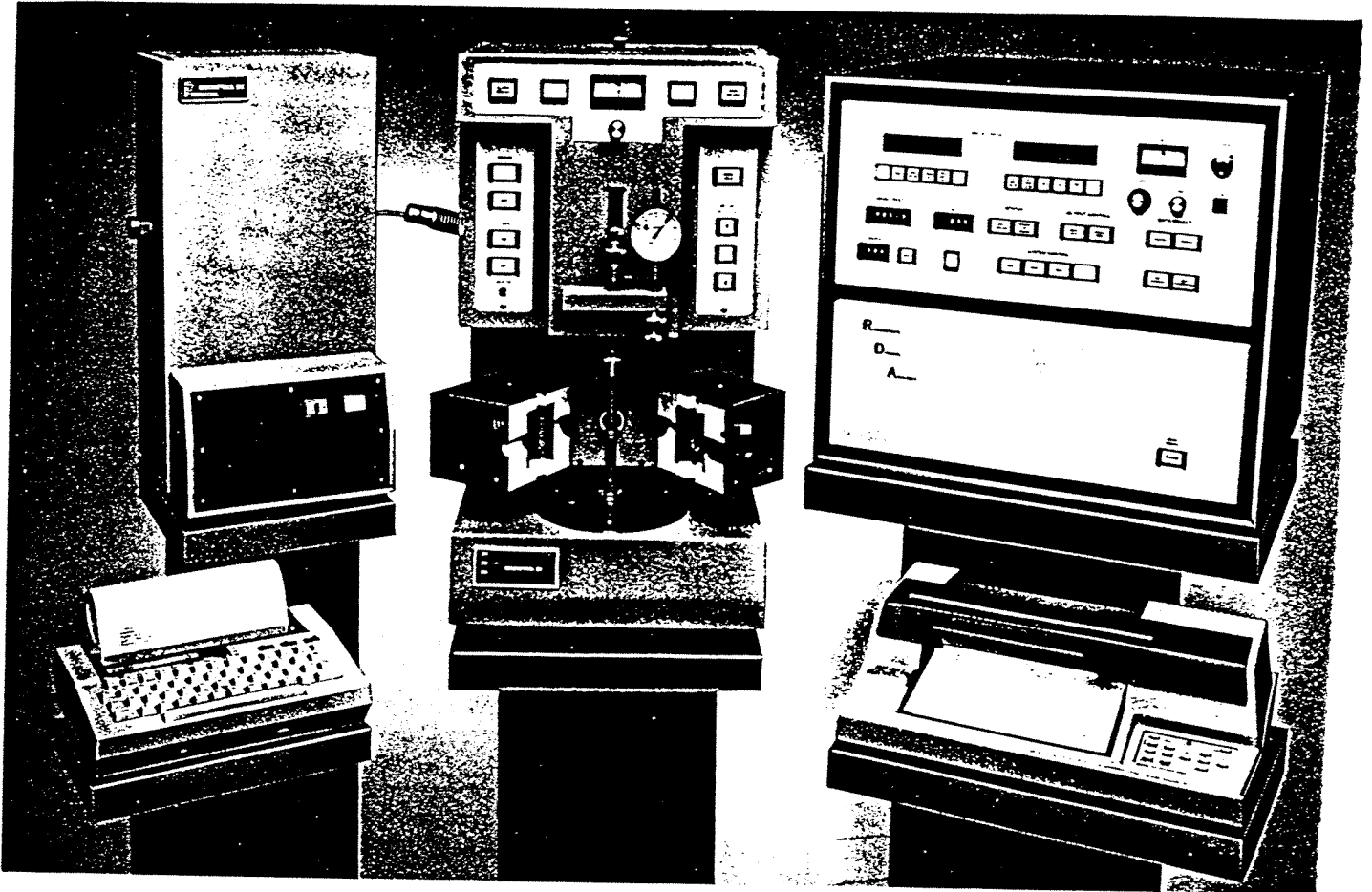


Figure 23.  
Rheometrics Dynamic Analyzer

In the experiments parallel plate geometry was used, with the exception of one experiment, which was conducted in the torsion mode. The decision to use parallel plates stemmed from the fact that the arrangement has been commonly used by other authors<sup>6,33,62</sup>. The choice of plate diameter (25 mm) was to ensure versatility of measurements, so that both phenomena, gelation and vitrification, could be recorded in the same experiment. Smaller plates, more suitable for monitoring of advanced stages of processing, had to be ruled out due to the resin bleeding problem resulting from the very low viscosity of the Narmco resin at low levels of conversion. If the viscosity itself were the main object of investigation, the larger plates (40 mm) would be advisable.

The material used in the parallel plate investigations was Narmco 'B' - stage resin, while for experiment in the torsion mode the Narmco prepreg was used. The thickness of resin placed between parallel plates was about 0.4 mm. The mode of test under the apparatus nomenclature was 'time/cure sweep'. The frequency of oscillation in the experiments was set at 1.6 Hz. After placing the material between the plates, the gap between them was fixed, not allowing for any axial movement. This was necessary to avoid squeezing the resin out from the gap at an early stage of the experiment.

Considering the extreme changes in material physical/mechanical properties during the processing, the 'auto' option was chosen for the strain, with a maximum value of 10% adjustable in 2% steps. The maximum allowable torque was specified as 60 g·cm. Under the mentioned mode the apparatus attempts to maintain a minimum stress which provides a satisfactory level of measured strain and stress. In the low viscosity region the strain is increased up to its specified limit to generate a sufficiently strong signal representing torque. In the region of material vitrification, the maximum, specified torque is used to generate the measurable strain signal.

During the experiment, the temperature of a material, storage modulus, loss modulus, and eventually, tangent of the phase angle between stress and strain (loss tangent) are recorded by the apparatus. On the basis of these records, which are presented in Figures 24a-31a, the determination of gelation

and vitrification points was carried out.

The point of gelation, for a single experimental record, was identified as a place of intersection of the storage modulus  $G'$  and loss modulus  $G''$  curves. The more rigorous procedure of searching for the moment where the ratio of both moduli does not depend on the applied frequency of oscillation could not be implemented due to time restrictions in the access to the RDA. Nonetheless, the investigations of other researchers<sup>6,33,62</sup> show that for frequencies in the range 1 - 10 Hz, the point of moduli intersection yields a very good approximation of the gelation moment. It may be noted also that the curves of both moduli in the vicinity of gelation become so steep that even if the ratio of the moduli corresponding to gelation is slightly different than 1, the resulting error in term of gelation moment is negligible.

The determination of the vitrification point from the records was difficult. In the absence of any clear suggestion in the literature, the intention was to look for any characteristic behavior of curves  $G'$ ,  $G''$ , and tangent of phase shift, which may indicate the point of vitrification. The latter two ( $G''$ , tangent) had to be ruled out, however, since in the vicinity of vitrification their readings were out of the sensitivity range of the apparatus. The area of the  $G'$  curve where the vitrification phenomena should be looked for remained a question. The work of Gillham<sup>24,27,73</sup> suggests that due to the decreasing rate of conversion in the vicinity of vitrification, the moment of vitrification is not to be expected during isothermal processing, but rather later, during final cooling. In this area of the records, either an increase, or sudden and pronounced decrease of the storage modulus  $G'$  appears, the latter suggesting, perhaps, breaking of a material. In the interpretation of the results, with one exception, this point of rapid decrease of  $G'$  was considered as an approximate vitrification moment.

A question may arise concerning the rationale of the assumption that the moment of material breaking may mark the moment of final vitrification. During thermoset processing, even under

isothermal conditions, the density of chain packing increases, leading to the shrinking of a material. This is especially true when a material approaches vitrification. The linear decrease of processing temperature during the final stage of the experiment additionally contributes to shrinkage. At the moment of vitrification the free volume disappears, making a material more brittle. All these, combined with the fact that the gap between plates is forcefully fixed, leads to the generation of stresses, and may lead to an eventual breaking of the material.<sup>59</sup>

In Figure 26a a typical record is presented. It may be seen that at a beginning of the cycle both curves,  $G'$  and  $G''$ , drop to a very low level and remain at it for 20 - 30 minutes, responding to the applied temperature. Later the advancement of conversion causes the curves to rise again. The curve of  $G''$  starts first but the rate of increase is higher for the  $G'$  curve so that the curves cross each other after the time of about 40 minutes. The point of intersection is considered as a point of gelation and is marked 'G' in the figure. Proceeding further, the curve of  $G''$  reaches local maximum and becomes chaotic (measurement is out of the sensitivity range). The curve of  $G'$  in the meantime increases at progressively decreasing rate forming a knee shape. A linear temperature decrease at the end of processing results in an increase of  $G'$ , followed by its sudden drop at the moment where vitrification is expected.

The procedure for the identification of the vitrification moment is not simple. In experiment 140°C/30min (Figure 24a) no break in a material is recorded, and a vitrification point is recognized as a moment when the curve of  $G'$  rising rapidly, reaches the high-level plateau. In experiment 170°C/140 C/180min (Figure 25a), and in experiment 170°C/60min(A) (Figure 26a), a clean drop in  $G'$  curve is recorded. It may be noticed, however, in these and in the other experiments that the resin seems to never break completely. In experiment 170°C/60min(B) the  $G'$  curve recovers when reheating is applied (Figure 27a), which is something to be expected. However, in experiment

170°C/120min(A) (Figure 28a), the curve 'recovers' during further cooling. This casts a doubt on whether the sudden drops of G' curve observed in the figures are really associated with material breaking, or rather with the displacement of the tool in its fixture under extensive stress.

In the record of the experiment using the torsion mode, the gelation point cannot be identified. Neither can the vitrification point be determined from the storage modulus curve. However, a thorough examination of the loss tangent curve shows an interesting oscillation (Figure 32b) for the time of processing of 170 min, which corresponds to the processing temperature of about 100 °C, while the vitrification is expected to take place at about 115°C. Nonetheless, since the oscillation is weak, agreement is only approximate, and on the basis of a single record no suggestion can be formulated.

#### 4.2.4 Discussion of the Results

A major inconvenience in further evaluation of the obtained results is that the points of gelation or vitrification found on experimental records are specified in terms of time and temperature, but not in terms of the degree of conversion. It is quite natural that for different temperatures of processing the time for gelation and vitrification to take place is different; this information, however, is not adequate for the evaluation of the results through necessary comparisons. The comparison can only be made on the basis of the degree of conversion and temperature. It should be recalled (Equation 34) that for any resin system, gelation is expected to take place at one specific value of the degree of conversion, and that the vitrification point can also be expressed as a function of the degree of conversion, with the addition of temperature of processing as a secondary parameter (Equation 36). In order to obtain values of the degree of conversion, the kinetics of conversion for the Narmco resin was utilized in the work to build the model of conversion in the form of a computer code based on numerical integration (see Chapter 3). The nature of the model allows it to be applied to any temperature/processing cycle, producing consecutive values of conversion as a function of time. The model was used to produce a curve of conversion as a function of time for each processing cycle of the experiments (Figures 24b-31b). From these curves the degree of conversion, corresponding to the time of identified gelation and vitrification, could easily be found.

In Table 1 the temperature of processing, time of processing at gelation, and degree of conversion at gelation for conducted experiments are provided. The identification of the gelation point from experimental records, as a point of inter-section of storage and loss modulus curves, did not create any serious problems. A minor problem may be reported in experiment 190°C/180min(B) (Figure 31a), where strong oscillation of  $G'$  and  $G''$  appeared directly before gelation.

The obtained experimental values of conversion at gelation are in a very narrow range (0.31 - 0.36), which is consistent with the theoretical value of conversion at gelation of 0.33<sup>6,7,8</sup>. This excellent agreement proves that the RDA technique is ideally suitable for the determination of gelation. It also strongly indicates that the theory of resin rheological behavior, combined with a high-quality kinetics model of conversion, is able to produce results very consistent with high-precision measurements.

It may be noticed from Table 1 that the degree of conversion at gelation slightly increases with the increase of the temperature of processing. This tendency, although in agreement with Serrano and Harran,<sup>62,63</sup> is much weaker than reported there, and its statistical significance is doubtful.

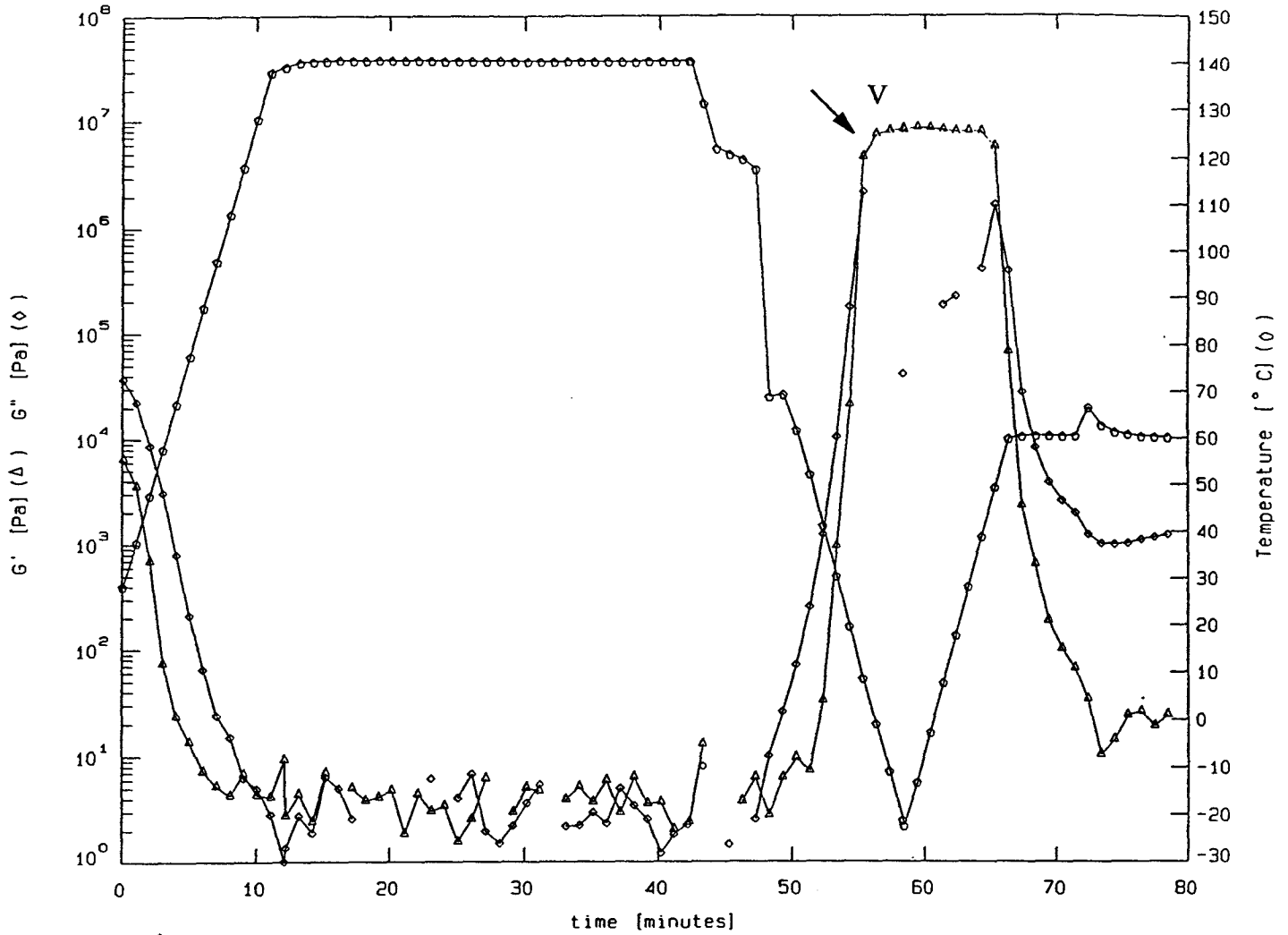
In order to conveniently discuss the experimental results of vitrification, the time of vitrification, the degree of conversion at vitrification, and the temperature of vitrification, the results are presented for all experiments in Table 2. The temperature at vitrification may be directly compared with the last column in the table, where temperatures of vitrification for the same values of conversion are calculated from the DiBenedetto equation<sup>48,49</sup>. The agreement is far from being perfect. Considering this, the spread of results, and weakness of the concept itself, the method, as it is, cannot be accepted as a primary tool for the determination of vitrification points. However, taking into account that determination of the vitrification point for some resin systems may be problematic even with the TBA technique, the tested method, may still prove to be of value as a supplementary technique after further experiments. In such eventual experiments special attention should be directed at the use of smaller plates, and utilization of readings of the indicator of axial forces.

#### 4.2.5 Determination of the Vitrification Point on the Basis of the Differential Scanning Calorimeter Measurements.

The concept of the technique takes advantage of the fact that due to free volume, the enthalpy of the material above the vitrification temperature is expected to substantially increase. The successful use of the method was reported in the work of Wisanrakkit.<sup>71</sup> In experiments conducted in the presented thesis, the samples of the Narmco resin were processed isothermally at 190 °C, for two hours, to the degree of conversion of about 0.9 and Tg was expected to be approximately 160 °C. The samples were later cooled and then heated again using a linear temperature increase. Results of the DSC are presented in Figures 33-36. Although various temperature increase rates were tested, the resulting differential heat consumption curves did not exhibit any behavior which would allow the identification of the vitrification moments.

#### 4.3 Contribution of the Author

The research effort within Chapter 4 consists of experiments conducted on RDA and DSC apparatuses and is aimed at the determination of gelation and vitrification points for various processing conditions. The applied methods are quite novel and there are very few publications on the subject.



Legend:

V - vitrification point

Figure 24a.

RDA record of processing 140 °C/30 minutes

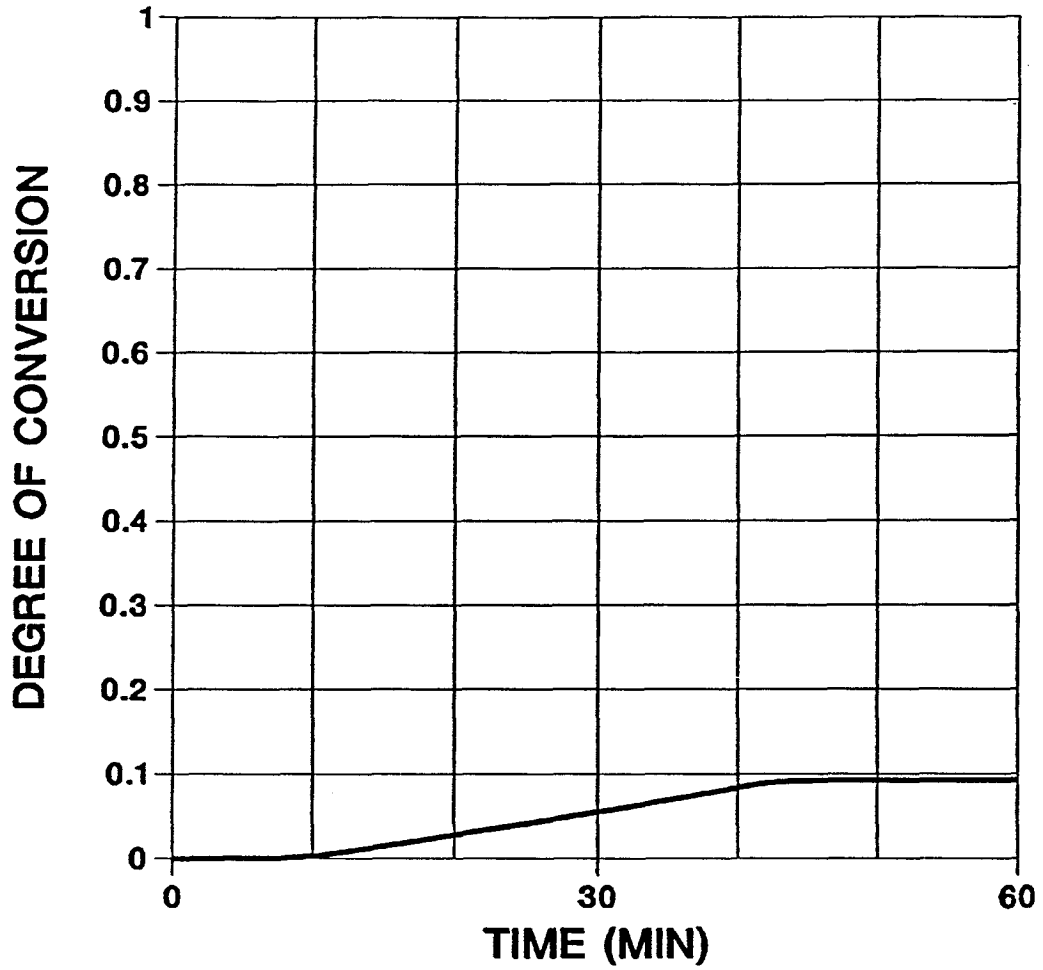
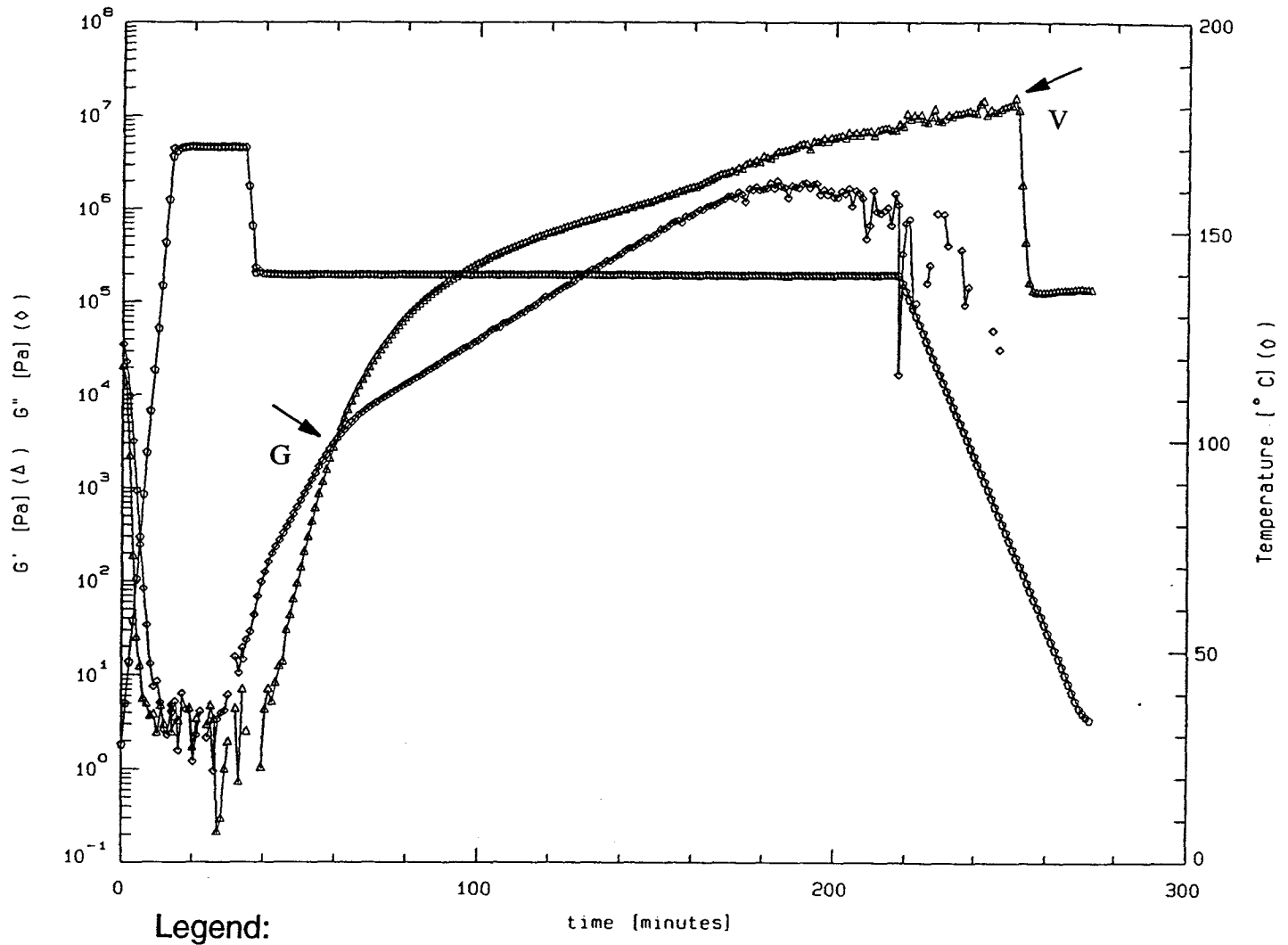


Figure 24b.

Degree of conversion for experiment 140 °C/30 minutes



Legend:  
 G - gelation point  
 V - vitrification point

Figure 25a.

RDA record of processing 170/140°C/180 minutes.

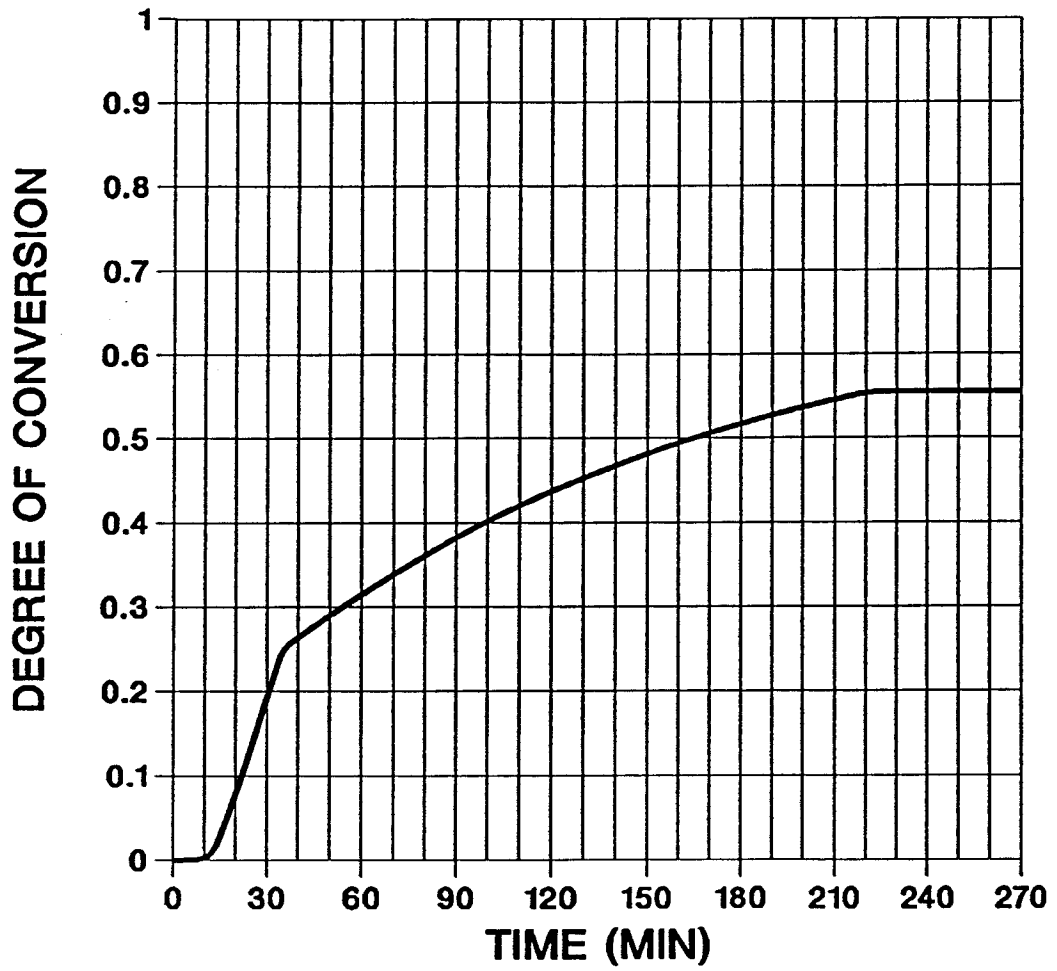


Figure 25b.

Degree of conversion for experiment 170/140°/180 minutes.

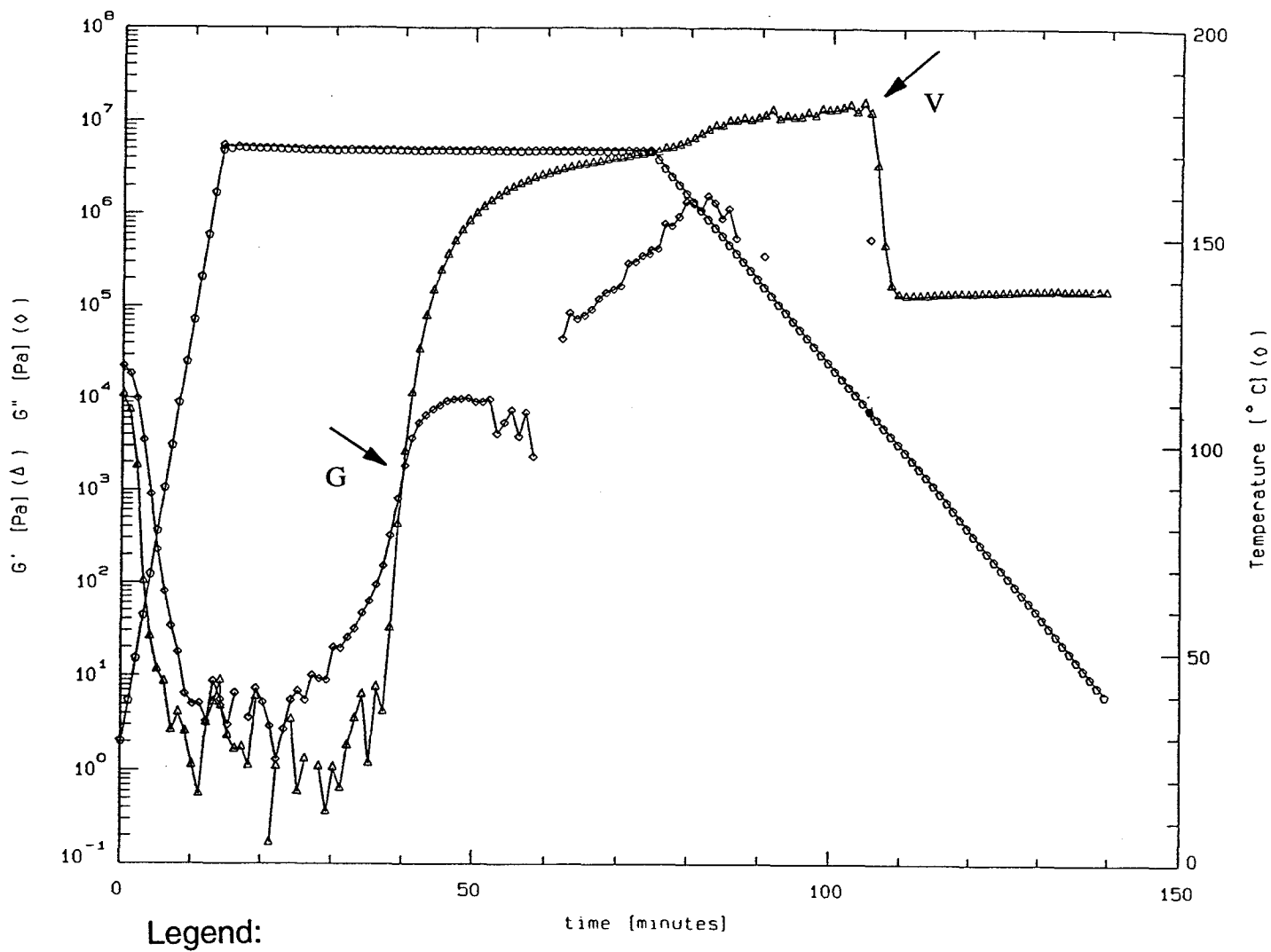


Figure 26a.

RDA record of processing 170°C/60 minutes (A).

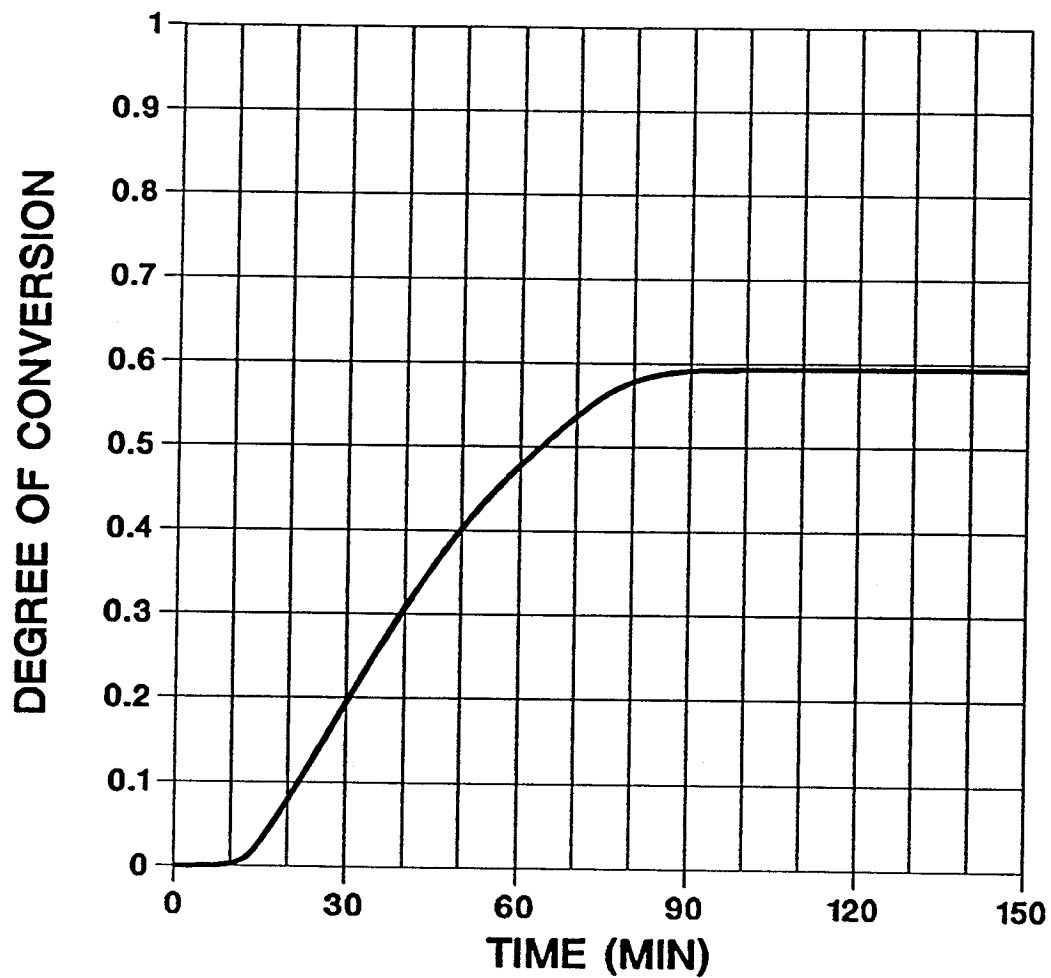
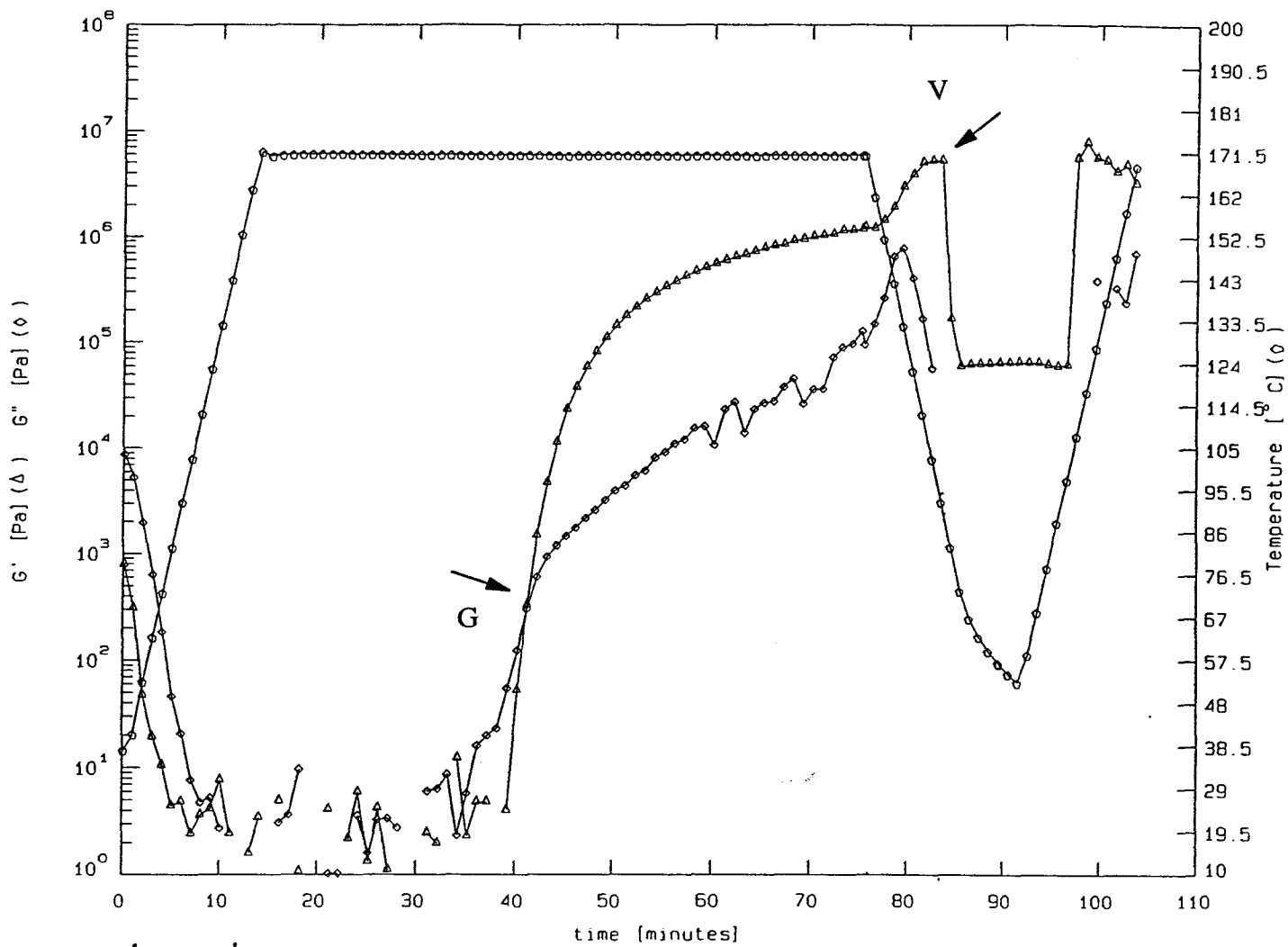


Figure 26b.

Degree of conversion for experiment 170°C/60 minutes (A).



Legend:

G - gelation point

V - vitrification point

Figure 27a.

RDA record of processing 170°C/60 minutes (B).

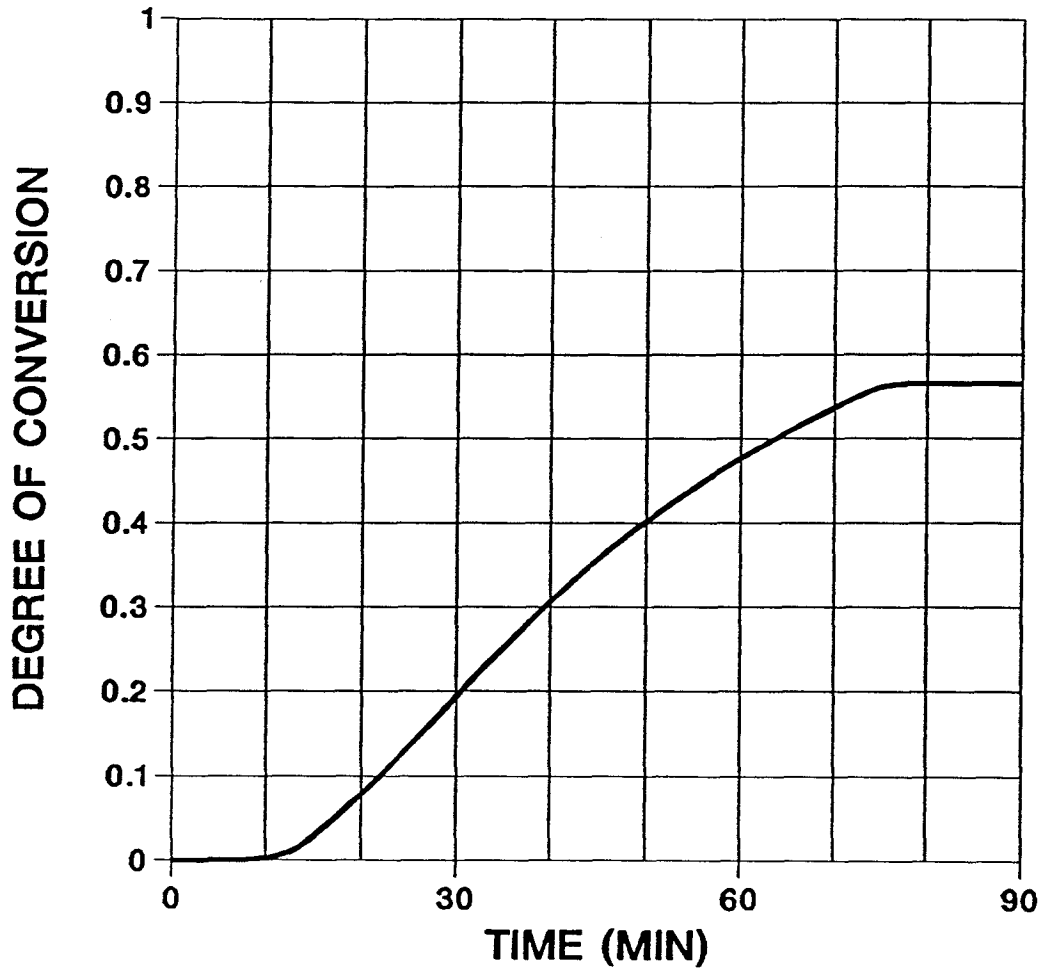
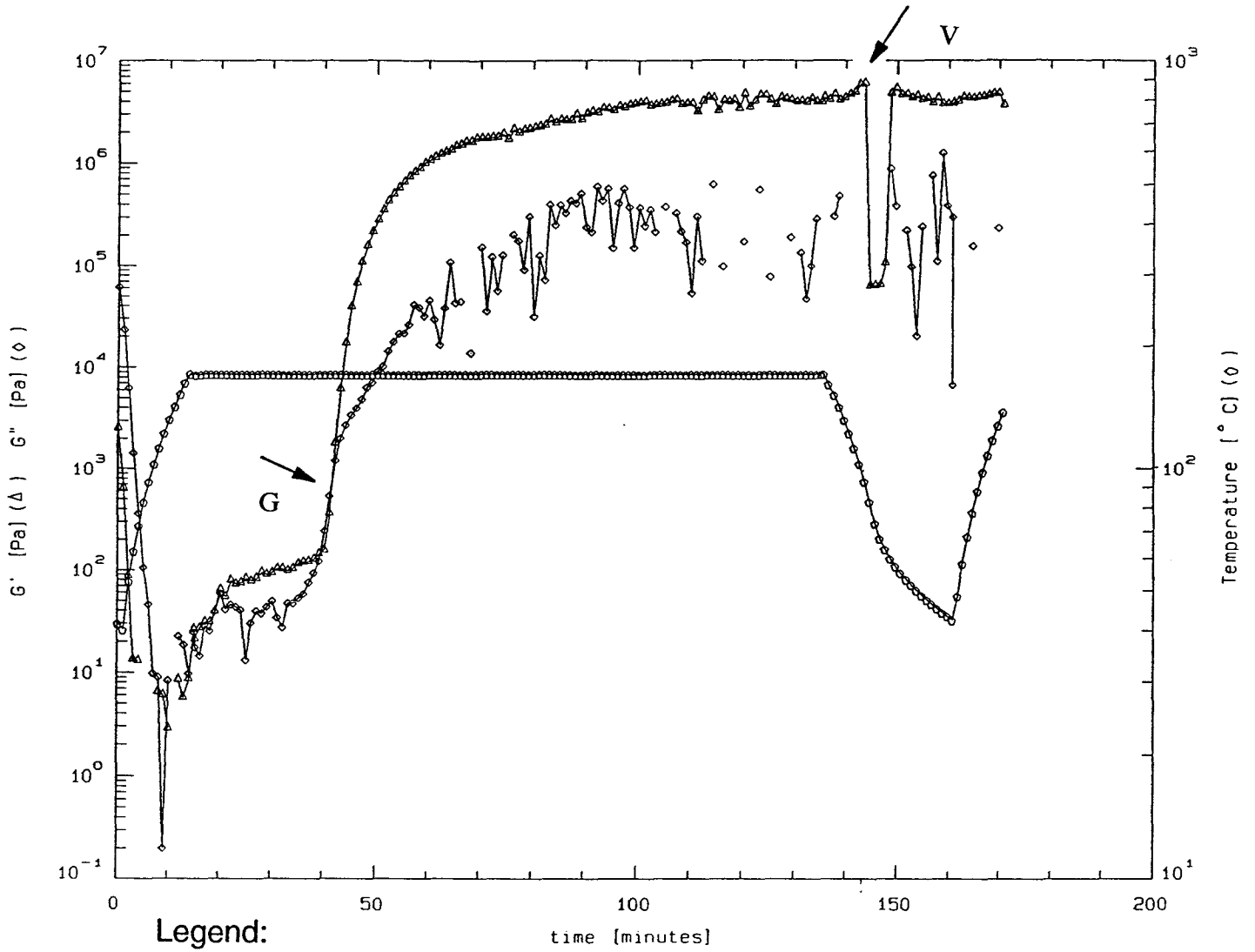


Figure 27b.

Degree of conversion for experiment 170°C/60 minutes (B).



Legend:  
 G - gelation point  
 V - vitrification point

Figure 28a.

RDA record of processing  $170^{\circ}$ C/120 minutes (A).

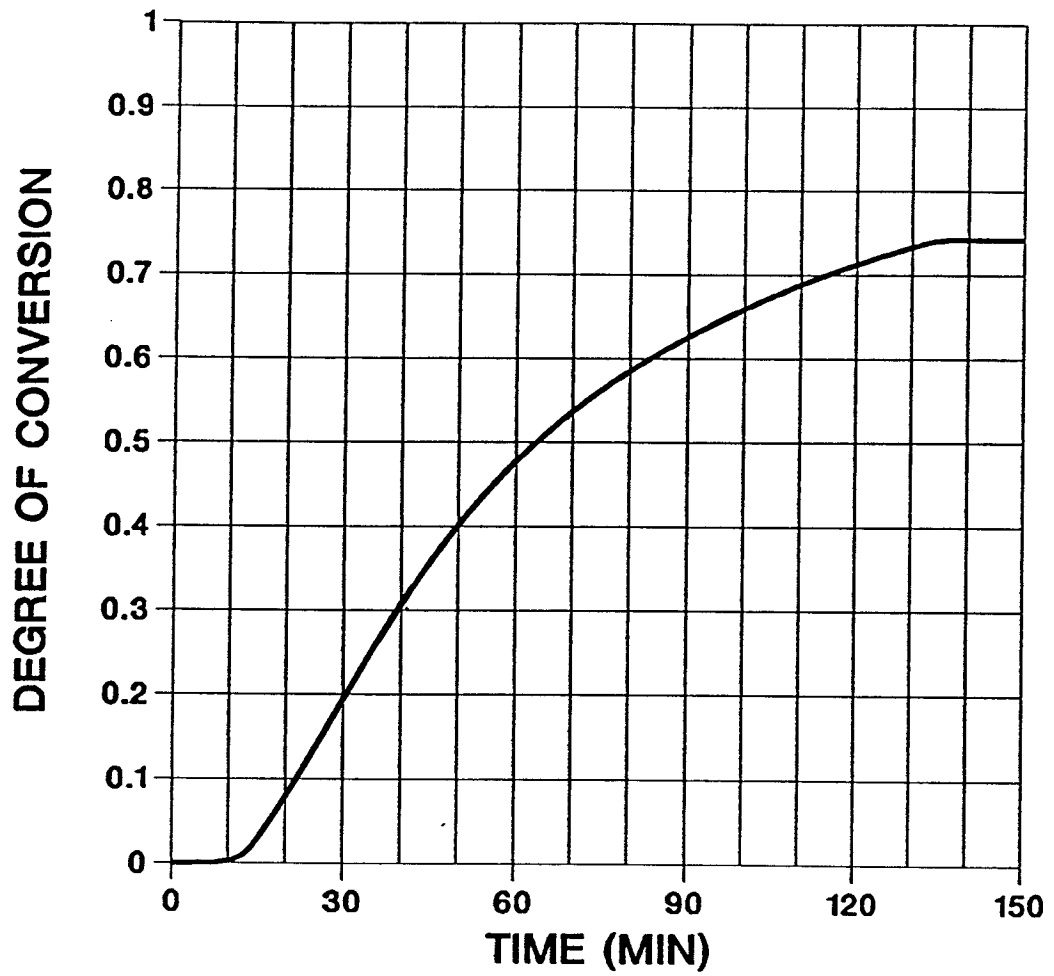
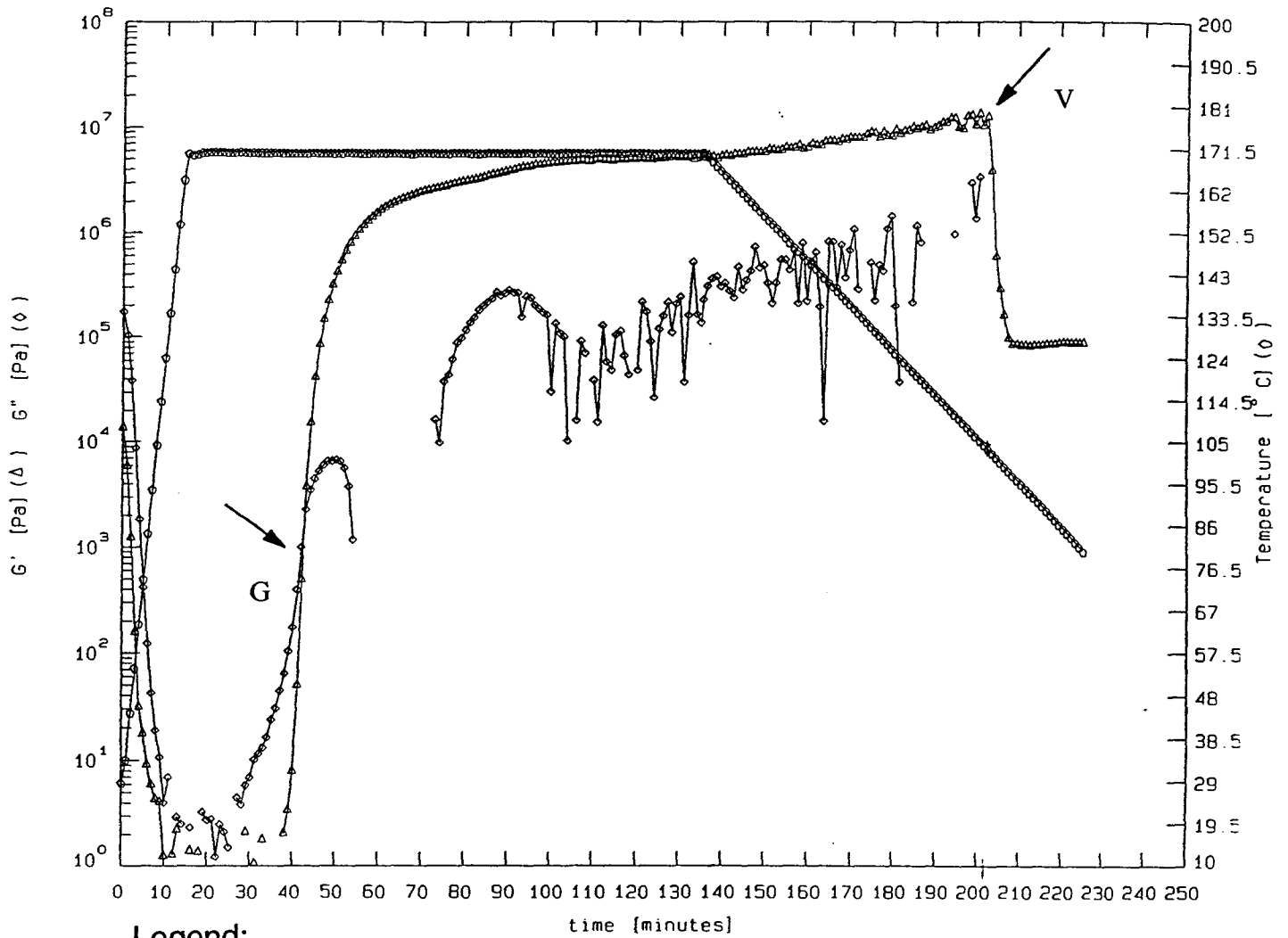


Figure 28b.

Degree of conversion for experiment 170°C/120 minutes (A).



Legend:  
 G - gelation point  
 V - vitrification point

Figure 29a.

RDA record of processing 170°C/120 minutes (B).

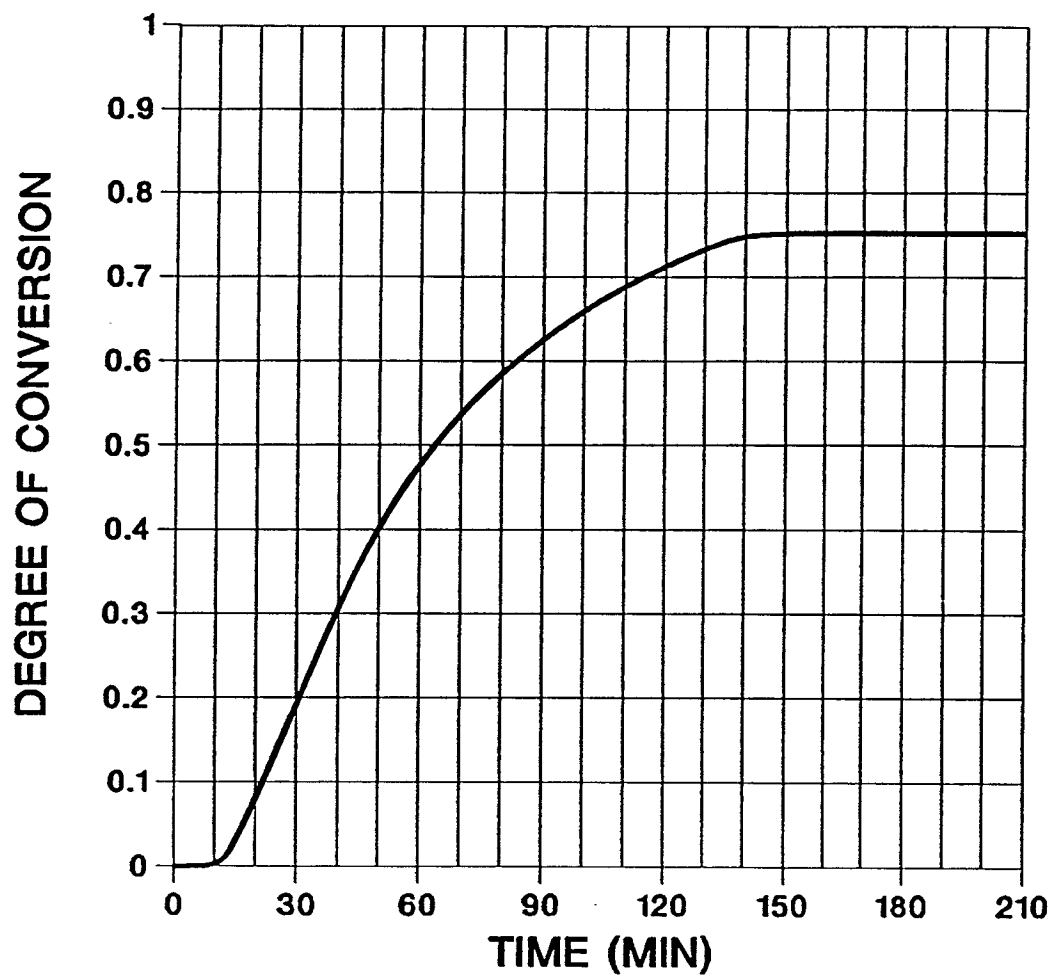


Figure 29b.

Degree of conversion for experiment 170°C/120 minutes (B).

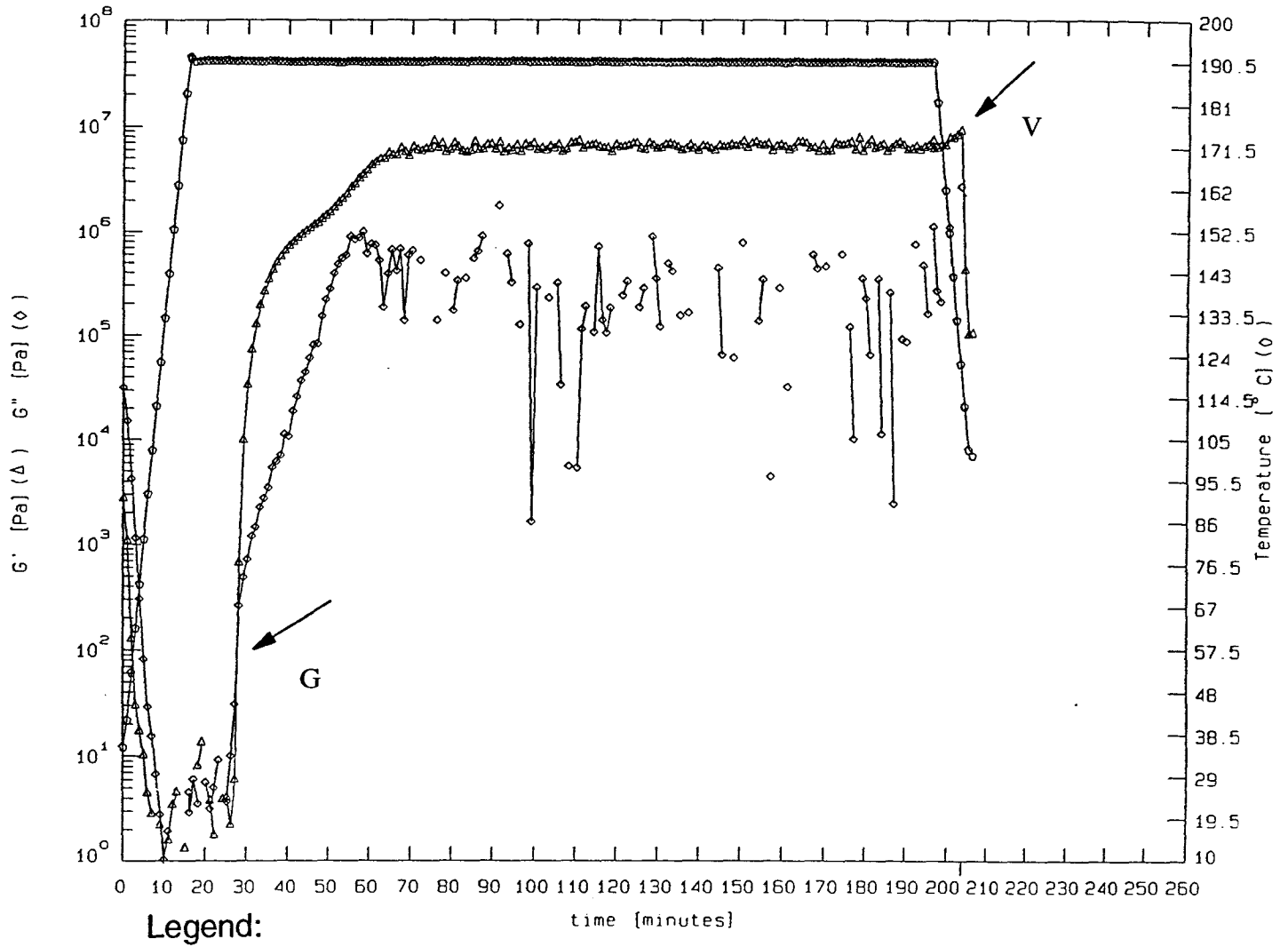


Figure 30a.

RDA record of processing 190°C/180 minutes (A).

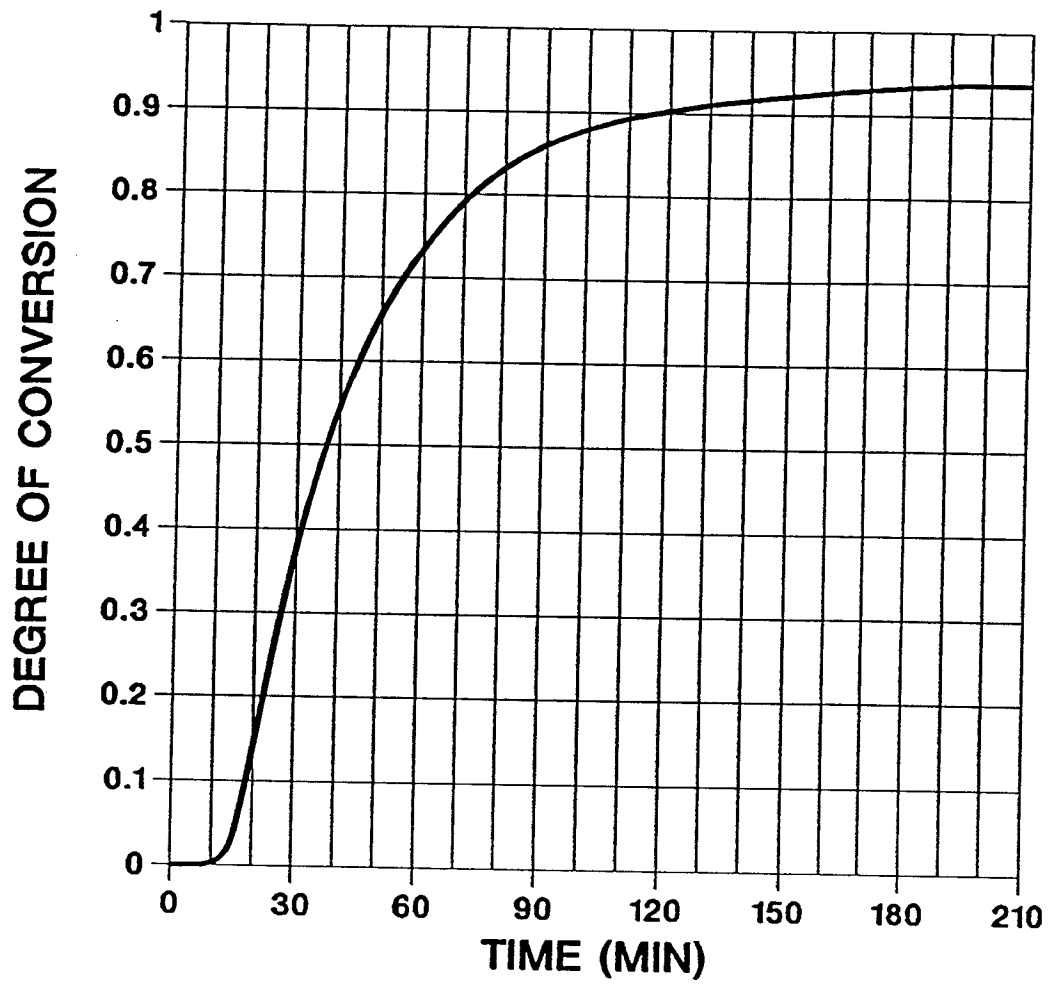


Figure 30b.

Degree of conversion for experiment 190°C/180 minutes (A).

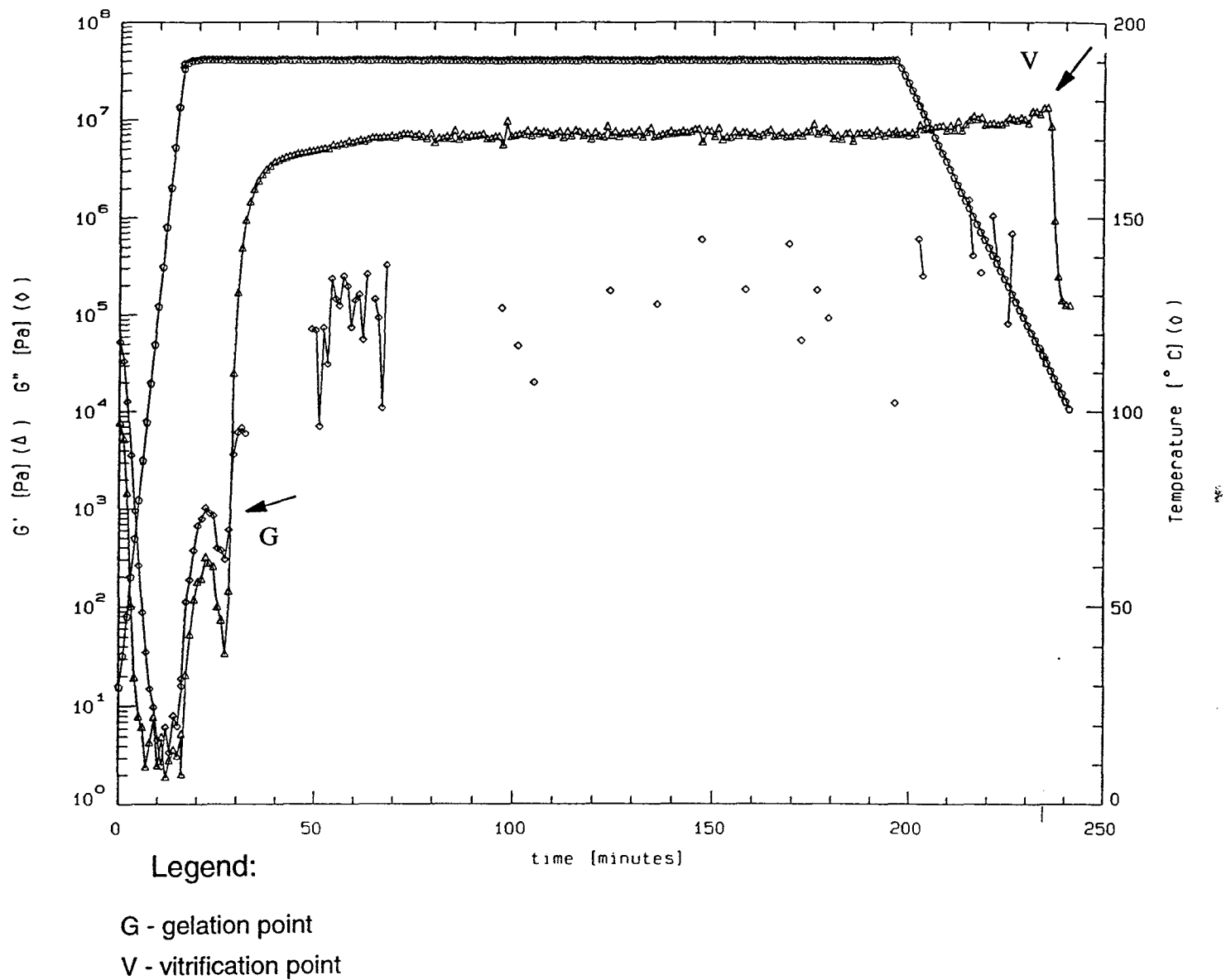


Figure 31a.

RDA record of processing 190°C/180 minutes (B).

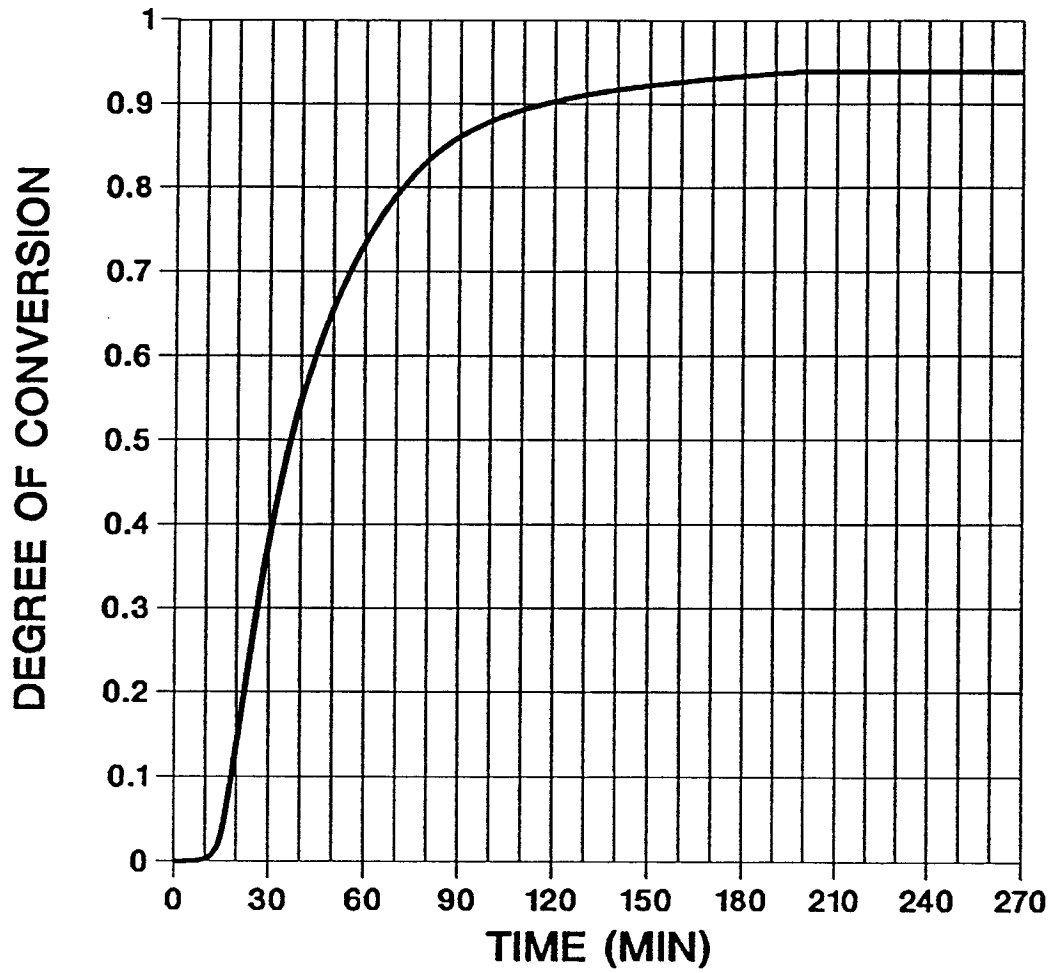


Figure 31b.

Degree of conversion for experiment 190°C/180 minutes (B).

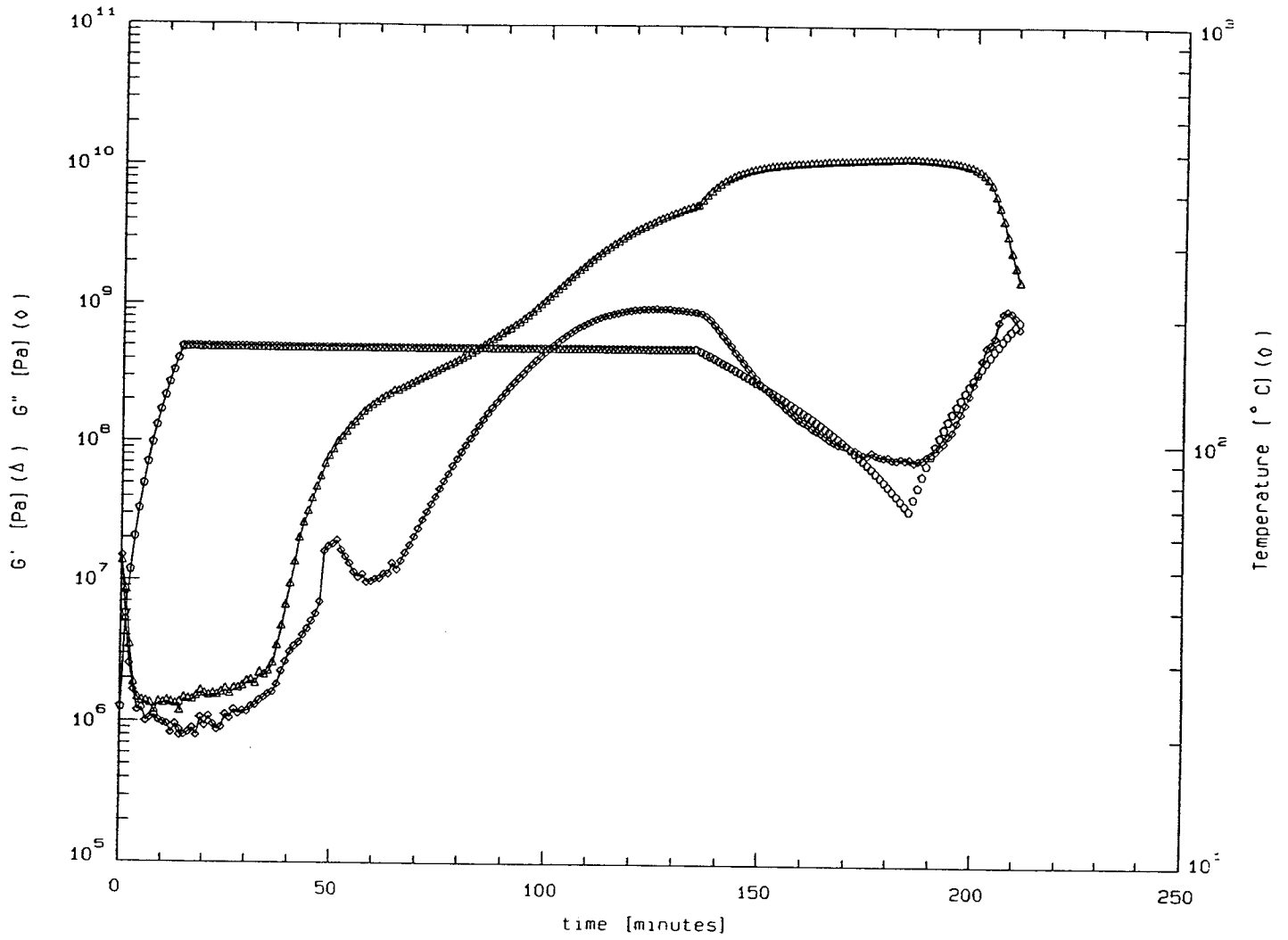


Figure 32a.

RDA record, torsion mode - temperature cycle and moduli  $G'$  and  $G''$ .

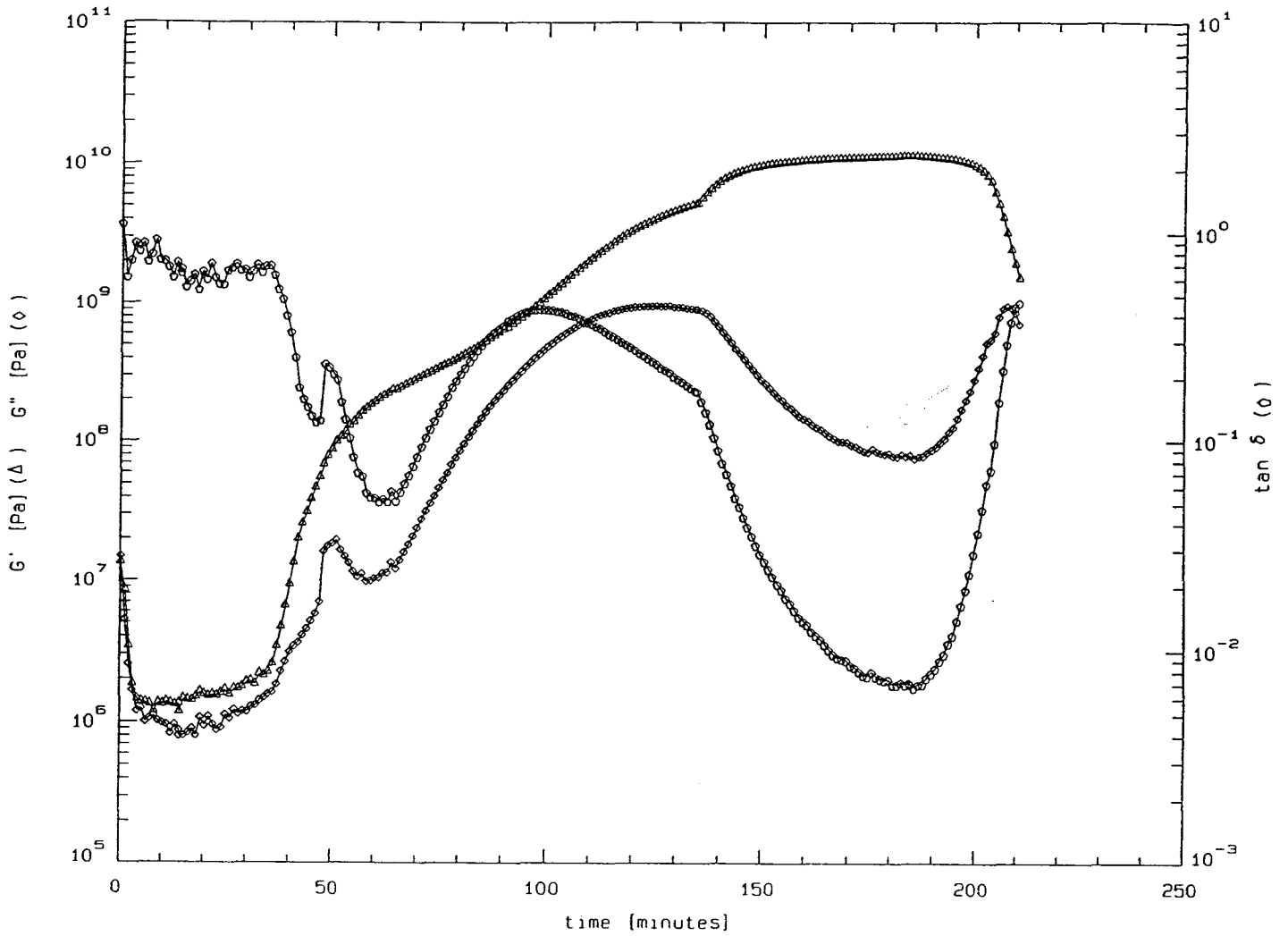


Figure 32b

RDA record, torsion mode - moduli  $G'$ ,  $G''$  and loss tangent.

Table 1.

Gelation Point - Experimental Data.

Experiment	Temperature at gelation ( C)	Time of gelation (min)	Degree of conversion at gelation
140°C /30 min	140	not gelled	not gelled
170/140° /180 min	140	60	0.31
170° /60 min (A)	170	40	0.31
170° /60 min (B)	170	41	0.32
170° /120 min (A)	170	40	0.31
170° /120 min (B)	170	42	0.32
190° /180 min (A)	190	29	0.35
190° /180 min (B)	190	30	0.36

Table 2.

Vitrification - Experimental and Theoretical Data.

Experiment	Time of vitrification  (min)	Degree of conversion	Temperature at vitrification  °C	Theoretical temperature of vitrification  °C
140°C/30 min	-	0.1	0	2.9
170/140°C/180 min	250	0.56	76.5	73.0
170°C/60 min (A)	103	0.59	108.0	79.0
170°C/60 min (B)	83	0.57	95.5	74.9
170°/120 min (A)	143	0.74	100.0	114.0
170°C/120 min (B)	202	0.76	104.0	119.0
190°C/180 min (A)	204	0.94	162.0	176.0
190°C/180 min (B)	233	0.94	112.0	176.0

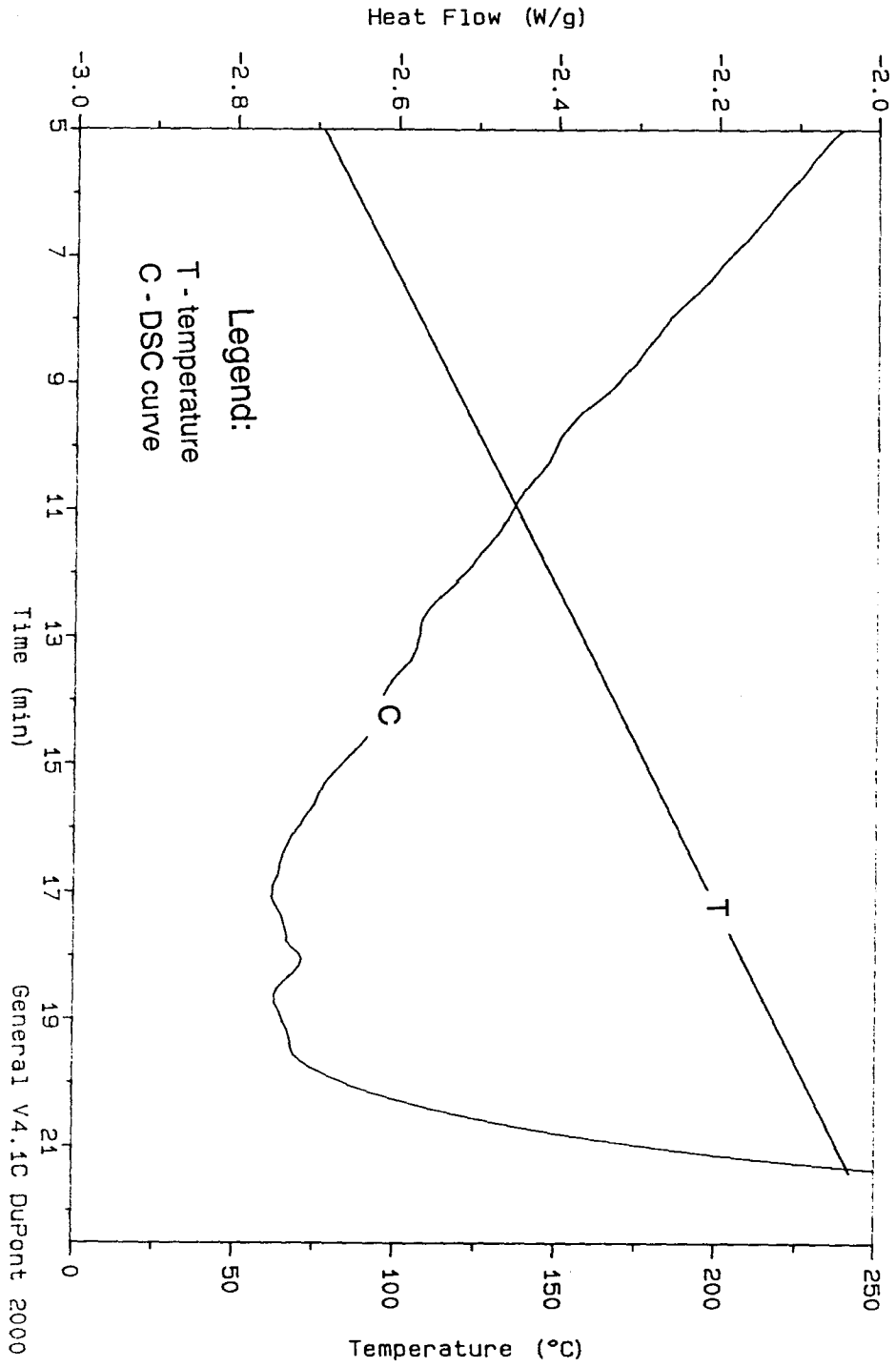
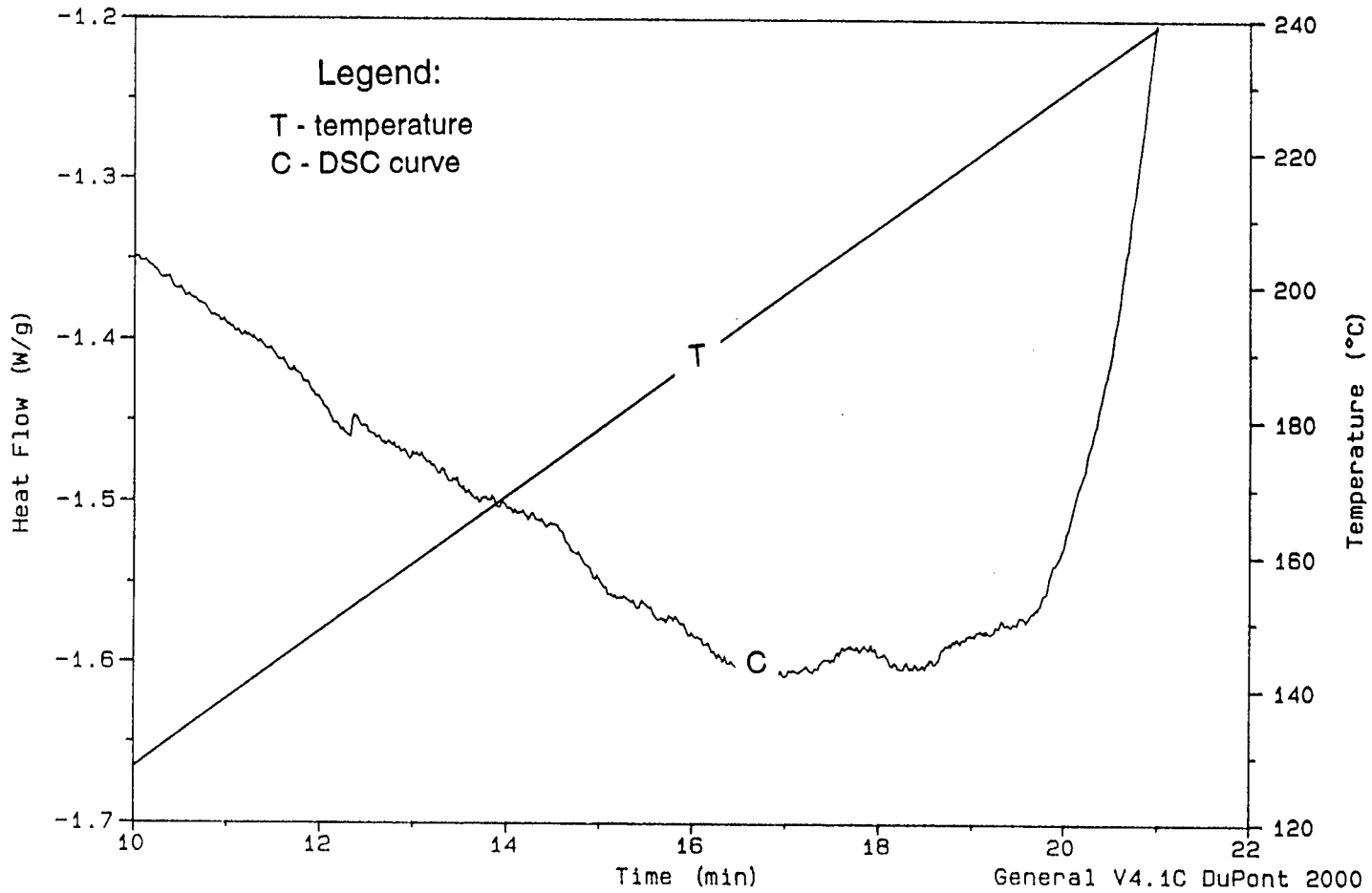


Figure 33.

DSC record, rate of temperature increase 10°C/minute.

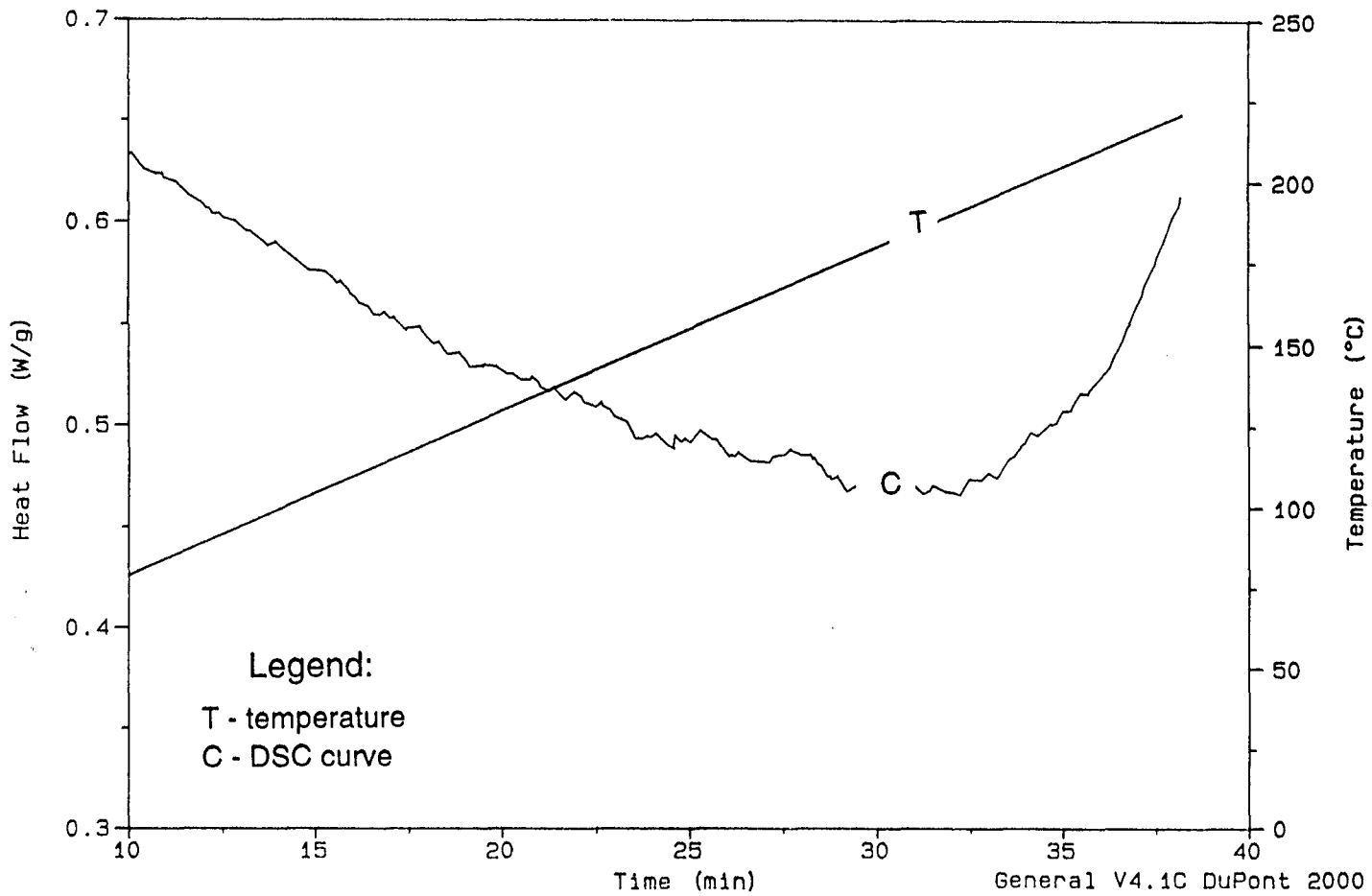
DSC record, rate of temperature increase 10°C/minute.

Figure 34.



DSC record, temperature increase 5°C/minute.

Figure 35.



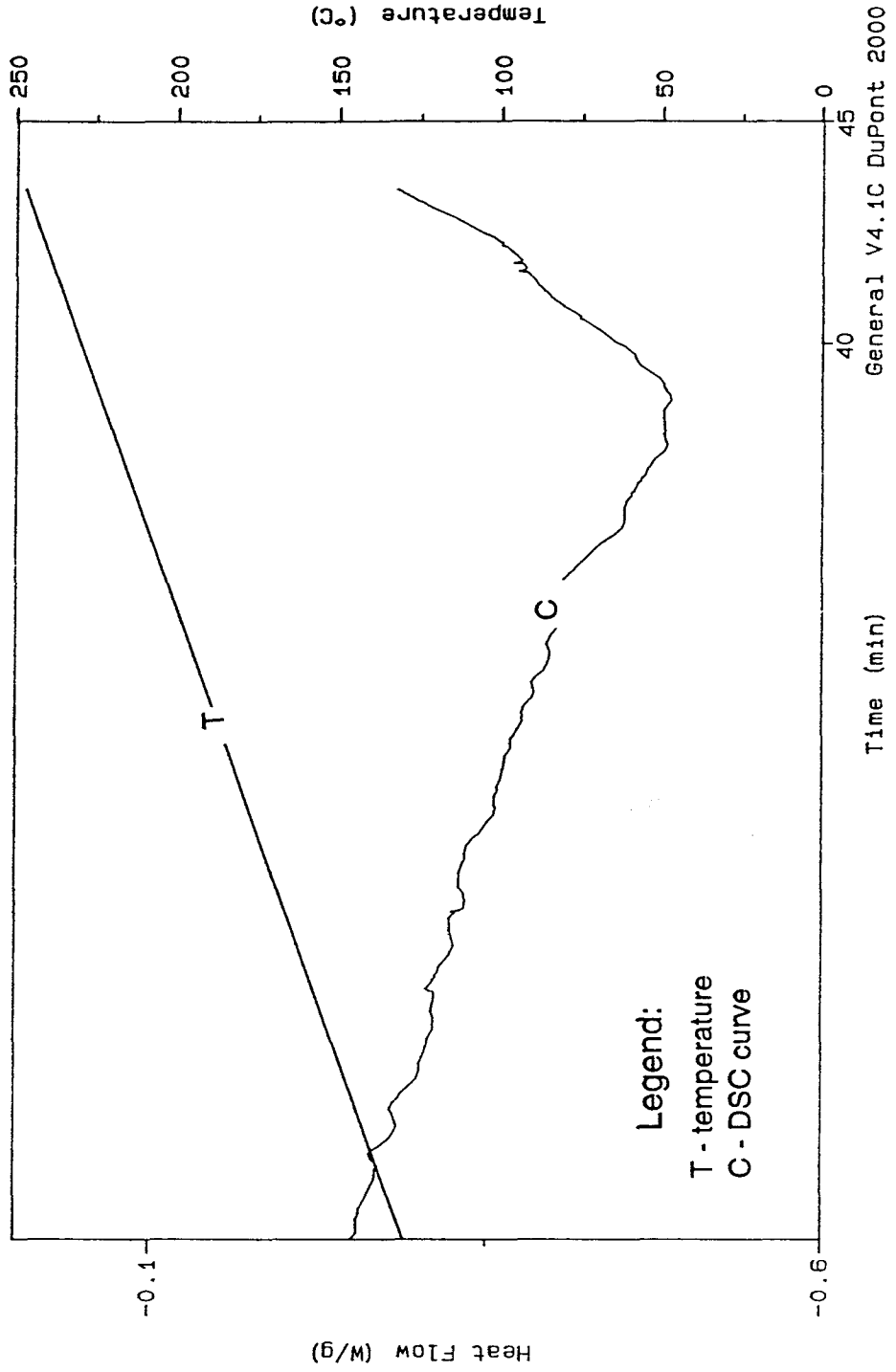


Figure 36.

DSC record, temperature increase 5°C/minute.

## 5. CURE DIAGRAMS

### AS A METHOD OF DISPLAYING INFORMATION OF RHEOLOGICAL CHANGES IN MATERIAL UNDER PROCESSING

#### 5.1 Gilham's T-T-T and C-H-T Diagrams

There are at least four possible states of the thermoset system, depending on temperature and degree of conversion; liquid, sol glass, gel rubber and gel glass. The transition in the state of material can be conveniently shown in the Gillham's T-T-T and C-H-T diagrams in time of processing versus temperature coordinates. The T-T-T diagram for isothermal curing is the better known of the two. Isothermal curing ensures a unique relationship between time of processing and degree of conversion for any temperature of processing, resulting from the kinetics of conversion implicitly incorporated into the diagram. The time of processing also represents the degree of conversion for a given temperature. As a result the degree of conversion could be eliminated as an independent variable, leaving only two; time and temperature.

It should be stressed that the T-T-T diagram shown in Figure 37 can be read only horizontally, and that shifting from one isotherm to another is not permissible in the diagram (unless certain additional procedures are employed). It may be noticed from the diagram that the gelation curve is of the decreasing exponential type, while the curve of vitrification is roughly 'S' shaped. It should also be remembered that vitrification causes a drastic slow-down of kinetics of conversion and under real conditions of processing often marks an end to further conversion.

At the beginning of processing, when the degree of conversion is low, the resin is in the liquid, ungelled state, unless the temperature is below the temperature of vitrification of an unprocessed resin,  $T_{g0}$ . For a low processing temperatures (below  $T_g$  gel) the vitrification comes first, before

gelation. For higher processing temperatures, the gelation comes first, leading to the formation of an unvitrified gel (gel rubber). Further processing in this range of temperatures results in vitrification of a resin, which occurs when the horizontal isothermal line of processing crosses the curve of vitrification. Physically,  $T_g$  is a property of a material and in thermosets is not a constant, but a function of the degree of conversion. With the progress of processing the  $T_g$  of a material rises, until it becomes equal to the temperature of processing. At this moment vitrification takes place. If processing continues, conversion, although very slow, still increases, and the  $T_g$  of a material becomes higher than the processing temperature, advancing the material deeper into the glassy state.  $T_g^\infty$ , the upper limit to which the  $T_g$  may proceed with the progress of conversion, corresponds to a fully converted resin ( $\alpha=1$ ). For temperatures of processing slightly below  $T_g^\infty$ , extended processing after vitrification may lead to full cure (the line of processing reaching the curve of full processing in the diagram). The diagram suggest that the only way of fast processing of a material to the level of full cure is to avoid the vitrification-related slow-down by applying (at least temporarily) a temperature of processing higher than  $T_g^\infty$ . However, the T-T-T diagrams show the danger of such a procedure through an existence of yet another curve - the line of upper devitrification. This is, in fact, the curve of material destruction, and can be reached even as a result of extended processing below  $T_g^\infty$ .<sup>22,23,24,26,27,28</sup>

The most important value of T-T-T diagrams is the understanding of the process that they provide. The advantage of the diagrams is that the kinetics of conversion is incorporated into the diagrams, so that the required time for processing, or time for characteristic events to occur may be read directly for a given temperature of isothermal processing. Moreover, the possibility of adding new features was suggested by Gillham<sup>27,53</sup> - the contours of iso-alpha, or iso- $T_g$ . These contours allow the shifting from one isotherm to another on the graph at different temperatures, making the diagrams more universal.

There is also another advantage of the diagrams related to the process of their creation. Since the use of the TBA technique allows for the identification of the moment of gelation as well as vitrification, within one experiment involving a continuous process of isothermal curing, the experiment conducted at any temperature level yields two characteristic points for the diagram, one belonging to gelation, the other to the vitrification curve. Using different temperatures of processing, the curves of gelation and vitrification can be determined, without involving the degree of conversion measurements, which may be difficult to determine for a slow progress of a reaction at low temperatures.

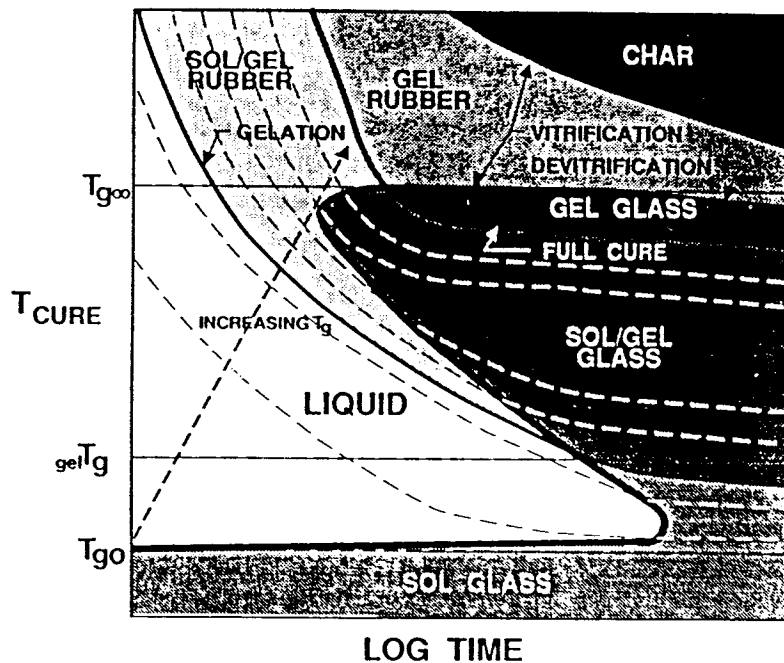


Figure 37.

Isothermal Time Temperature Transformation (TTT) Cure Diagram

In order to further expand the applicability of the T-T-T diagram - the Continuous Heating Transformation (CHT) diagram was proposed. The diagram is built in the same way as T-T-T diagrams, and contains the same information, except that it is valid for heating with a linear temperature increase rather than for isothermal heating.<sup>71,72,73</sup>

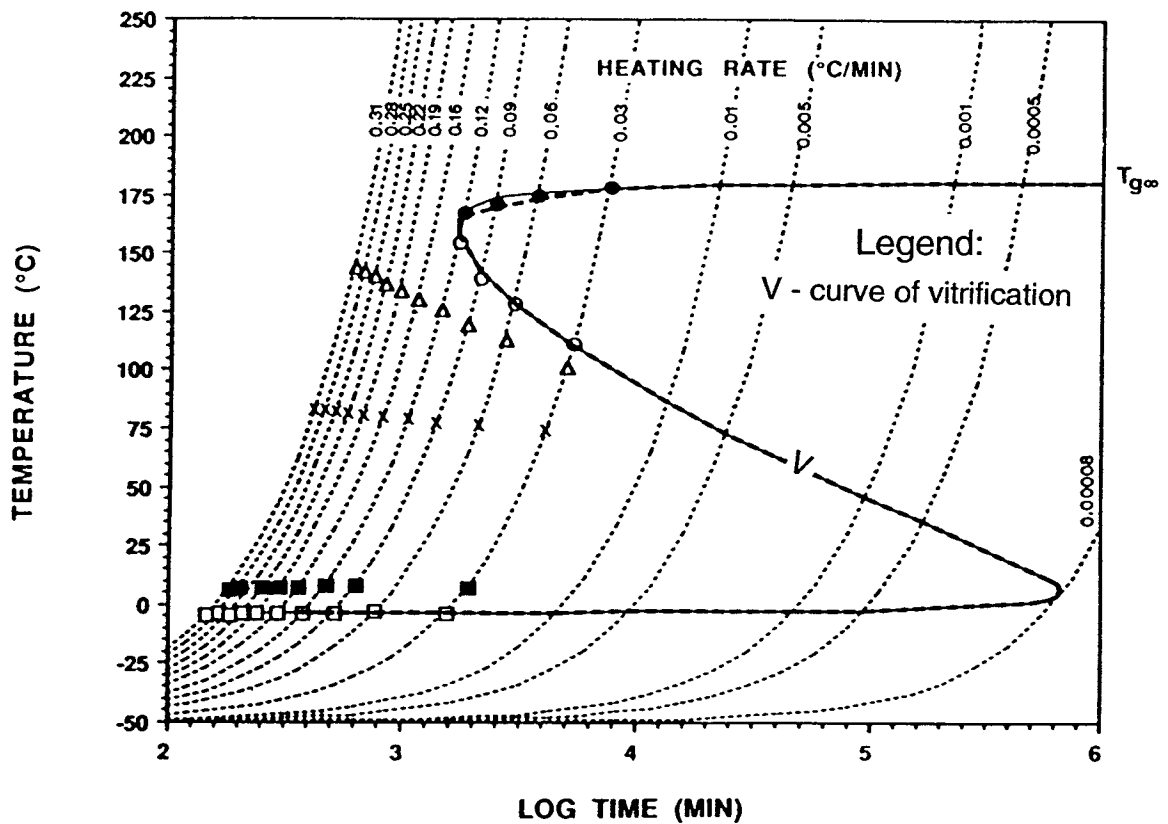


Figure 38.

Continuous Heating Transformation (CHT) Cure Diagram

## 5.2 $\alpha$ -T-T Diagram - The Concept

Despite the mentioned advantages, the Gilham's diagram is not as suitable as an element of modelling of thermoset processing as it is for isothermal processing. Even if thermal cycles applied in processing are isothermal, the resulting temperature history at locations distant from the tool may not be isothermal. The changes in the kinetics of resin conversion are more likely to happen than the changes in rheology. In the case of altered kinetics, the Gilham's diagrams lose their validity, since the kinetics is a built-in element of their structure. If, however, the kinetics could be somehow separated from resin rheology in the process of diagram creation, only the kinetics would have to be adjusted.

The proposed concept of an algorithm that could be applied to any processing cycle stems from the fact that the point of gelation and the point of final vitrification for a resin system can be easily expressed as a function of the degree of conversion and temperature. Gelation is expected to occur at a constant value of conversion, while the point of vitrification is conveniently described by the DiBenedetto equation<sup>49</sup>. Both curves may be plotted on the grid of the degree of conversion versus temperature of processing. In order to place the point of processing in the same figure, its coordinates, the momentary temperature of processing and degree of conversion, must be determined. The latter can be calculated only if the model of the kinetics of conversion is available. The method does not require isothermal conditions of processing, but the display it produces is inferior to Gilham's diagram. Due to the system of coordinates used in the diagram, the time of processing cannot be read directly from the graph produced, and the curve of upper devitrification from Gilham's diagram cannot be easily incorporated into the graph.

The objective of this work was to create an algorithm based on the presented concept, while looking for improved forms to comprehensively display the complex information produced. The research

effort resulted in the development of a system that calculates and graphically presents the progress of thermoset processing. The system can be applied to non-isothermal processing and accounts for the degree of conversion as well as phase changes in a material. The newly proposed diagrams reintroduce time into their system of coordinates.

### 5.3 Structure and Operation of the Proposed System

In order to build the proposed system for a new material, three elements are needed: gelation and vitrification curves, expressed as a function of the degree of conversion,  $\alpha$ ; the kinetic model of conversion; and diagrams displaying the information of the two previously mentioned elements in a clear and an efficient fashion. All these elements and their interaction are presented in Figure 39. For any specific time and temperature history, the kinetic model employing numerical integration calculates the momentary degree of conversion. The momentary temperature of processing,  $T$ , provides the remaining coordinate of the point, representing the state of processing in the  $\alpha$ - $T$  coordinate system.

The system presented here is developed for the Narmco resin. For this material, there exists an excellent mathematical model of the kinetics of conversion, developed by Cole<sup>15,16</sup>, based on a mechanistic approach, which was incorporated into the system. The value of conversion at gelation and the parameters of the DiBenedetto vitrification curve were adopted from various literature sources.<sup>6,7,8,34,67,68</sup> Both gelation and vitrification parameters were further verified experimentally, as presented in the previous chapter.

In order to develop the system for any other resin the parameters in the rheological element of the system have to be adjusted and the model of kinetics of conversion has to be replaced, perhaps completely. There are no specific requirements concerning a model of conversion to be incorporated into the system. However, the accuracy of the model will affect the accuracy of the system. In the absence of a mechanistic model of kinetics the possibility exists of experimentally fitting one of existing simplified expressions, using the DSC technique.

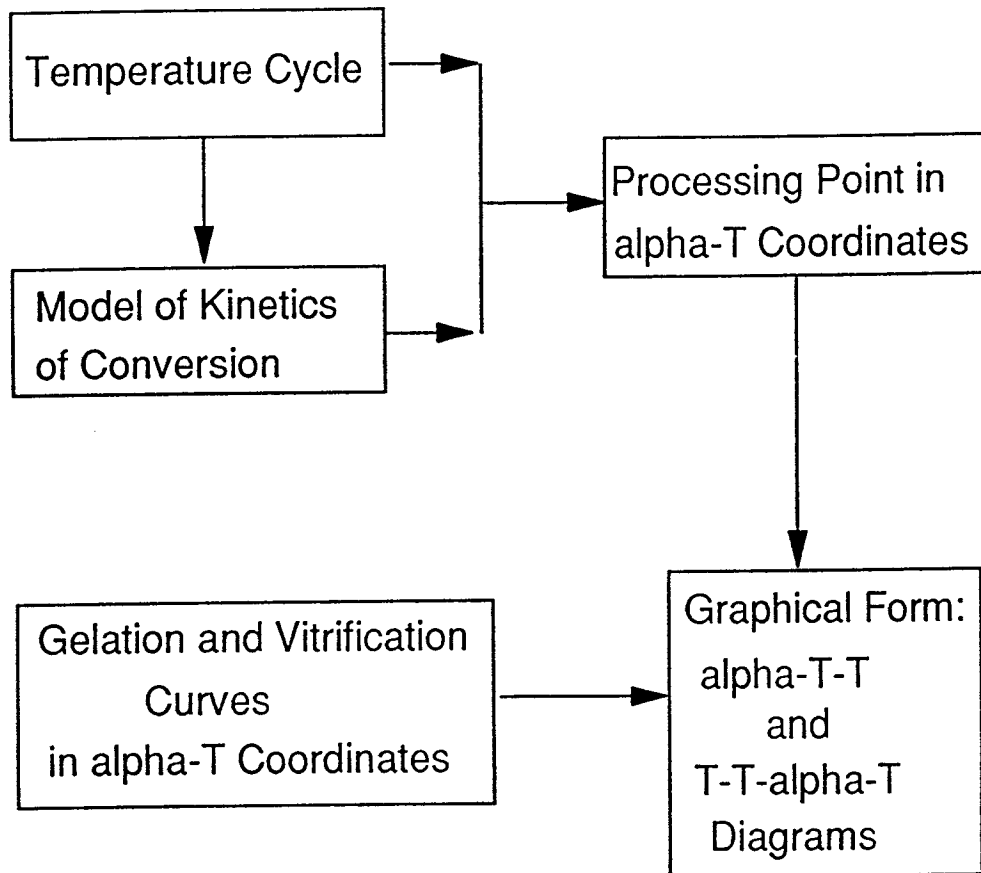


Figure 39.  
Structure of the system

#### 5.4 Interaction of the Proposed System With a Thermal Model of Composite Processing.

During a curing process, a material is exposed to an elevated temperature and pressure for a specific length of time. The modelling of composite processing consists of at least two main models: heat transfer and resin flow. In a typical processing arrangement, the temperature is applied to a heating tool adjacent to one side of a composite, while the other side is insulated by a bleeder and a vacuum bag. Due to low thermal conductivity of a material and strong exothermic effect of the chemical reactions, the temperature in the material differs from location to location. The most pronounced difference is one between the temperature in the material adjacent to the heating tool and the temperature on the far-side of the location; this difference depends on the overall thickness of the composite. The difference is visible even for a composite a few millimeters thick, and becomes significant for a thicker one, thereby creating a need for modelling of this thermal phenomenon. Any thermal model requires information on the exothermic reaction of conversion and in this way, depends on material-related information. The interaction of a thermal model of composite processing and the system presented here is shown in Figure 40. The temperature cycle applied to a heating tool provides boundary conditions for a heat transfer model, which in turn calculates the temperature distribution across material. A conversion kinetics model, interacting with other elements of the system, utilizes the temperature distribution to calculate local rates of conversion, which are used by a heat transfer model and treated as heat sources. The conversion model numerically integrates the rates of conversion to calculate the momentary degree of conversion for different locations in the composite.<sup>52</sup>

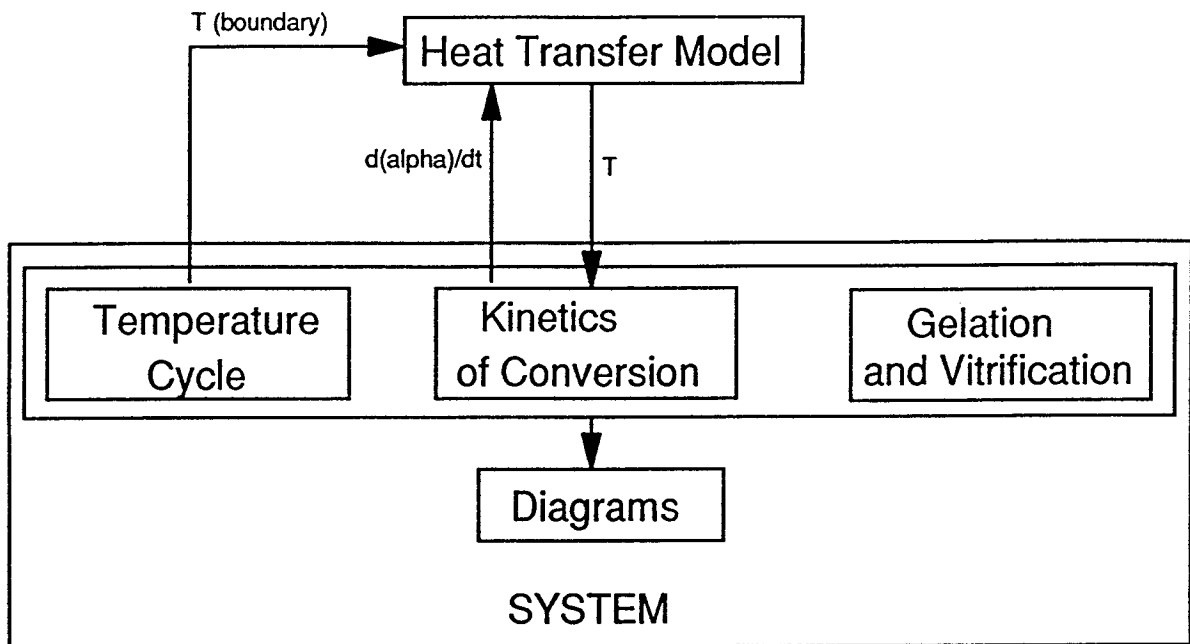


Figure 40.

Interaction of the proposed system with a thermal model

### 5.5 $\alpha$ -T-T and T-T- $\alpha$ -T Diagrams - Graphical Output of the System

In Figure 41 the results of the proposed system, obtained for a temperature cycle similar to that suggested by the producer, are displayed. The diagrams consists of three parts. Part I displays an assumed temperature cycle. In Part II this temperature history is used by a kinetic model of conversion to obtain the degree of conversion as a function of time. Part III presents the main part of the  $\alpha$ -T-T diagram which contains the curve of gelation (G), the curve of vitrification (V), the line of full cure, and the curve of processing (P). The curve of processing is marked with small circles. The marks are drawn for approximately 10 min time intervals, as a way to introduce time into Part III, which otherwise uses a conversion-temperature system of coordinates. The three-part diagram not only contains the complete information about a material under specific processing conditions, but the configuration of the graphs also provides an additional advantage. It allows for the determination of the time of processing for any point on the processing curve. This can be done either by drawing a vertical line from the point to the curve of conversion below (Part II) and then reading the time horizontally, or by drawing a horizontal line from the point on the temperature curve (Part I), and then reading time vertically. Usually only one of these two ways is practical.

It should be noted that even if the temperature cycle is fixed, there are still three parameters of processing in the diagram: time, temperature and degree of conversion. This is the reason why a complex alpha-T-T diagram consists of three different parts. Another option for representing an equivalent amount of information is to develop a three-dimensional image, as shown in Figure 42. The 'x' and 'y' coordinates are time and temperature, so that the thermal cycle of processing can be drawn in the base of the graph. The 'z' coordinate is the degree of conversion. The curves of gelation and vitrification take the form of surfaces. The thermal cycle of processing shown in Figure 42 is the same as that shown in Figure 41. Since surfaces of gelation and vitrification sometimes

obstruct the view of the processing curve, the same graph can be shown without the mentioned surfaces. This is done in Figure 43 where the curve of processing is produced exclusively. The non-continuities of the curve mark its cross-section with the gelation and vitrification surfaces.

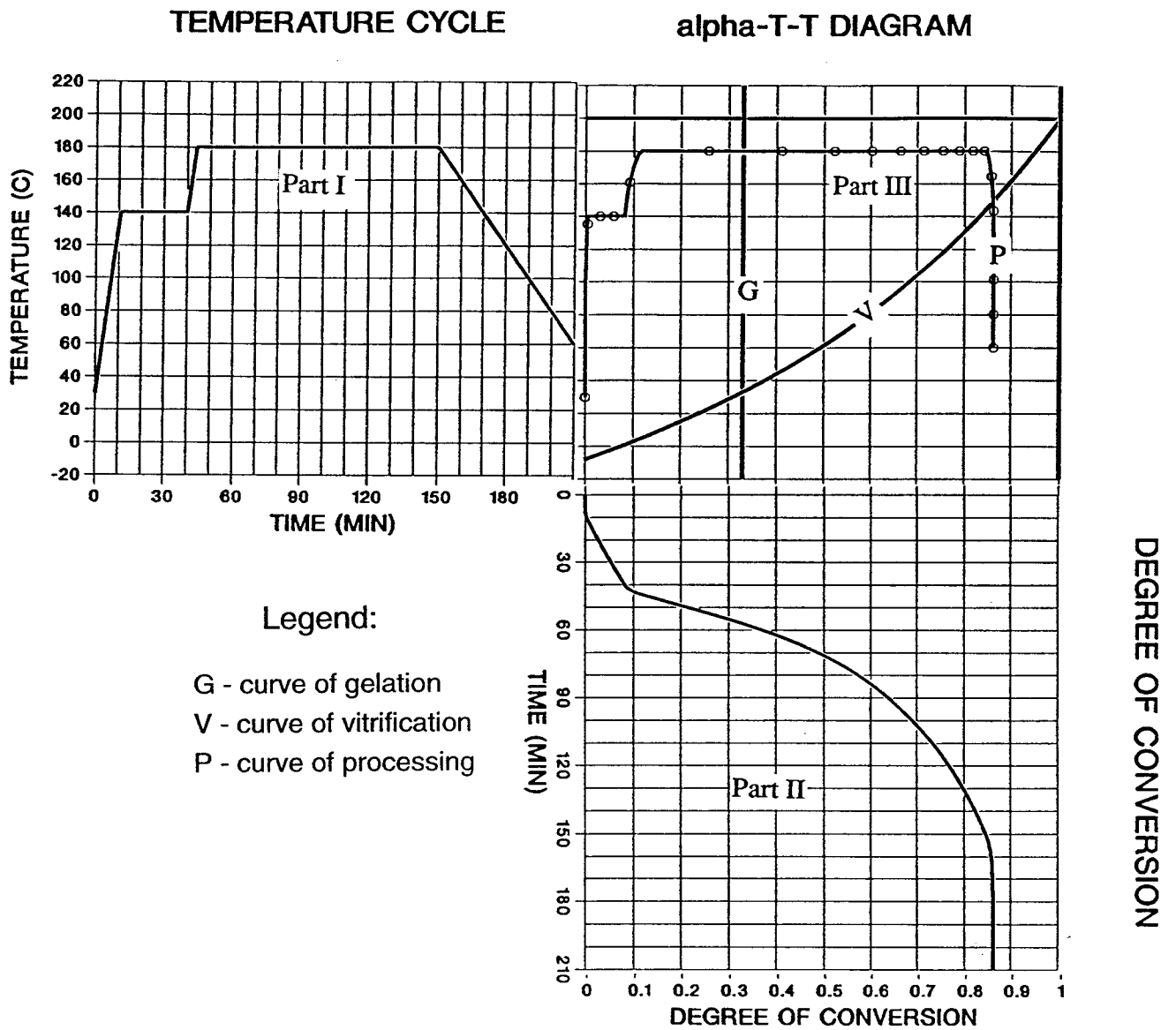
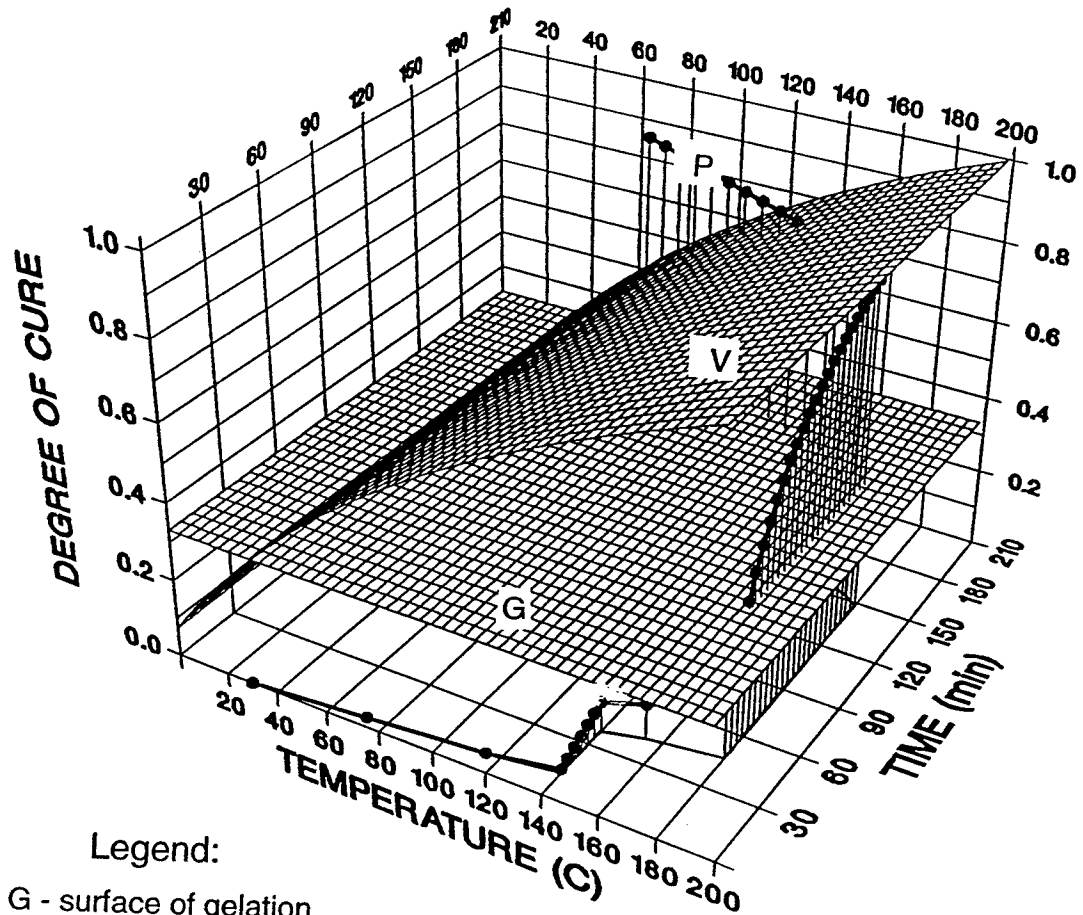


Figure 41.

Comprehensive  $\alpha$ -T-T diagram  
 for manufacturer suggested temperature cycle.



Legend:

- G - surface of gelation
- V - surface of vitrification
- P - curve of processing

Figure 42.

T-T- $\alpha$ -T diagram

for manufacturer suggested temperature cycle.

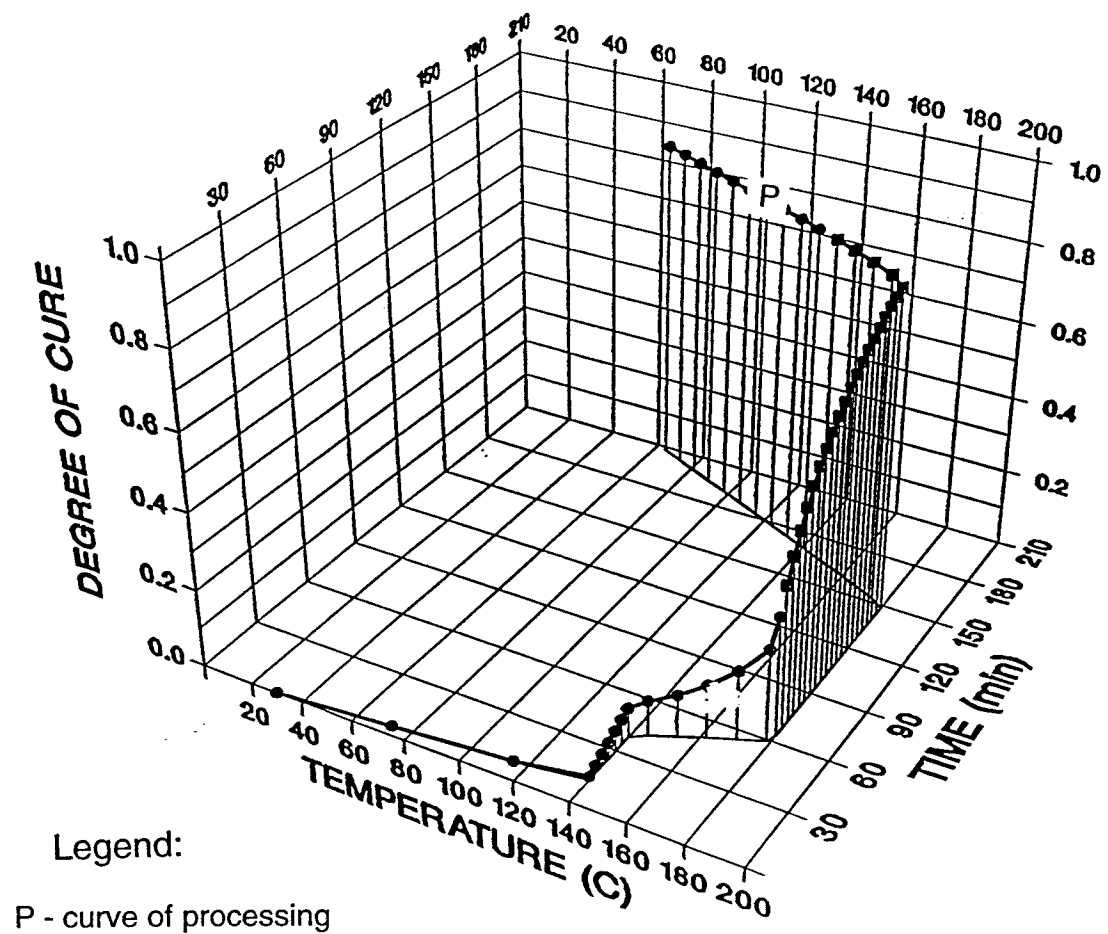


Figure 43.

T-T- $\alpha$ -T diagram without surfaces of gelation and vitrification

## 5.6 Applications

### 5.6.1 - RDA Tests

As it was mentioned in Chapter 4 of the Thesis, the major problem in completing RDA tests was a limited access to the apparatus. In order to maximize the utilization of the equipment a very detailed plan of experiments was required. This was made feasible by the use of the system and  $\alpha$ -T-T diagrams which allowed predictions of the moment of gelation and vitrification in advance, avoiding useless experiments, and eliminating any waste of time in a single experiment. The complete set of figures presenting alpha-T-T diagrams in tests is shown in Figures 44-51.

Test	Figure
140°C/30 min	in figures 44 a,b,c
170/140°C/180 min	in figures 45 a,b,c
170°C/60 min (A)	in figures 46 a,b,c
170°C/60 min (B)	in figures 47 a,b,c
170°C/120 min (A)	in figures 48 a,b,c
170°C/120 min (B)	in figures 49 a,b,c
190°C/180 min (A)	in figures 50 a,b,c
190°C/180 min (B)	in figures 51 a,b,c

Table 3.  
List of RDA experiments

In parts 'c' of the listed figures, points of gelation and vitrification identified from experiments are marked.

A typical example of processing is presented in Figure 50. Figure 50a shows the thermal cycle used in isothermal processing at temperature 190°C, and Figure 50c presents the progress of processing

in  $\alpha$  - T system of coordinates. The curve of processing in figure 50c is marked with small circles. The moment of gelation is expected to occur at an intersection of the curve of processing with a vertical line of gelation. However, according to RDA measurements, the gelation takes place slightly later, at the point marked as 'G'. At an advanced stage of processing in its isothermal part, the increasing density of circles in the curve of processing indicates a rapid slow-down of conversion, caused by the fact that the processing curve approaches the curve of vitrification. Vitrification phenomenon is expected to occur during final cooling of the resin, when the processing curve crosses the vitrification curve. The moment of vitrification as determined from RDA experiments, however, comes a little later. Its location on the curve of processing is marked by 'V'.

Figures 44 a,b,c show that the experiment 140°C/30min was designed for the investigation of rheological behavior of a resin at a very low level of conversion, processed at a low temperature. Consequently, no gelation phenomena is recorded, and special cooling arrangements are required for resin vitrification. Figure 45 shows the processing at 170°C/140°/180m in which is supposed to reach gelation at a low temperature of processing. However, in order to accelerate the process of conversion, and to make the experiment shorter, the elevated temperature of 170 C is applied at the beginning, and reduced later in the process, before the important transitions take place. The series for processing at 170 C are conducted for two different lengths of processing: 1h (Figure 47) and 2h (Figure 48) to investigate the conditions in the vicinity of the manufacturer-suggested cycle. Finally, the experiments using the processing at 190 C for an extended period of time (Figure 50 and 51) were designed to explore the behavior of a material which is being converted to a very high degree with the use of very high temperature.

$\alpha$ -T-T Diagrams provided, in advance, the information of temperature cycles, yielding a full range of processing conditions. Without the support of the diagrams the described variety of processing would not be achieved in such a limited time.

## TEMPERATURE CYCLE

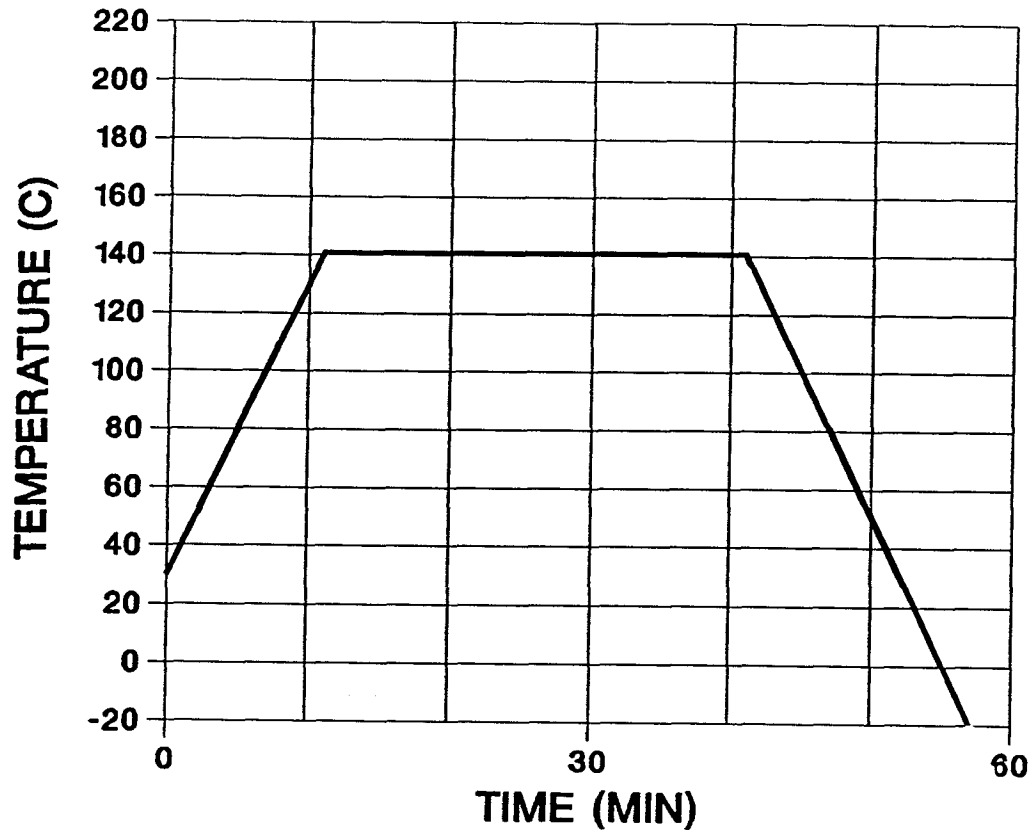


Figure 44a.

Temperature cycle in test 140°C/30 min.

## DEGREE OF CONVERSION

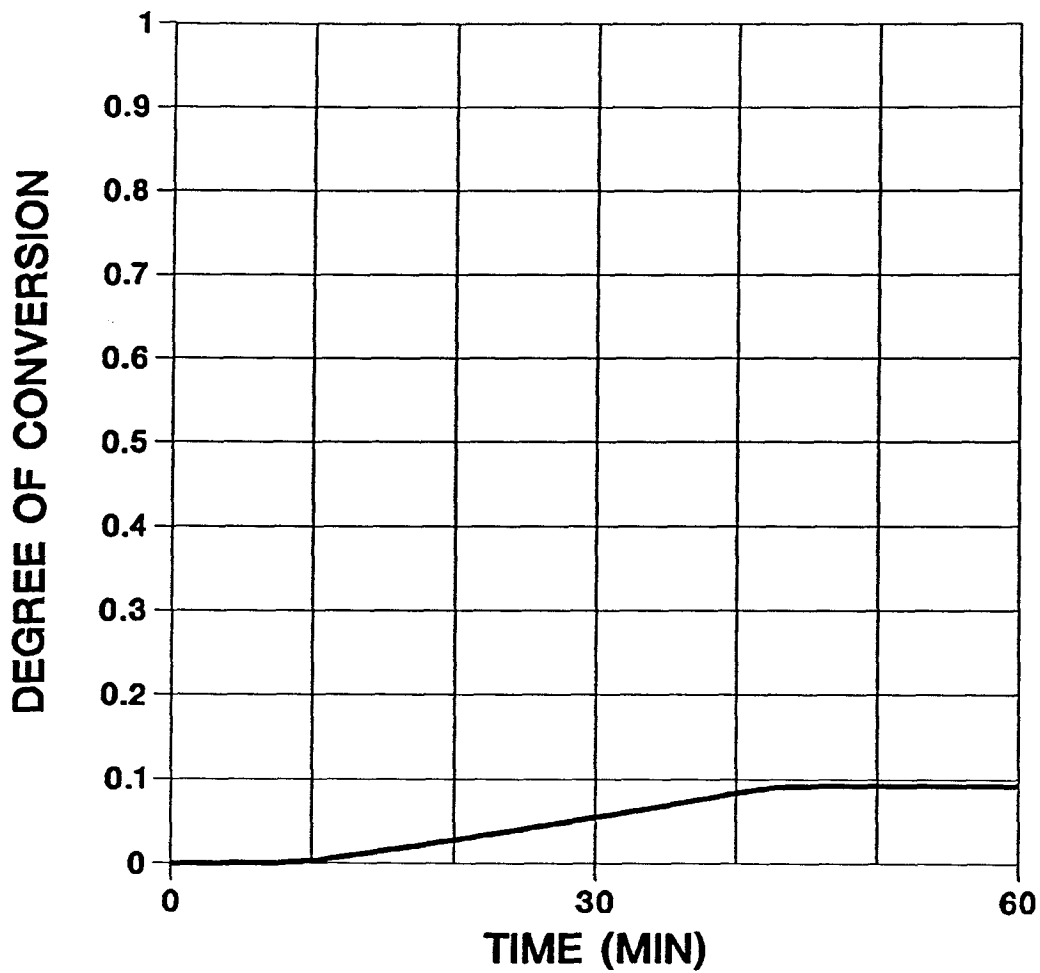
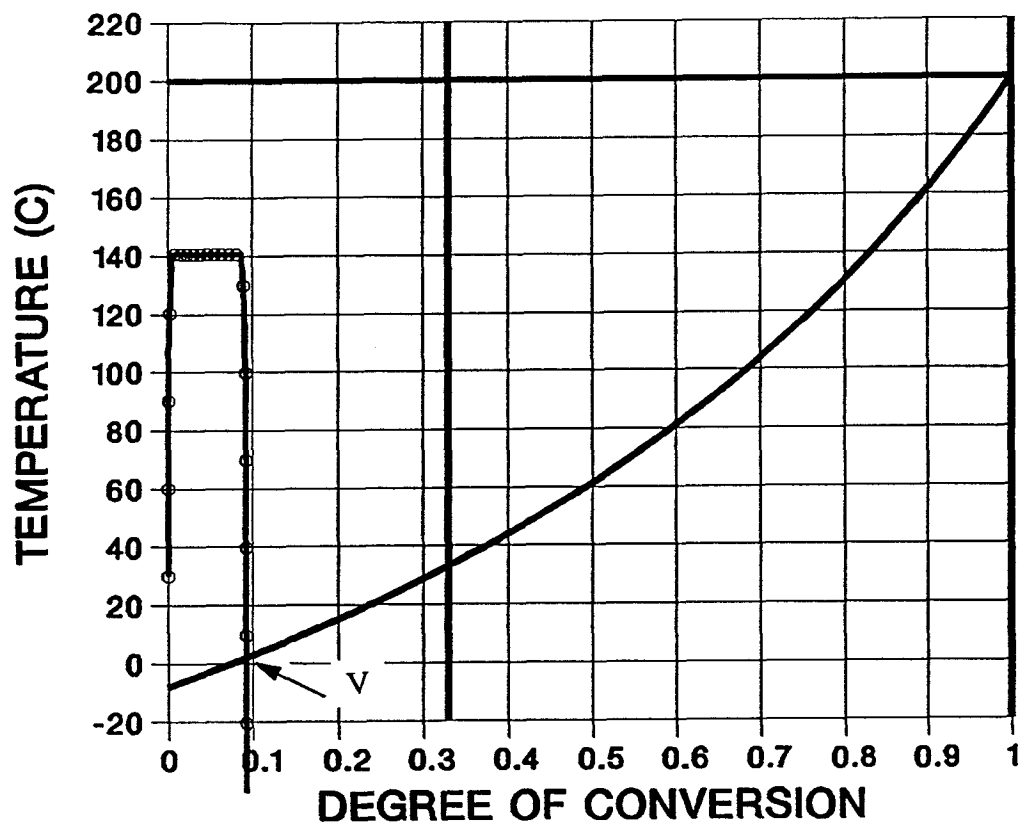


Figure 44 b.

History of degree of conversion for test 140°C/30 min.

## alpha-T-T DIAGRAM



Legend:

V - experimental vitrification

Figure 44c.

$\alpha$ -T-T diagram showing processing curve for test 140°C/30 min.

## TEMPERATURE CYCLE

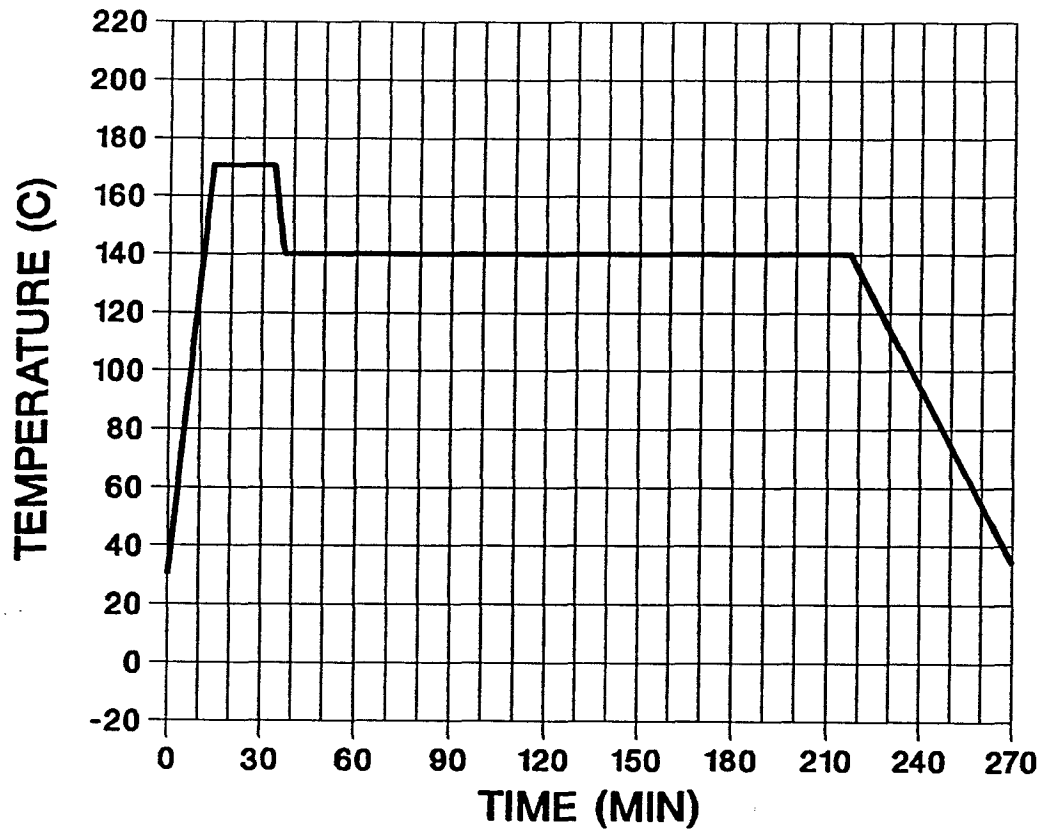


Figure 45a.

Temperature cycle for test 170°C/140°C/180 min.

## DEGREE OF CONVERSION

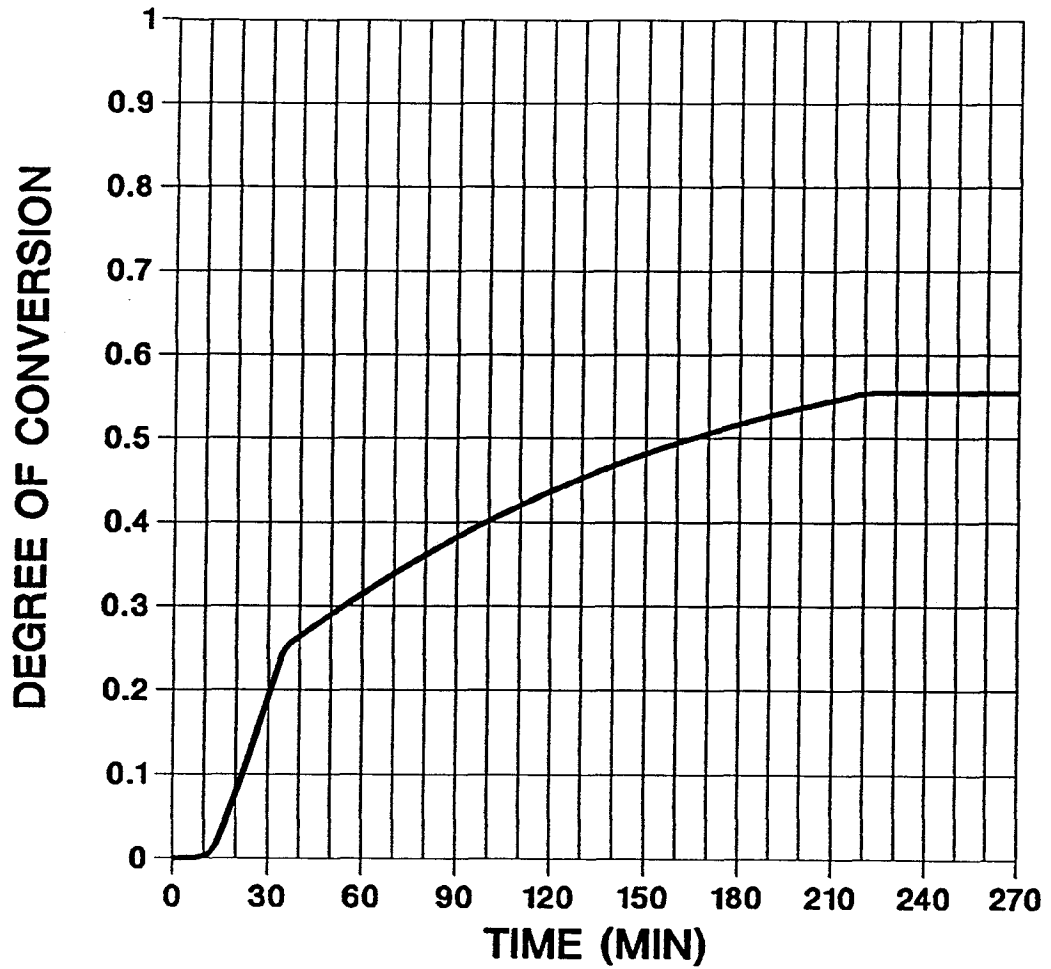


Figure 45b.

History of degree of conversion in test 170°C/140°C/180 min.

## alpha-T-T DIAGRAM

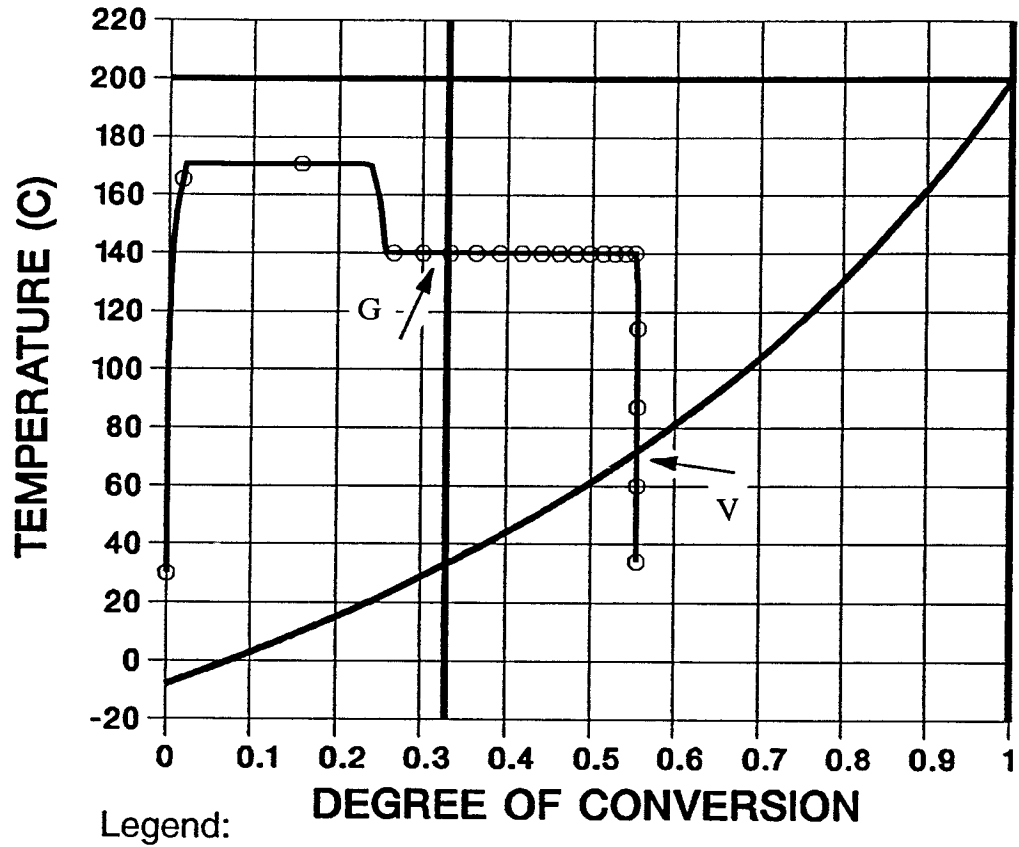


Figure 45c.

$\alpha$ -T-T diagram showing processing curve in test 170°C/140°C/180 min.

## TEMPERATURE CYCLE

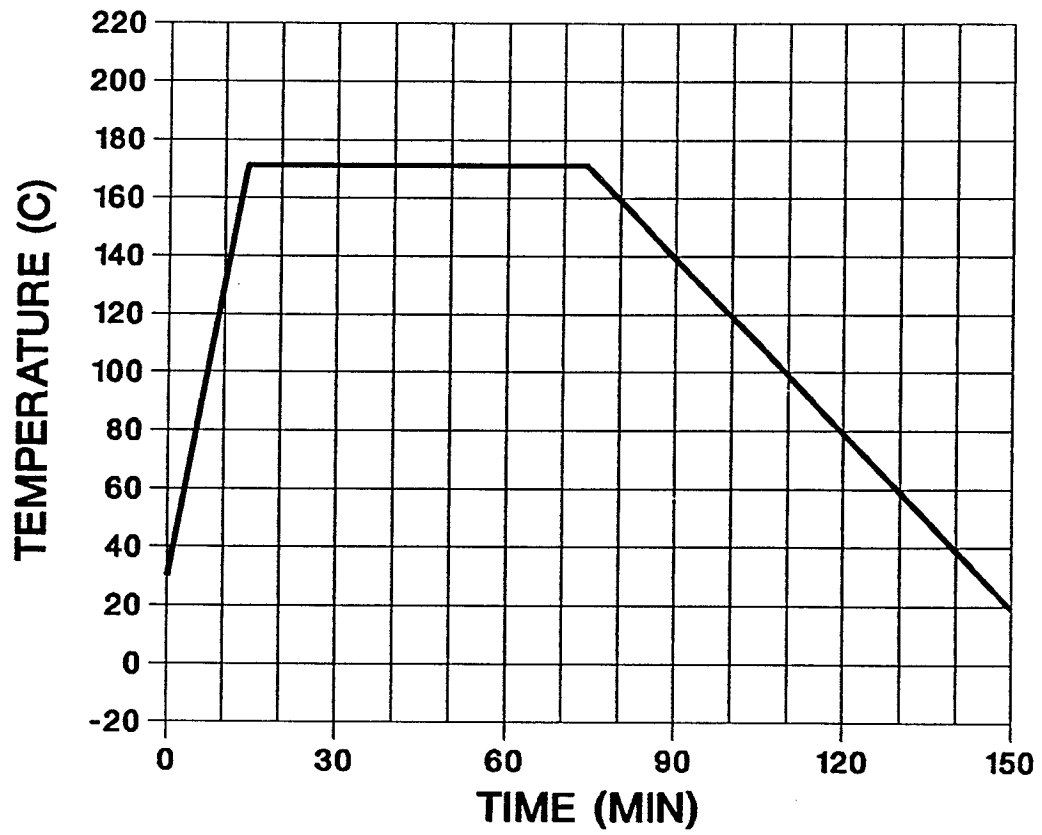


Figure 46a.

Temperature cycle in test 170°C/60 min (A).

## DEGREE OF CONVERSION

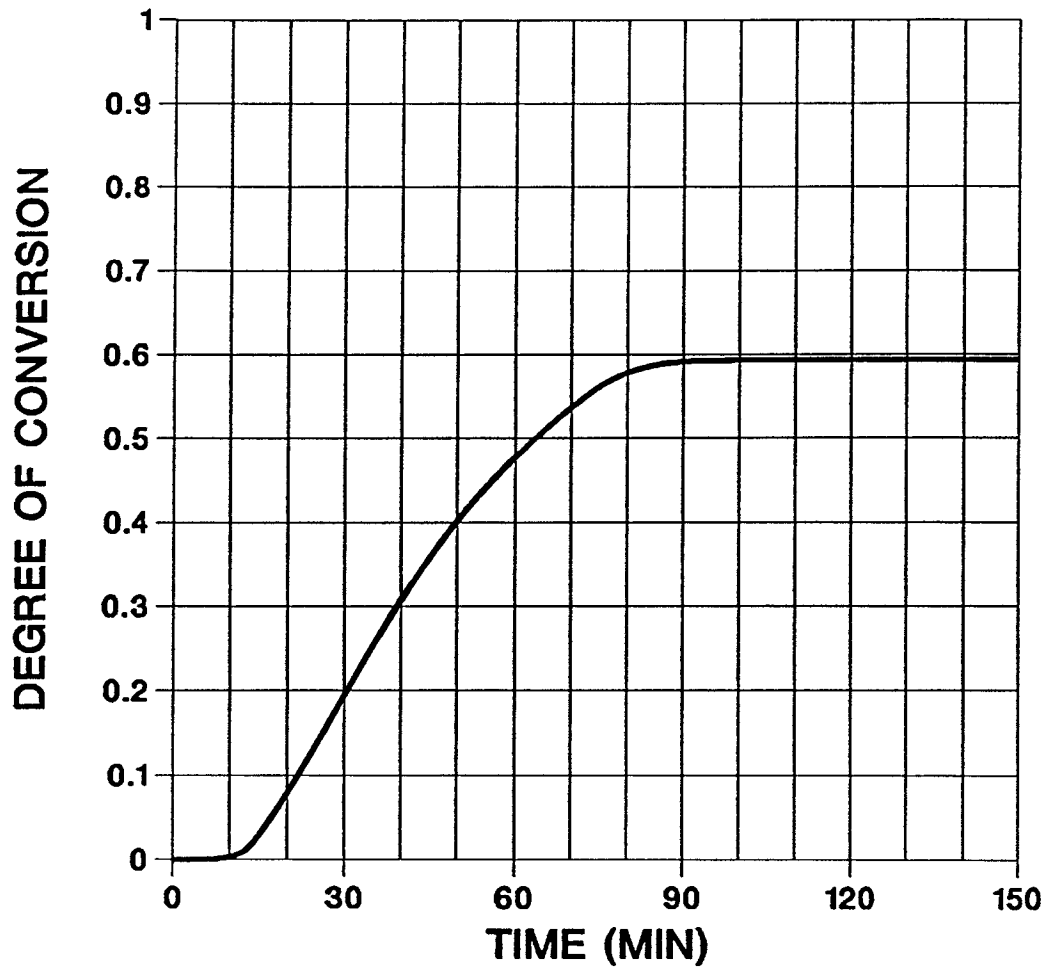
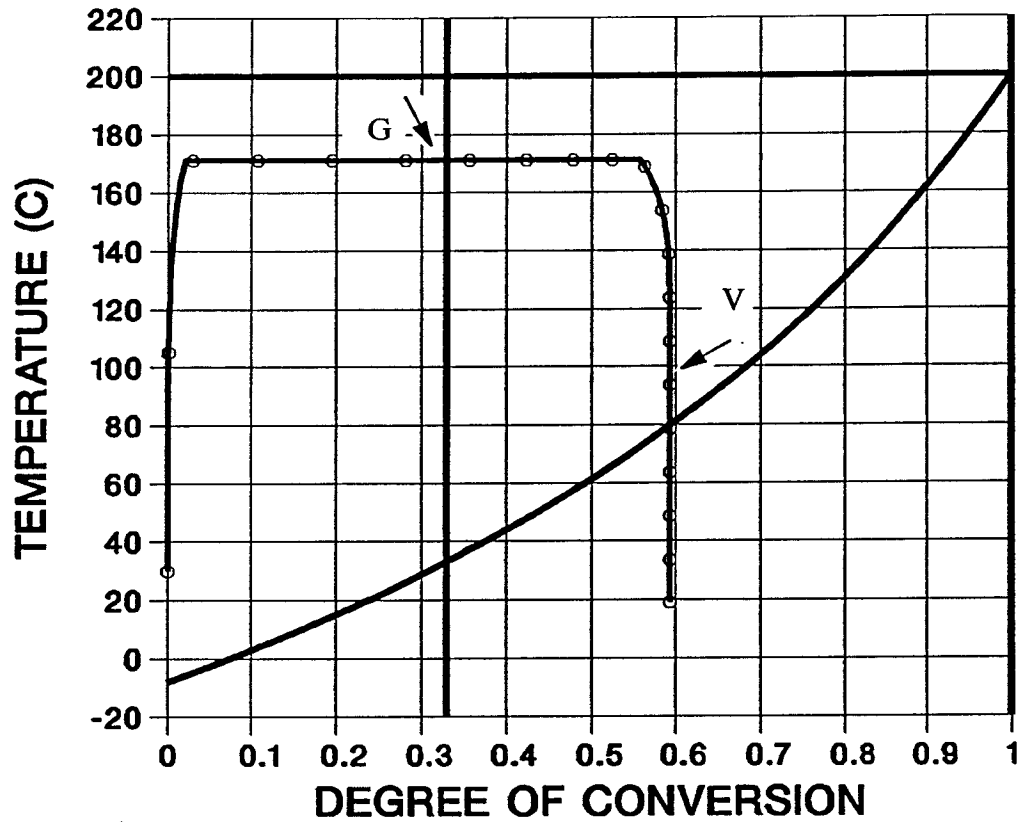


Figure 46b.

History of degree of conversion in test 170°C/60 min (A).

## alpha-T-T DIAGRAM



Legend:

G - experimental gelation

V - experimental vitrification

Figure 46c.

$\alpha$ -T-T diagram showing curve of processing in test 170°C/60 min (A).

## TEMPERATURE CYCLE

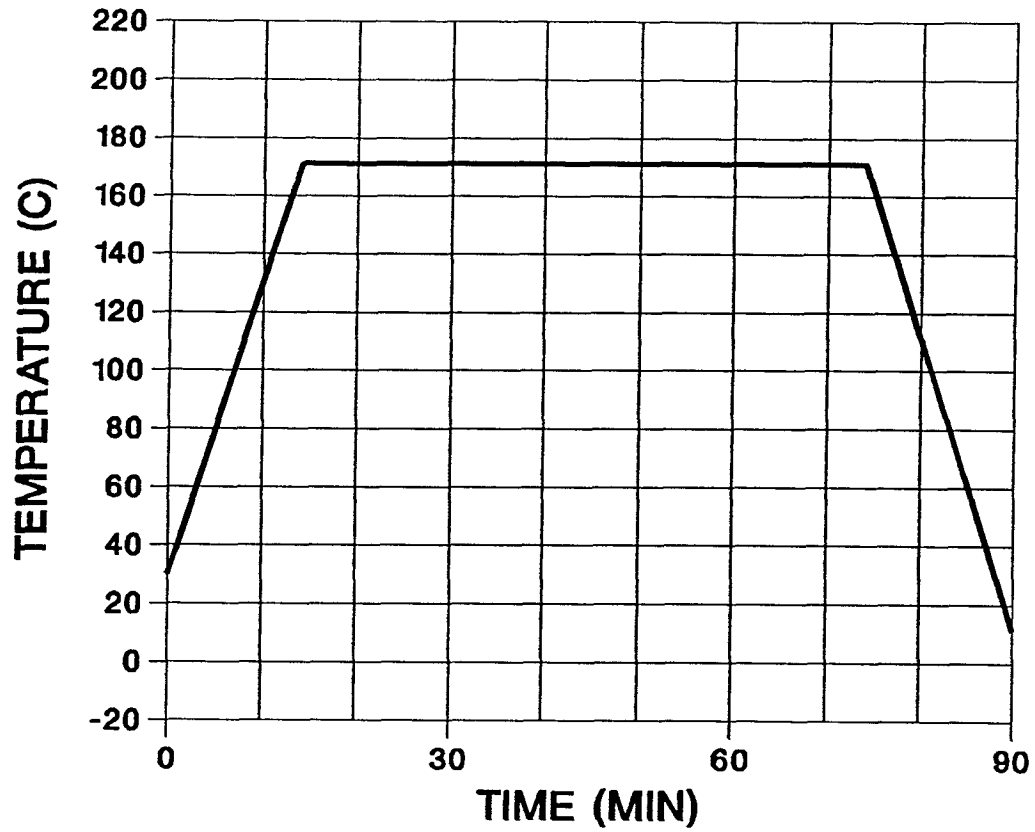


Figure 47a.

Temperature cycle in test 170°C/60 min (B).

## DEGREE OF CONVERSION

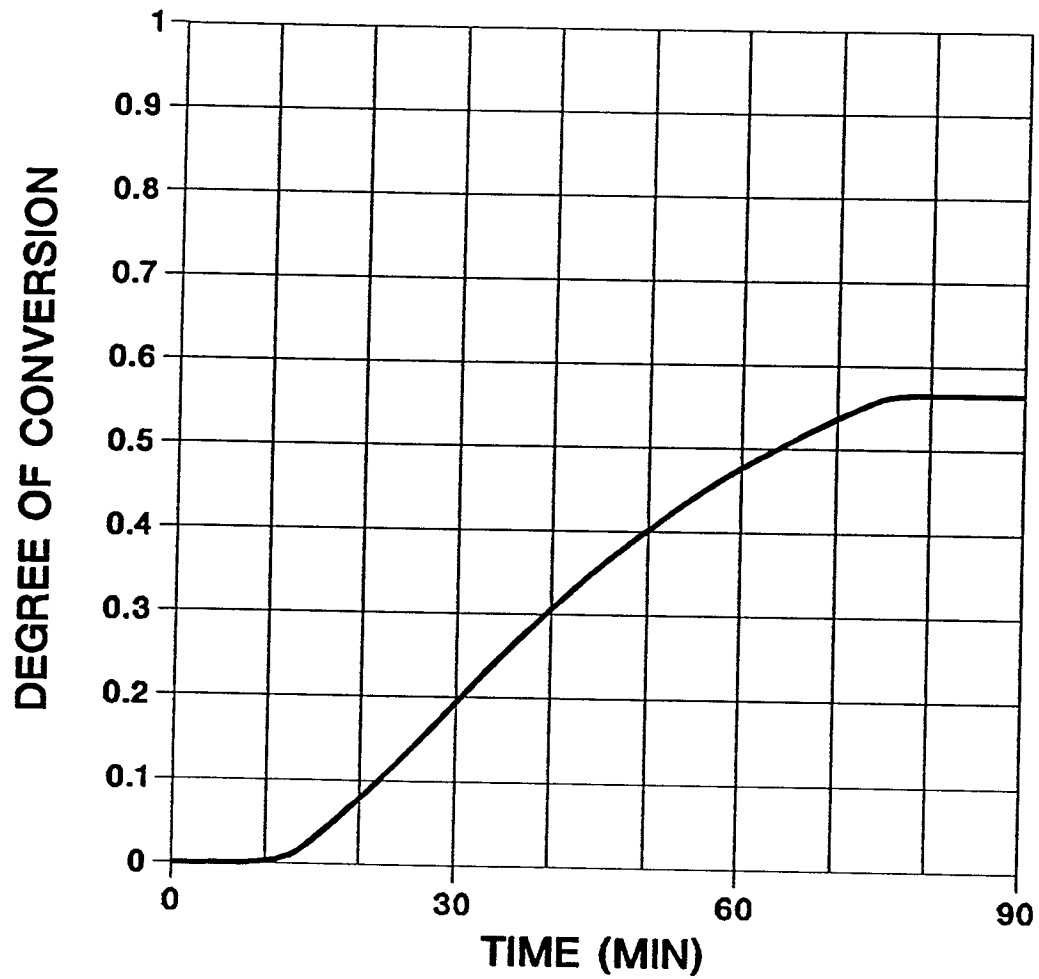
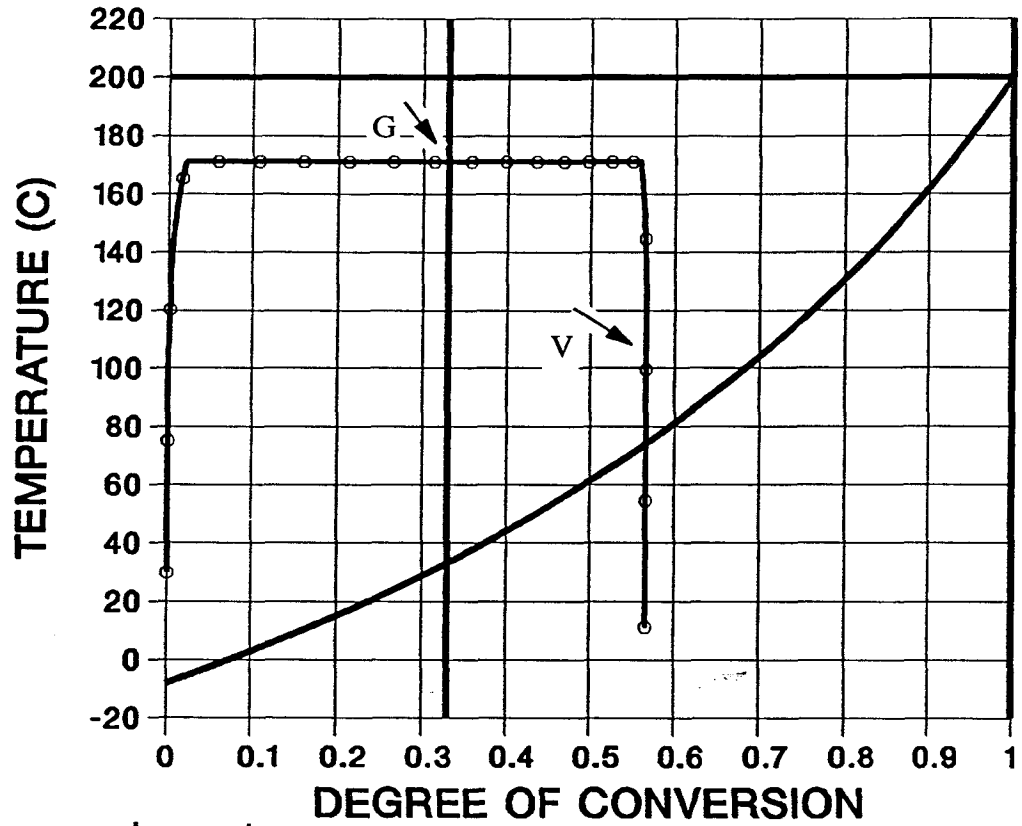


Figure 47b.

History of degree of conversion in test 170°C/60 min (B).

## alpha-T-T DIAGRAM



Legend:

G - experimental gelation

V - experimental vitrification

Figure 47c.

$\alpha$ -T-T diagram showing processing curve in test 170°C/60 min (B).

## TEMPERATURE CYCLE

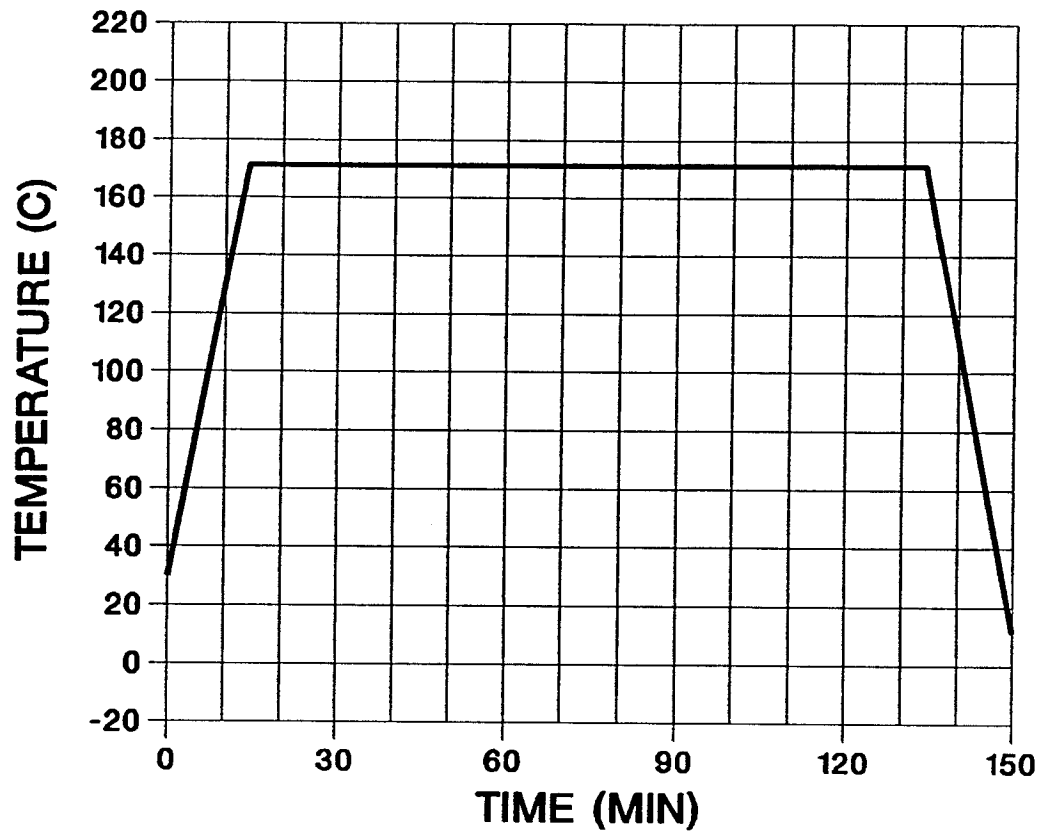


Figure 48a.

Temperature cycle in test 170°C/120 min (A).

## DEGREE OF CONVERSION

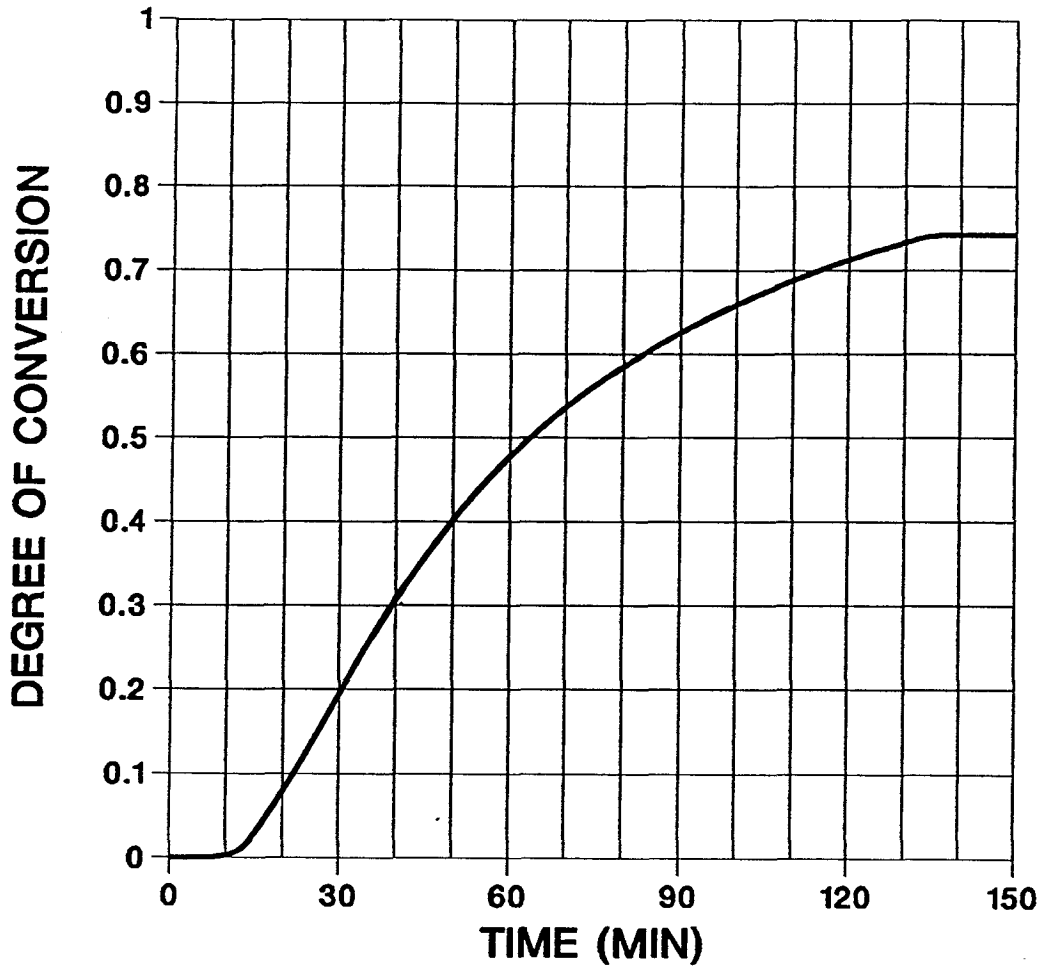
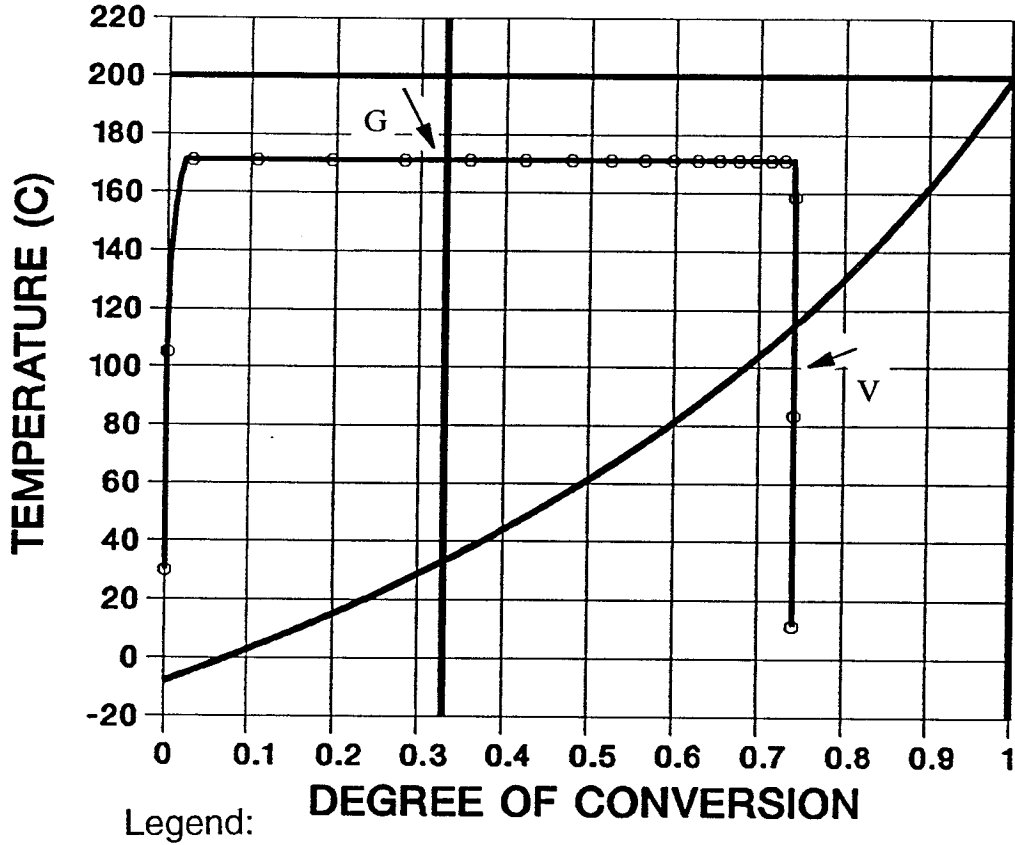


Figure 48b.

History of degree of conversion in test 170°C/120 min (A).

### alpha-T-T DIAGRAM



Legend:  
 G - experimental gelation  
 V - experimental vitrification

Figure 48c.

alpha-T-T diagram showing processing curve in test 170°C/120 min (A).

## TEMPERATURE CYCLE

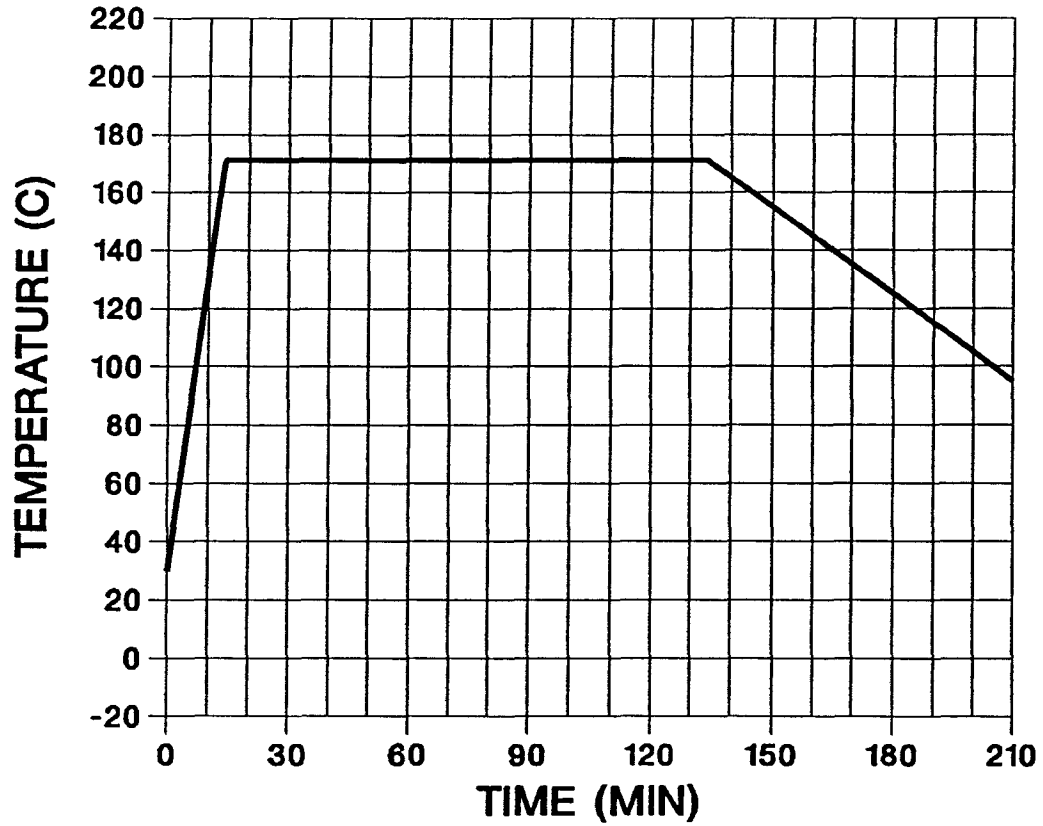


Figure 49a.

Temperature cycle in test 170°C/120 min (B).

## DEGREE OF CONVERSION

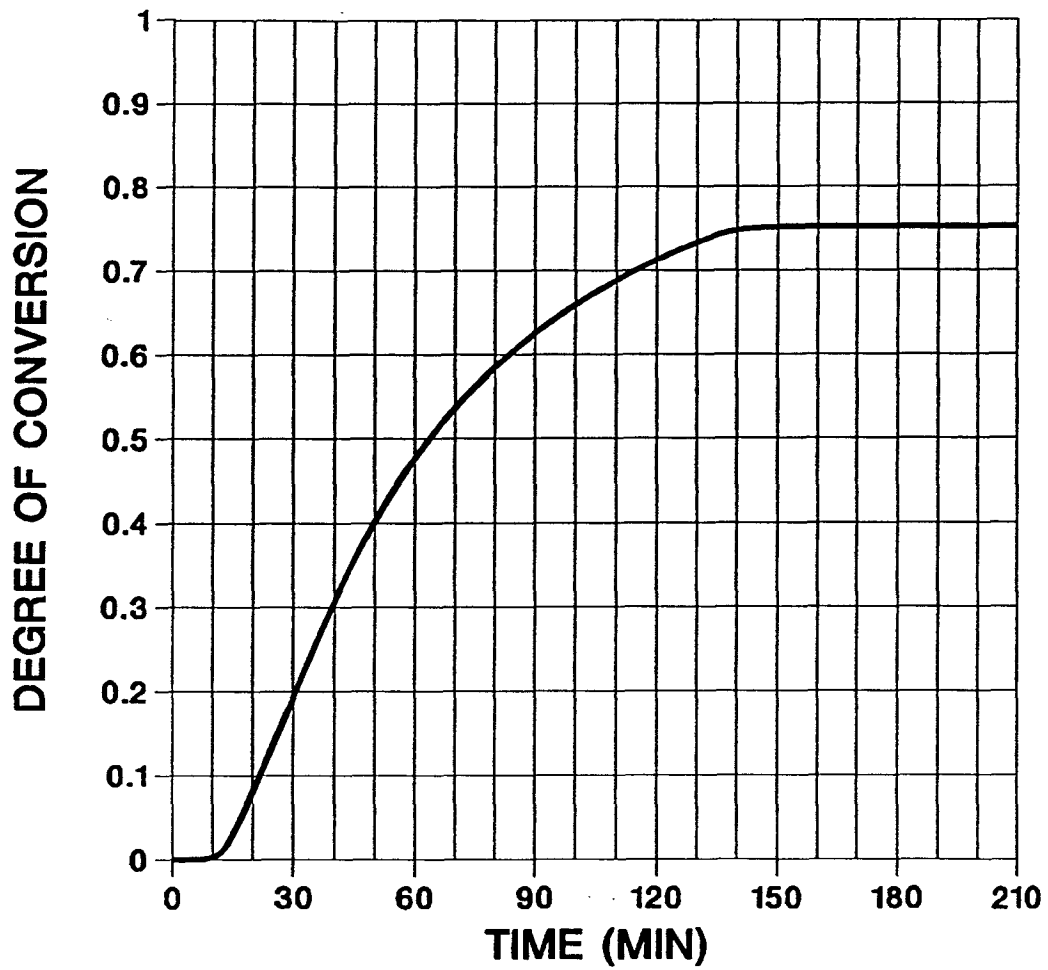


Figure 49b.

History of degree of conversion in test 170°C/120 min (B).

## alpha-T-T DIAGRAM

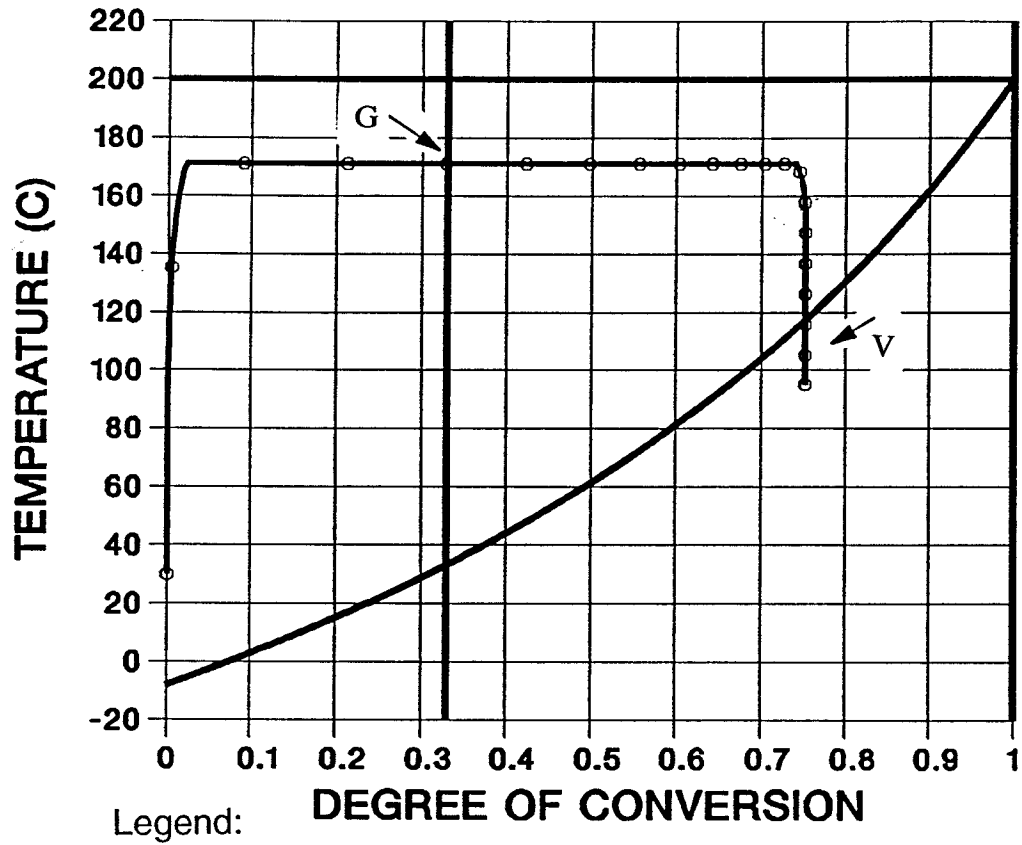


Figure 49c.

$\alpha$ -T-T diagram showing processing curve in test 170°C/120 min (B).

## TEMPERATURE CYCLE

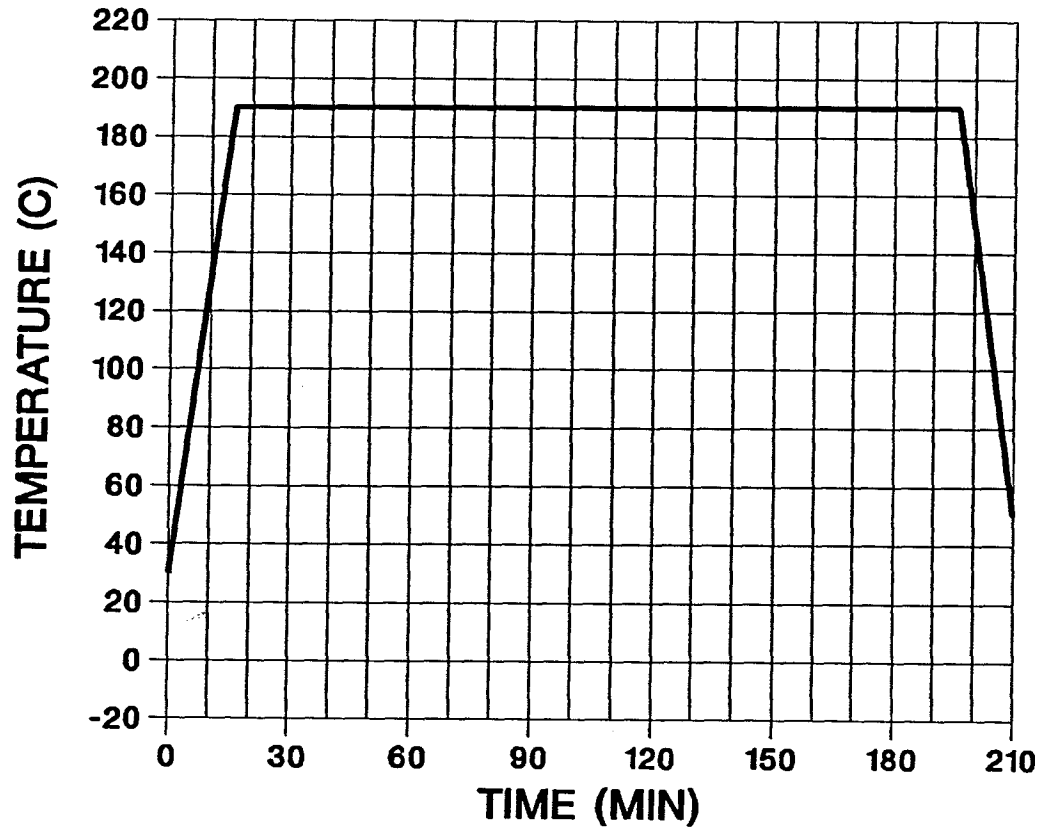


Figure 50a.

Temperature cycle in test 190°C/180 min (A).

## DEGREE OF CONVERSION

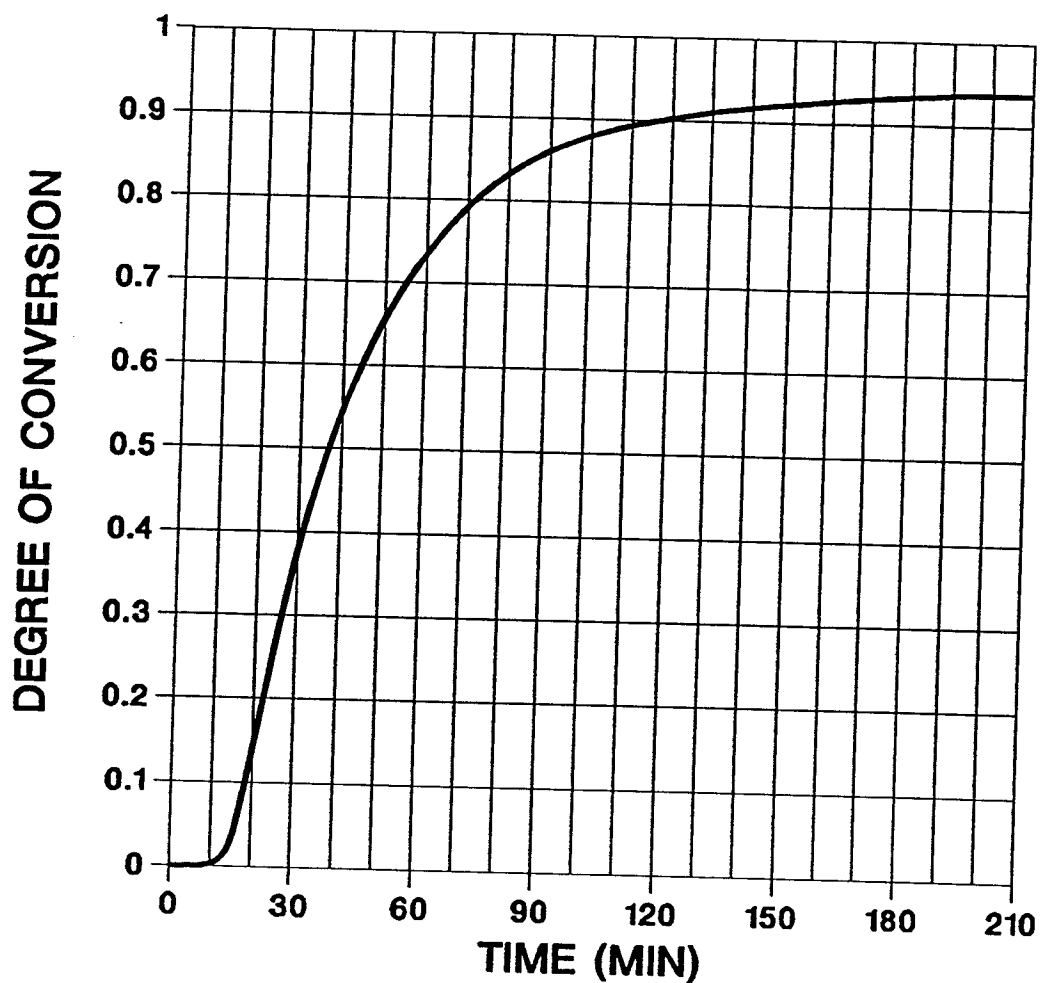
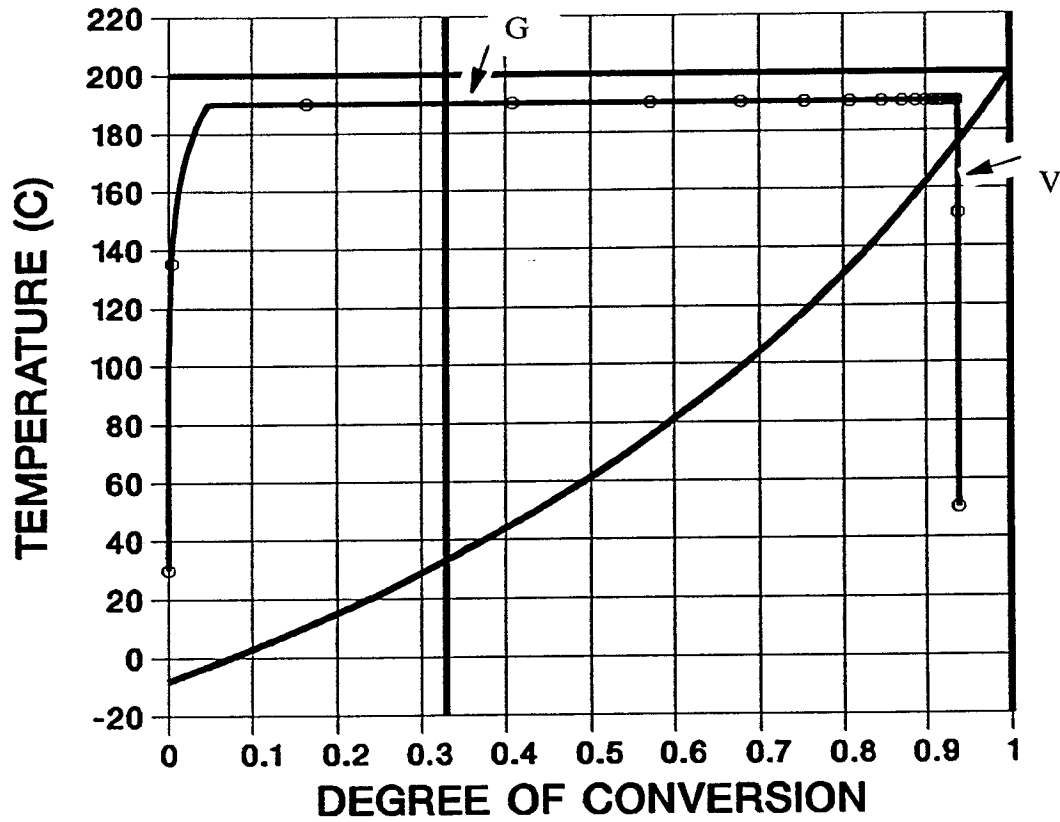


Figure 50b.

History of degree of conversion in test 190°C/180 min (A).

## alpha-T-T DIAGRAM



Legend:

G - experimental gelation

V - experimental vitrification

Figure 50c.

$\alpha$ -T-T diagram showing processing curve in test 190°C/180 min (A).

## TEMPERATURE CYCLE

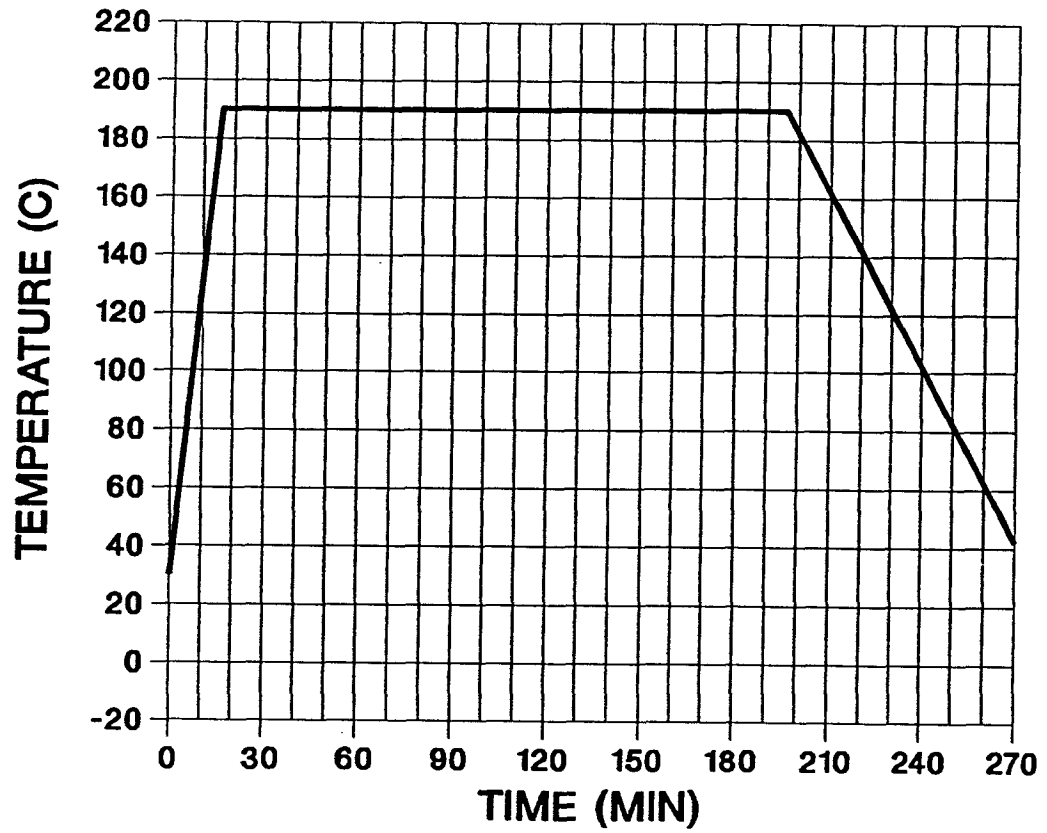


Figure 51a.

Temperature cycle in test 190°C/180 min (B).

## DEGREE OF CONVERSION

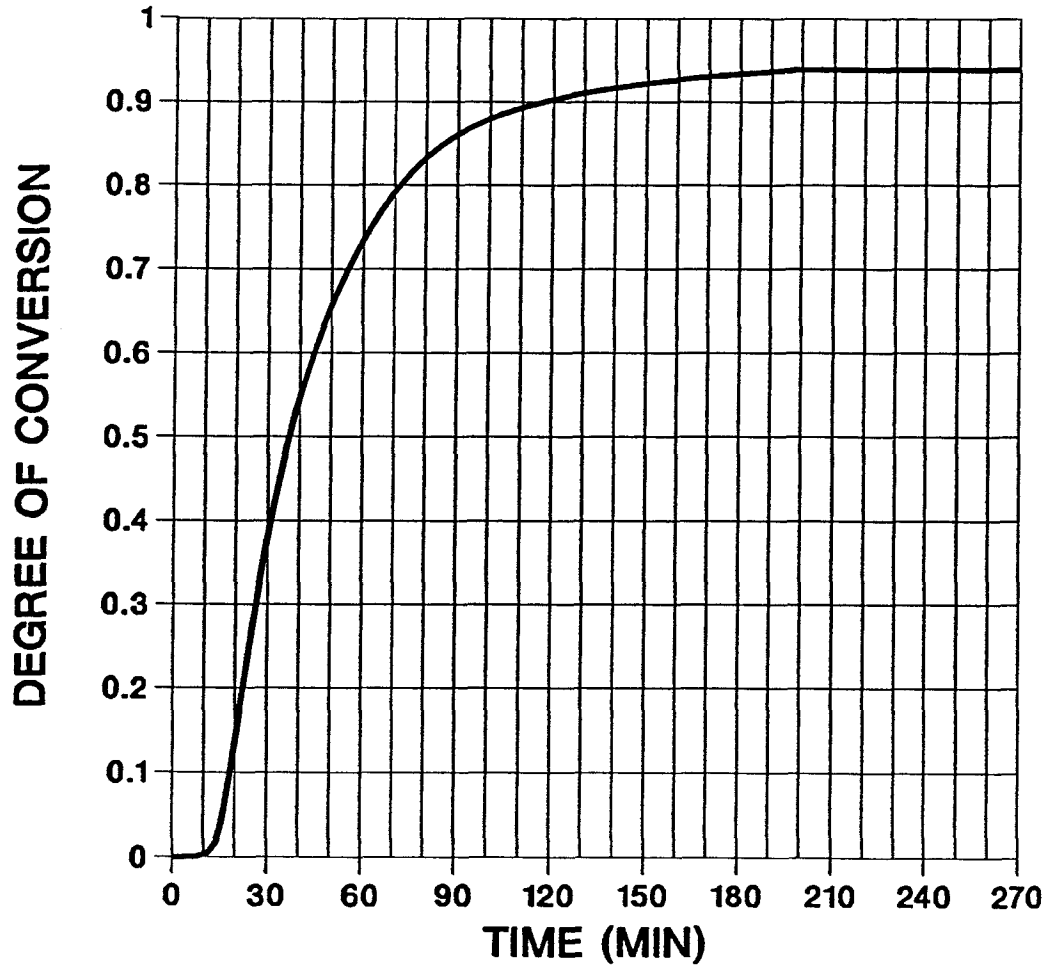
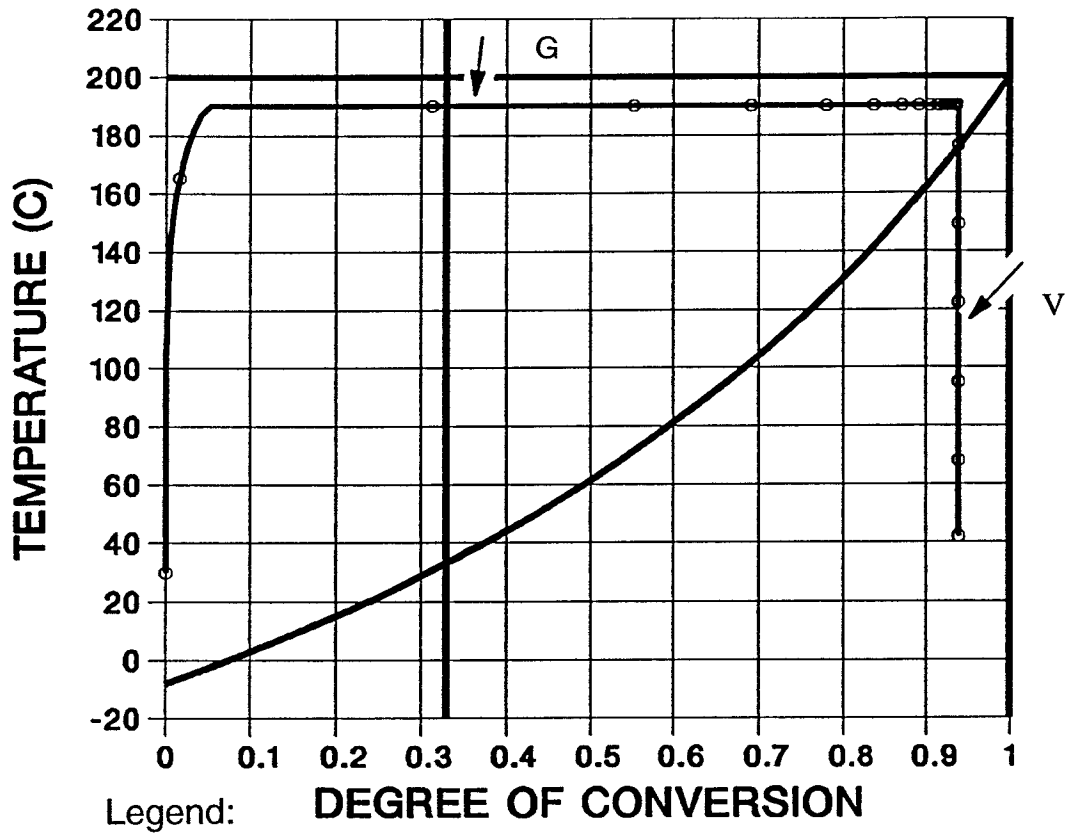


Figure 51.

History of degree of conversion in test 190°C/180 min (B).

## alpha-T-T DIAGRAM



Legend:  
 G - experimental gelation  
 V - experimental vitrification

Figure 51c.

$\alpha$ -T-T diagram showing processing curve in test 190°C/180 min (B).

### 5.6.2 $\alpha$ -T-T Diagram in Thick Composites Processing

In thick materials, different locations usually have a different temperature history and therefore a different degree of conversion, different glass transition temperature, and different moment of vitrification. All these differences result in a different structure of a material and the creation of additional stresses. The alpha-T-T diagram provides information on which point vitrifies first and its temperature of vitrification. Figure 52 shows a diagram which was generated by combining the processing information from the presented system with a realistic prediction of temperature for a layer of the Narmco resin 4.5 mm thick<sup>52</sup>. In each part of the diagram in Figure 52 two curves are present - one for the location in the processed material that is adjacent to the heating tool (marked with circles) and the other for the opposite side location (marked with triangles). Part I of the diagram shows the assumed curing cycle at the tool, and the resulting temperature cycle at the other side of material, with a high temperature peak due to the exothermic heat of conversion. The peak is responsible for the high degree of conversion observed for the far-side location in Part II of the diagram. Finally, in Part III there are two curves of processing. The auxiliary lines connecting the curves are drawn to connect processing points of the same processing time. When the temperature of processing starts decreasing at the end of the cycle at a rate of 2 °C/minute, the temperature in both locations is nearly the same. However, the far-side location obtained a higher degree of conversion, and therefore vitrifies first at the temperature of 150°C. The material at the tool vitrifies about 10 minutes later at the temperature of 135 °C. As a result of the applied processing cycle, the structure and degree of contraction of the material differs from location to location. The structure of the material at the far-side location was probably negatively affected by the temperature of processing, exceeding 220°C for a period of time. It may be concluded from the diagram that the moment of gelation was reached at different times in different locations.

In Figure 53 an T-T- $\alpha$ -T diagram containing the same cycle of processing as figure 52 is presented. Unfortunately, the surfaces of gelation and vitrification obscured the view and had to be removed from the graph.

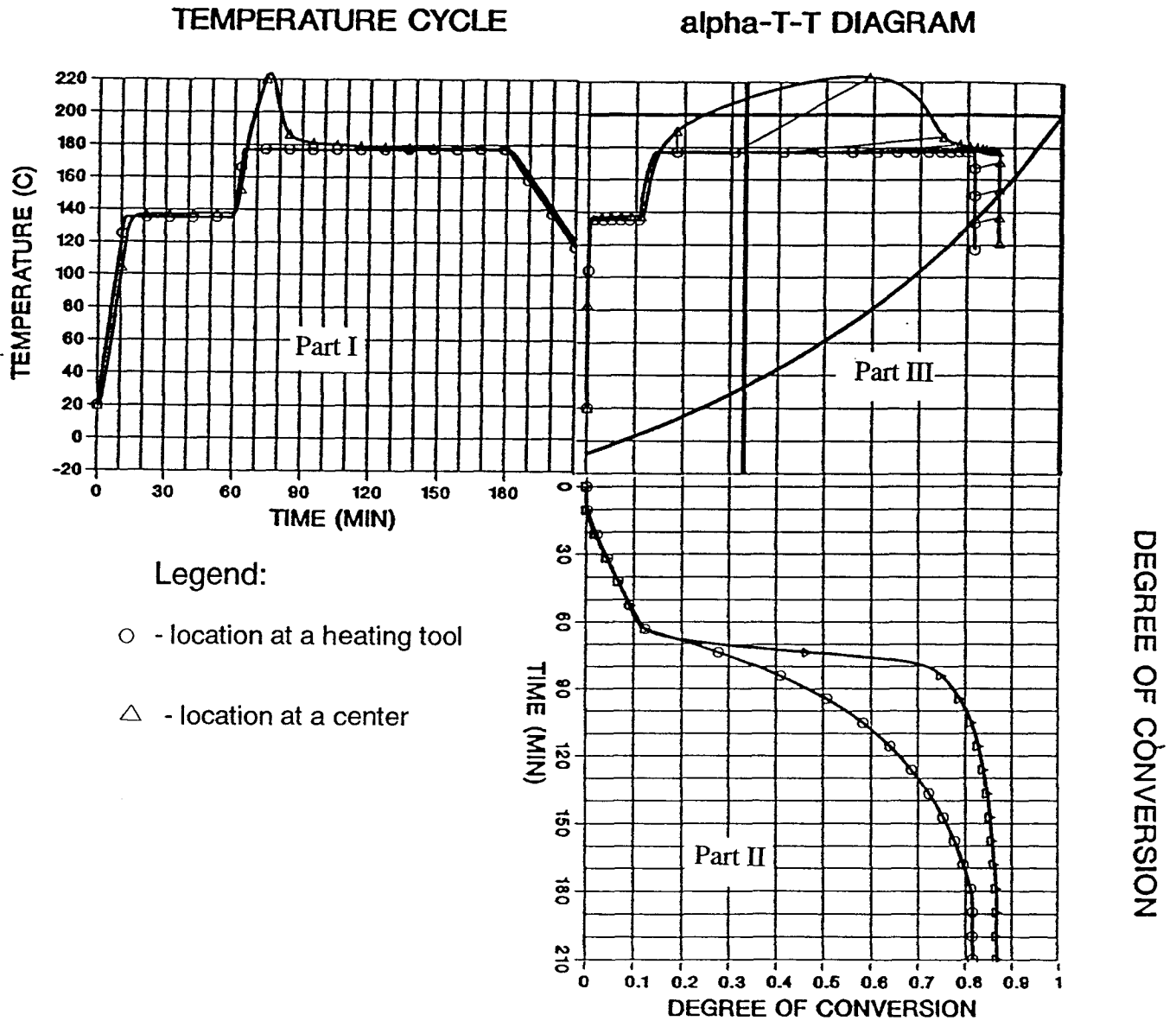


Figure 52.

$\alpha$ -T-T diagram in thick composite processing

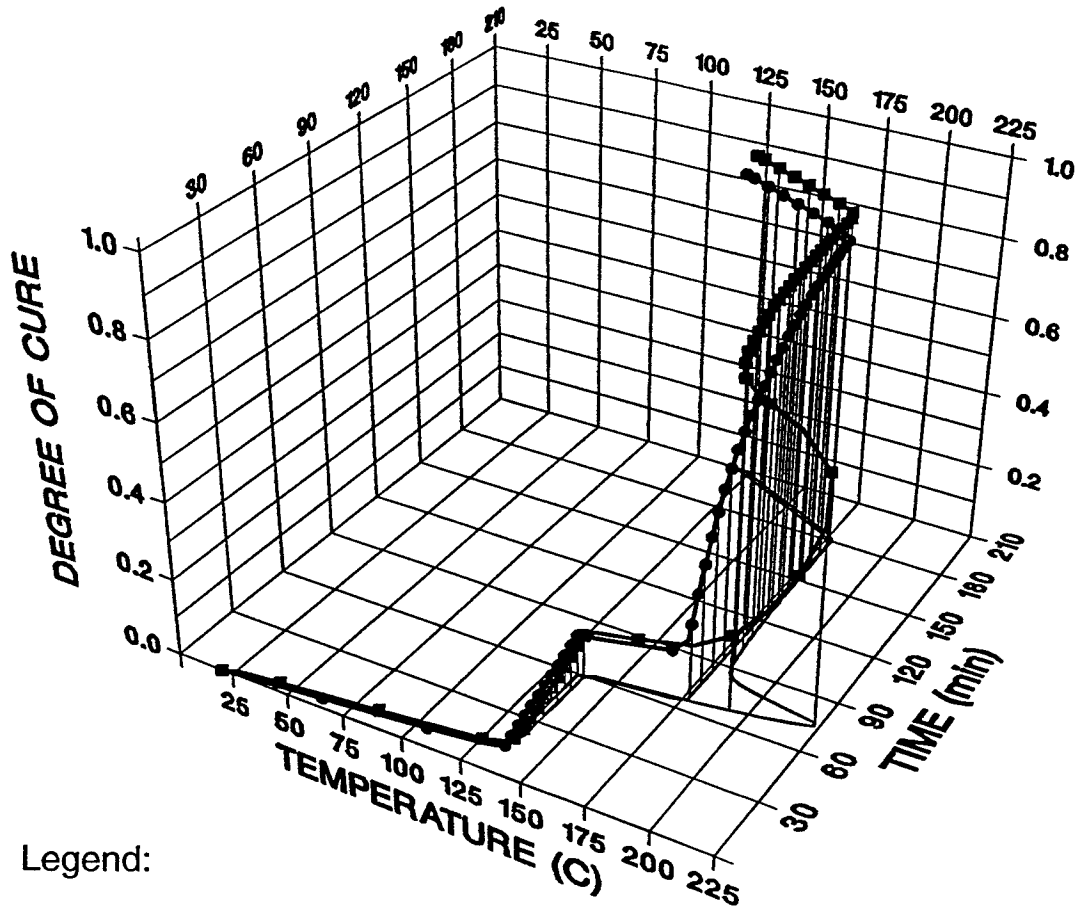
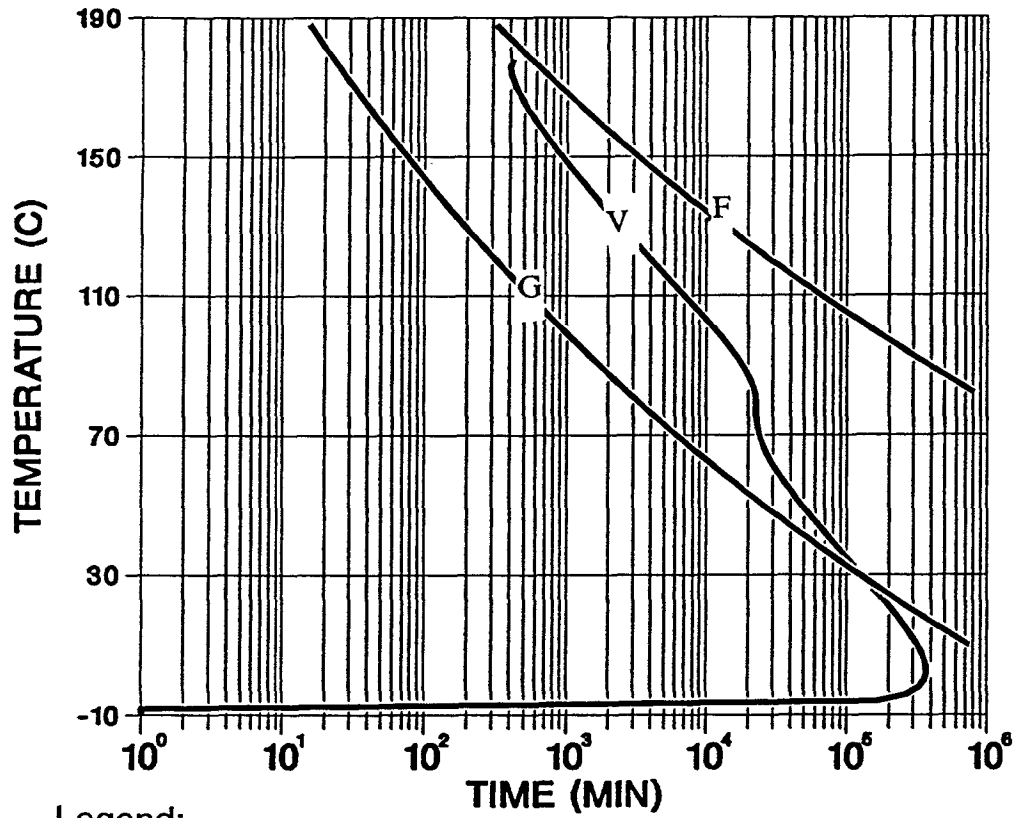


Figure 53.

T-T- $\alpha$ -T diagram in thick composite processing.

### 5.6.3 Generation of T-T-T Diagram

The  $\alpha$ -T-T and T-T- $\alpha$ -T diagrams previously presented are supposed to contain basic information equivalent to that of the T-T-T diagrams, but to be more universal in their applications. If this is so, it should be possible to produce the T-T-T diagrams using the proposed system. The T-T-T diagram may be generated by running consecutive simulations of isothermal processing for various temperature levels, waiting for gelation and vitrification to occur, and plotting both points in the time-temperature system of coordinates. This exercise has been conducted for the Narmco resin and the resulting T-T-T plot is presented in Figure 54. The only technical problem which was experienced was a necessity for fine tuning of the variable time increments for processing, especially in the range of low temperature processing. In the figure, the curve of gelation, vitrification and full cure are present; their shape is consistent with Gillham's diagrams. Discussion of the devitrification curve is beyond the scope of this Thesis. It should be realized, however, that the produced diagram has a limited accuracy, since the kinetics of conversion used by the system has never been verified for temperatures below 130°C. Also, in this specific exercise, the vitrification-related slow-down of conversion reaction was not accounted for.



Legend:

- G - gelation curve
- V - vitrification curve
- F - full cure curve

Figure 54.

T-T-T diagram for Narmco resin.

### 5.7 Contribution of the Author

Chapter 5 covers the main research effort of the author:

- (1) the concept of the system
- (2) the concept of  $\alpha$ -T-T and T-T- $\alpha$ -T diagrams
- (3) realization of the system and the diagrams in a form of a computer program for the Narmco resin
- (4) application of the system and diagrams for the simulation of processing, using a manufacturer suggested cycle and devised temperature cycles applied in RDA experiments
- (5) utilization of the system to produce a T-T-T diagram
- (6) application of the system and diagrams for the simulation of the processing of thick composites

The research is original and was performed exclusively by the author. It should be noted that the objective of this work is to provide a modelling element representing material behavior, rather than the modelling of the entire process, so that the modelling of thermal phenomena of the process are out of the scope of this work. The temperature of material in a central location used in Chapter 5.6.2, addressing the processing of thick composites, was re-printed from another work.<sup>52</sup>

## 6. APPLICATION OF ALPHA-T-T DIAGRAM TO CHARACTERIZE THE RAPID THERMOSET PROCESSING (RTP) METHOD

The RTP method, proposed by Breitigam, Bauer and May <sup>9</sup>, partly replaces the processing in the autoclave by processing in a pre-programmed furnace, cutting the cost of production. The method takes advantage of the fact that initial vitrification does not cause the slow-down in the kinetics of the reaction of conversion, this slow-down takes place in the vicinity of the final vitrification point. As a result, in a certain range of processing parameters, the state of the material exists in which the resin has the stiffness of a solid, but the rate of conversion is not negatively affected. In terms of the degree of conversion-temperature coordinates (Part III of the  $\alpha$ -T-T diagram), the curve of processing in the RTP mode should be on the right side of the initial vitrification curve, but may not approach the vicinity of the final vitrification curve.

The intention of the research effort presented here was to examine the feasibility of creating a processing diagram which can be used as a tool to optimize the processing cycle for RTP. The exercise is a hypothetical one, since the Narmco resin, for which the system was developed, is not very suitable for RTP processing. It has too low a degree of conversion at gelation, a low temperature of vitrification of B-staged resin, and the range of the verified applicability of the conversion model incorporated into the system does not cover processing below 130°C. Yet, if this hypothetical attempt proved to be successful, the same approach could be applied to any real case.

The first step in the research was to determine the shape and the analytical form of the initial vitrification curve in the  $\alpha$ -T coordinates. This was done on the basis of the same RDA records which were used for the verification of gelation and final vitrification curves. The moment of initial vitrification was recognized in the records as a midpoint of the 'knee' of the storage modulus ( $G'$ ) curve, with an arbitrary safety margin added. The identified curve of initial vitrification, "IN", is

shown in Part III of Figure 55. It was found that the original DiBenedetto equation, which is used routinely to analytically express the curve of final vitrification in  $\alpha$ -T coordinates, can be easily adapted to provide an analytical form of the initial vitrification curve, as well.

In the second step of the investigation, an attempt was made to find the ideal trajectory of the RTP processing curve in  $\alpha$ -T coordinates. In order to ensure the maximum effectiveness and, consequently, the shortest possible time of processing, the curve of processing should be parallel and run as close as possible to the initial vitrification curve. After introducing an additional safety margin, the correct curve of processing was assumed, as shown in Part III of Figure 55. Once this curve was known, it was discovered that the system could be easily altered to be run in a partly reversed mode, identifying for consecutive time increments the correct temperature cycle from the assumed processing curve in the  $\alpha$ -T coordinates. This correct or optimum curing cycle is presented in Part I of Figure 55 in which the temperature rises very slowly over an extended initial processing period, and very rapidly at the end of processing. Two inter-related aspects should be emphasized in connection with the curve generation:

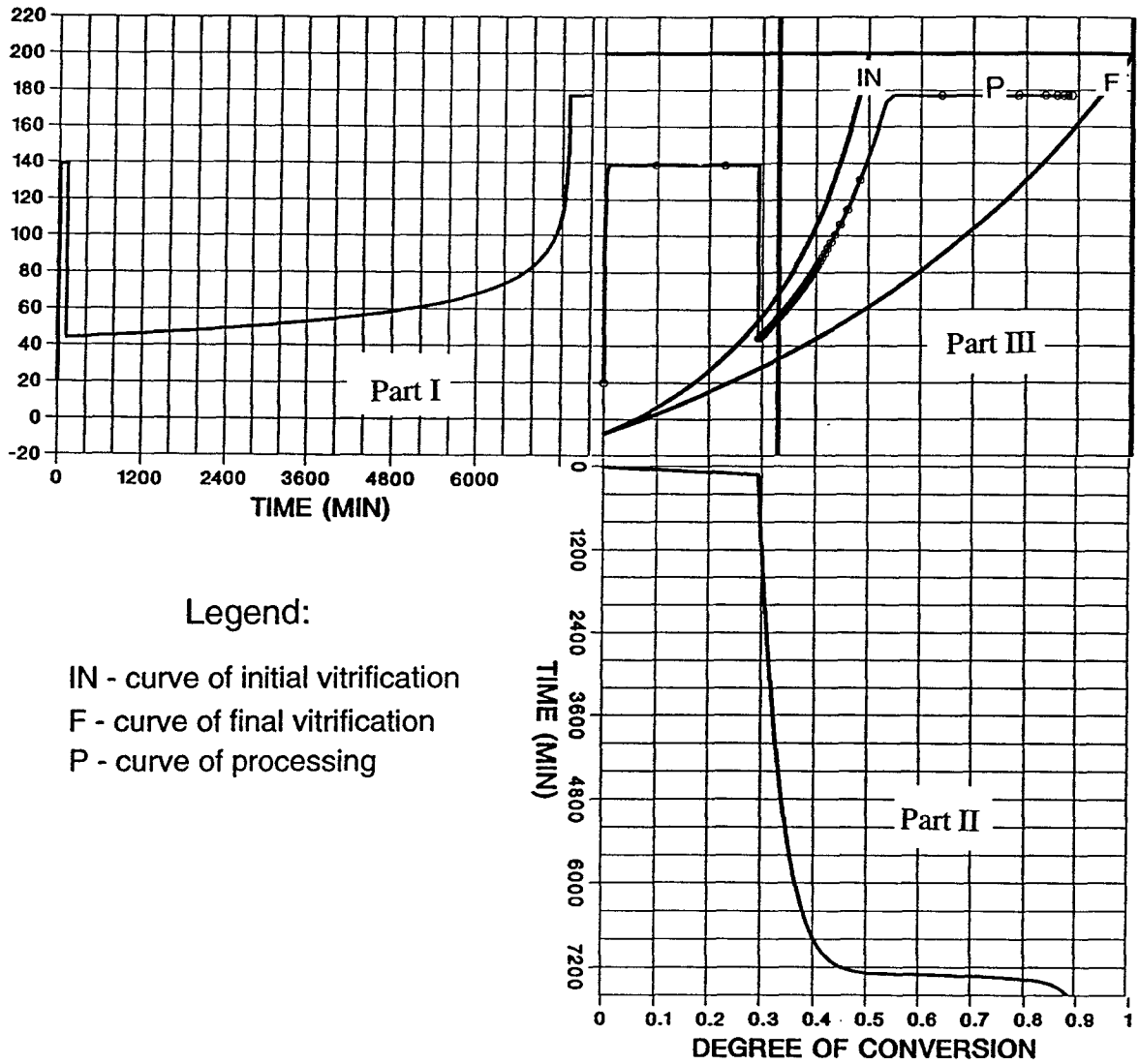
- (1) The only alternative way to obtain an acceptable thermal curve of processing is by performing very laborious experiments involving the TBA technique and a trial-and-error approach.
- (2) Any idea of simplifying the presented thermal curve, by linearization and safe application of even slower rate of temperature increase may look tempting, but is, in fact, very risky. Any alteration of the presented curve requires repeated calculations involving  $\alpha$ -T-T diagrams.

### 6.1 Contribution of the Author

The modelling effort and resulting diagrams presented in Chapter 6 are original and performed solely by the author. The proposed approach is the only existing one to design the RTP process from theoretical consideration. The practical importance of the approach, however, depends on the practical importance of the RTP method itself.

TEMPERATURE CYCLE

alpha-T-T DIAGRAM



Legend:

- IN - curve of initial vitrification
- F - curve of final vitrification
- P - curve of processing

Figure 55.

$\alpha$ -T-T diagram in RTP processing.

## 7. CONCLUSIONS

Thermoset-based composites are often classified as high - performance materials. On the other hand, they are also frequently considered as non-dependable, with a poor reproducibility of finished product properties. Two factors contribute to the latter. First, thermosets are extremely sensitive to the parameters of processing and may be easily damaged by processing errors. At the same time, the control of thermoset processing and the equipment used in the process may seem primitive, creating a deceiving impression of simplicity and promoting carelessness in production.

The first generation of mathematical models was developed to eliminate processing errors. Ironically, however, the models shared the over-simplistic approach, not to the process itself, but rather to the material being processed. A situation was thus created, where numerous groups of material specialists, usually with chemical backgrounds, were making tremendous advances in the understanding of chemical reactions and in network structure formation (rheology). This progress was nearly neglected by groups of scientists, usually with non-chemical backgrounds, making their own substantial contribution in modelling of the heat and mass transfer phenomena associated with the process. In modelling, preference was given to experimentally-based, simplified expressions for kinetics of conversion, rather than the complex expressions worked out by chemists. The objective of modelling was to ensure that a rigid prescription for correct processing, called the manufacturer-suggested processing cycle, was executed throughout the material to the greatest extent possible. The understanding of how this suggested cycle was formulated, and consequently, to which extent, and how it could be altered without causing harm to the processed material was beyond the scope of the modelling, excluding the possibility of modelling becoming a part of this formulation process. Even the basic, well-known rheological phenomena, such as gelation and vitrification, which do affect either the variables included in modelling (rate of heat generation, temperature), or the final properties of the product, have been neglected in the early modelling efforts.

It is not that the importance of the rheological phenomena was not recognized at all in the area of thermoset processing. The need for occasional processing of very thick layers of resin taught scientists to take advantage of the vitrification-induced slow-down of conversion. It was also learned that for a slow, linear temperature increase, the state of the material is 'sliding' along the vitrification curve, always slightly above the curve. There was, however, no scientific tool to visualize these aspects of processing.

Here the concept of this thesis originated. The objective was to create a modelling element representing rheological information on the material under processing, and to produce the complex generated rheological information in a comprehensive and transparent graphical form. The modelling element was developed in the work as the proposed system, and the graphical form is represented by  $\alpha$ -T-T and T-T- $\alpha$ -T diagrams.

The proposed system presented in the Thesis, with its graphical output as  $\alpha$ -T-T, and T-T- $\alpha$ -T diagrams, provides full information on a material under processing. It plots the progress of processing, characterized by time, temperature and the degree of conversion relative to the major material transformations: gelation, initial vitrification, and final vitrification. It is capable of predicting a diffusion-controlled slow-down of the reaction of conversion caused by final vitrification, the temperature of final vitrification, and the moment of initial and final vitrification.

The information contained in the diagrams is enriched in the case of thick material processing, when the progress of processing in one characteristic location may be directly related to the progress in another location, providing the time sequence for vitrification.

The diagrams, especially the  $\alpha$ -T-T diagram, have two roles to fulfill: to provide information and to improve understanding of the processing. One glance at the location of a processing point allows for determination of the state of the material and current values of the processing variables. The

choice of a degree of conversion as an abscissa in the main part of the  $\alpha$ -T-T diagram seems uncomfortable for a beginner, but teaches one to think in categories of material structure. For someone who has become familiar with the processing diagrams, gelation is no longer a change of physical state, but rather a certain stage in network formation. Similarly the temperature of glass transition is no longer a temperature, but rather a property of a material related to the density of the network, and naturally increasing with the progress of processing.

The system, and the diagrams proposed in this work are developed from the theory of the process and no experimental proof of their validity is required. A need exists, nonetheless, to demonstrate their eventual applications and capabilities. From this point of view, the experimental part of the work is of secondary importance, and was intended to give reality to the produced examples, providing the system with real kinetics of conversion, and real rheology of the Narmco resin. For the author, it was an opportunity to become familiar with experimental techniques and problems related to the determination of kinetics, and rheological characterization of a resin system.

The latest generation of kinetics of conversion models, represented by Cole's mechanistic model, proved to be very well suited to the kinetic requirements of the system. For real conditions of processing, the range of model validity is more than sufficient. For more theoretical applications, however, it would be beneficial to ensure the validity of the model for temperatures below 130 °C. The expression for the conversion slow-down that occurs near vitrification would also have to be reexamined to be applicable for low temperatures.

The RDA technique allowed for dependable and accurate identification of the gelation point. Unfortunately neither this technique nor the DSC technique used in the work were fully satisfactory in determining vitrification. The RDA records, however, allowed for a comfortable identification of initial vitrification phenomena.

The diagrams presented, and the proposed system, although novel today, are only the first step in equipping the existing processing models with material-related information. It is expected, however, that they will provide a solid base for other steps, and other more sophisticated applications which are yet to be developed. Even within the current work, the additional element of the curve of initial vitrification was added to the basic  $\alpha$ -T-T version. Similarly, the contours of iso-viscosity may be added as viscosity is a function of the degree of conversion.

With the recent publication of the RTP method<sup>9</sup> an unexpected opportunity to demonstrate one of the future, more sophisticated applications of the diagram arose - an opportunity to utilize the diagrams as the only existing tool for the optimization of the thermal processing cycle. The application of the system to the method shows a completely new perspective on the function of the diagrams. The "ideal" curve of processing, in  $\alpha$ -T co-ordinates was determined first, and on the basis of the curve, the system found the correct optimum temperature cycle to be applied.

Today when the work is completed, modelling of the processing of thermoset-based composites is slowly changing. There is a general acceptance of the idea to include material-related information in models of processing, and progress is being made in this direction. It gives a great personal satisfaction for the author to be able to state that even such modelling precursor as Professor G. Springer of Stanford University accepted the need for an element responsible for material behavior in his work.

## REFERENCES

1. Adabo, H.E., Williams, R.J., *J. Appl. Pol. Sci.*, 27, 1327 (1982)
2. Apicella, A., " Developments in Reinforced Plastics" Ch.5, Protchard ed., New York (1986)
3. Apicella, A., et all., *J. Appl. Pol. Sci.*, 29, 2083 (1984)
4. Berglund, L.A., Kenny, J.M., *SAMPE J.*, 2, 27 (1991)
5. Berry, G.C., Fox, T.G., *Adv. Pol. Sci.*, 5, 856 (1968)
6. Bidstrup, S.A., Ph.D. Thesis University of Minnesota (1986)
7. Bidstrup, S.A., Macosco, C.W., *J. Pol. Sci.*, 28, 691 (1990)
8. Bidstrup, S.A., Sheppard, N.F., *Proceedings ACS Symp.* 175 (1987)
9. Breitigam, W., Bauer, R., May, C., ACS International Symposium, 33, 511, (1992)
10. Castro, J.M., Macosco, C.W., *Soc. Plast. Eng. Tech. Papers.*, 26, 434 (1980)
11. Chambon, F.J., *J. Rheol.*, 31, 803 (1987)
12. Chambon, F.J. and Winter, H.H., *Pol. Bulletin*, 13, 499 (1985)
13. Chan, L.C., Nae, H.N., Gillham, J.K., *J. Appl. Sci.*, 29 3307 (1980)
14. Chiang-Ying, Dynes, P., *J. Appl. Pol. Sci.*, 27 569 (1982)

15. Cole, K.C., *Macromolecules*, 24 3093 (1991)
16. Cole, K.C., Hechler, J.J., Noel, D., *Macromolecules*, 24 3098 (1991)
17. Cole, K.C., Noel, D., "Physicochemical Characterization of High-Performance Fibre-Reinforced Organic-Matrix Composites" NRC Report (1988)
18. Du Pont Inc. (Ed.) "Theory of Operation of the Du Pont 982 Dynamic Mechanical Analyzer"
19. Du Pont Inc. (Ed.) "DSC Operator's Manual"
20. Du Pont Inc. (Ed.) "TMA 2940 Operator's Manual"
21. Dusek, K., *Pol. Bulletin*, 13, 321 (1985)
22. Enns, J.B., Ph.D. Thesis Princeton University (1982)
23. Enns, J.B., Gillham, J.K., *J. Appl. Pol. Sci.* 28, 2567 (1983)
24. Enns, J.B., Gillham, J.K., "Polymer Characterization" *Amer. Chem. Soc. Advances in Chemistry Series* 203, 27 (1983)
25. Flory, P.J., "Principles of Polymer Chemistry" Cornell University Press, New York (1953)
26. Gan, S., Gillham, J.K. and Prime, R.B., *J. Appl. Pol. Sci.* 37, 803 (1986)
27. Gillham, J.K., "Developments in Polymer Characterization" Dawkins England (1982)
28. Gillham, J.K., Bena, J.A., *J. Appl. Pol. Sci.* 18, 951 (1974)
29. Graesley, H., Account of Chemical Research 10 (1983)

30. Gupta,A.,et all., *J.Appl.Pol.Sci.*, 28, 1011 (1983)
31. Halpin,J.C., Kardos,J.L.,Dudkovic,M.P., *Pure & Appl.Chem.*,55, 895 (1983)
32. Harran,D., Laudouard,A., *J.Appl.Pol.Sci.*, 32, 6043 (1984)
33. Harran,D., Laudouard,A., *Rheol.Acta*, 24, 63 (1985)
34. Havlicek,I., Dusek,K., "Crosslinked Epxies" Walter de Gruyter & Co.(Ed.) New York (1987)
35. Hinrichs,R., Thuen,J.M., "Characterizing Rheological Cure Behavior of Epoxy Composite Materials, Narmco Materials Inc. Report 92627
36. Holly,E.E., et al., *J.Non-Newt Fluid*, 27, 17 (1988)
37. Horie,K., et al., *J.Appl.Pol.Sci.*, 8, 1357 (1970)
38. Kamal,S., *Pol.Eng.Sci.*, 13, 59 (1973)
39. Kamal,M.R., Ryan,M.E., *Polym.Eng.Sci.*, 20, 859 (1980)
40. Kenny,J.M.,Apicella,A., *Pol.Eng.Sci.*, 29, 972 (1989)
41. Kenny,J.M.,Maffezoli,A.,Nicolais,L., *Compos.Sci.Technol.*, 38, 339 (1990)
42. Kenny,J.M.,Trivisano,A., *Pol.Eng.Sci.*, 31, 1426 (1991)
43. Loos,A.C., Springer.G.S., *J.Comp.Mat.*, 17, 135 (1983)
44. Macosco,C.W.,Miller,D.R., *Macromolecules*, 9, 199 (1976)
45. May,C.A., "Chemoreology of Thermosetting Polymers" ACS Symposium Series 227, Washington (1983)

46. May,C.A., et all., ACS Symposium Proceedings (1983)
47. McGrath.J.E., ACS Symposium Proceedings (1992)
48. Mijovic,J.,Lee,Ch.H., *J.Appl.Pol.Sci.*, 37, 889 (1989)
49. Nielsen,L.E., *J.Macromol.Sci.*, C3, 69 (1969)
50. Nielsen,L.E., "Polymer Rheology" Marcel Dekker (Ed.), New York (1982)
51. Osinski,B.A., *Polymer*, 34, 752 (1993)
52. Osinski,B.A., SAMPE Conference Proceedings Toronto (1992)
53. Pang,K.P.,Gillham,J.K., *J.Appl.Pol.Sci.*, 37, 1969 (1989)
54. Pascault,J.P., Williams,R.J., *J.Pol.Sci.*, 28, 88 (1990)
55. Plazek,D.J.,Frund,Z.N., *J.Pol.Sci.*, 28, 431 (1990)
56. Prime,R.B.,"Thermal Characterization of Polymeric Materials"  
Turi,E.A.,(Ed.) Academic Press, New York (1981)
57. Rabinowitch,E., *Trans.Faraday.Soc.* 33, 1225 (1937)
58. Read,B.E.,Dean,G.D.,Duncan,J.C.,"Determination of Dynamic Moduli  
and Loss Factors" Rochester (Ed.) New York 1991
59. Reometrics Inc. (Ed.) "Understanding Rheological Testing" (1990)
60. Roller,M.B., *Pol.Eng.Sci.*, 15, 406 (1975)
61. Sanford,W.,McCullough,R.J., *J.Pol.Sci.*,28, 973 (1990)
62. Serrano,D.,Harran,D., *Pol.Eng.Sci.*, 29, 531 (1989)

63. Serrano,D., et al., *J.Pol.Sci.*, 39, 679 (1990)
64. Shu-Sing Chang, SAMPE Symposium Proceedings (1992)
65. Tung,C.Y.,Dynes,P.J., *J.Appl.Pol.Sci.*, 27.569 (1982)
66. Vinogradov,G.V.,Malkin,Y., "Rheology of Polymers", Springer-Verlag (Ed.) Berlin (1980)
67. Williams,R.J., Benavente,M.A., RuseckaiteR., *Pol.Eng.Sci.*, 30, 1140 (1990)
68. Williams,R.J., Private Correspondence
69. Winter,H.H., ASTM Conference Proceedings Detroit (1988)
70. Winter,H.H., *Pol.Eng.Sci.* 27, 1698 (1998)
71. Wisanrakkit,G., Ph.D. Thesis Princeton University (1990)
72. Wisanrakkit,G., Gillham,J.K., *J.Coat.Tech.*, 62, 35 (1990)
73. Wisanrakkit,G.,Gillham,J.K., *J.Appl.Pol.Sci.* 42, 2453 (1991)